Montanuniversität Leoben – University of Leoben
Department Metallurgie – Department of Metallurgy
Nichteisenmetallurgie – Nonferrous Metallurgy

# Master Thesis

Title:

## Technical optimization and economic evaluation of the lead bath recycling process

Author:

Benjamin Böckl, BSc

Supervisors:

Priv.-Doz. Dipl.-Ing. Dr.mont. Jürgen Antrekowitsch

Dipl.-Ing. Dr.mont. Alois Unger

Leoben, June 2015

**NON-FERROUS METALLURGY**
MONTANUNIVERSITY
A-8700 LEOBEN

Benjamin Böckl

September 2014

# TECHNICAL OPTIMIZATION AND ECONOMIC EVALUATION OF THE LEAD BATH RECYCLING PROCESS

The focus of the present thesis is on the technical optimization and economic evaluation of the so called lead bath recycling process. With this pyrometallurgical process, strategic metals like zinc, lead and silver are recovered from dumped slags generated in the lead- and zinc industry. The innovation of this process is based on its flexibility, which offers the opportunity to treat a large portfolio of residues with the same strategic metals in them. Furthermore, the valuables are recovered in different fractions, where each one represents a saleable intermediate product.

The first part of the research deals with the optimization of the slag metallurgy, which potentially increases the recovery of the valuables and reduces the energy usage of the process. The theoretical knowledge has to be confirmed by several experiments using the hot stage microscope at the chair of nonferrous metallurgy at the University of Leoben. Based on the most promising results, technical scale trials with a resistance furnace are scheduled afterwards. These future results are supposed to represent the input data for prospective trials in the next bigger scale on the Top Blown Rotary Converter. For this next development step, mass and energy balances have to be calculated.

In addition to the technological part, the economic calculation is meant to represent the second part of the thesis in order to validate the project feasibility. The obtained data from former trials in the TBRC and the previously calculated mass and energy balance provide the input information for further calculations. The most important cost drivers for a possible realization are supposed to be identified and divided into capital expenditure, operational expenditure as well as the earnings from the achieved products. This calculation should be performed for three different scenarios and for two types of residues in total. The Imperial Smelting slag is meant to represent the type of residue with the lower content of strategic metals and the further investigated lead Blast Furnace slag characterizes the type with the higher valuable content. The three calculated scenarios are divided in a realistic case, which is based upon provided data as close to reality as possible, a best case- and a worst case scenario. Their aim is to show the influence of the different input parameters as well as the broad horizon of the project.

At the end, both technological and economic results are supposed to be presented. The technological results should contain an answer to the possible optimization measures and their potential, while the economic part is expected to be able to indicate whether the process is economically feasible and profitable.

Leoben, September 2014

# Statutory Declaration

I, Benjamin Böckl declare that I have authored this thesis independently, that I have not used other than the declared sources and that I have explicitly marked all material which has been quoted either literally or by content from the used sources.

Leoben, May 2015

_____

Benjamin Böckl

# Acknowledgement

First of all I want to thank Priv.-Doz. Dipl.-Ing. Dr.mont. Jürgen Antrekowitsch for the possibility to compose this thesis at the “Christian Doppler laboratory for Optimization and Biomass Utilization in Heavy Metal Recycling”. In cooperation with the chair of nonferrous metallurgy of the Montanuniversitaet Leoben, the CDL provided all the necessary raw materials and equipment for the trials and excellent guidance. Apart from the professional working conditions, Dr. Antrekowitsch and his colleagues were very understanding for my travel plans at the end of my studies, which deserves extra gratitude from me.

Particularly special thanks are due to Dipl.-Ing. Dr.mont Alois Unger, who supported me throughout the thesis. His knowledge and dedication to the thesis have been most helpful from the introduction to the topic at the very beginning, to the experimental design and procedure, right through to the correction of the written thesis. His effort and commitment was absolutely unique and I appreciate all his help and advice. I could not have wished for a better supervisor.

My sincere thank you to Dipl.-Ing. Dr.mont. Stefan Steinlechner, who helped me obtain realistic economic data from existing comparable plants, which was very important for the economic evaluation.

I also want to thank Dipl.-Ing. Josef Fasching, who introduced me to the hot stage microscope and helped analysing the phase composition of the valuable metals with the scanning electron microscope.

At this point I also want to thank my father Robert Hilger, who supported me a lot and provided unworried conditions for my studies, my mother Anna Maria Böckl for her faith in me, her encouragement and all her sacrifices for me. Many thanks also to my grandparents Helga & Herbert Böckl for everything they’ve done for me in the past years. I also should like to mention Gerald Ratich, who has been very supportive. Furthermore I want to thank my friends in Leoben, especially my flat mates, who made my time so enjoyable from the first day throughout my studies.

Last but not least I want to thank my beloved girlfriend Dominique Heuritsch for her patience, her understanding for my long periods of absence and her uncompromising support, whenever I need her.

# Abstract

This master thesis presents the most important technological and economic aspects of the “lead bath recycling process” in a Top Blown Rotary Converter (TBRC). Due to limited lead resources, stringent landfill regulations, as well as environmental- and sustainability reasons, the simultaneous recovery of the contained valuable metals of lead slag from primary production processes should be promoted. The aim of the thesis is to optimize the recycling process in order to run it more efficiently and make it more competitive. To achieve this, various influencing factors on the valuable recovery efficiency are identified and tested in two series of laboratory scale- and technical scale experiments. The focus is on fluxes that affect both the melting temperature and the viscosity of the slag, leading to reduced energy consumption and an increased valuable metal recovery rate. The thesis is supported by the usage of a scanning electron microscope, where the present phases of the valuable metals in the slag are determined.

The second part of the master thesis is an economic evaluation of a simulated industrial plant. Three different scenarios with two different slags as raw material are developed and calculated, due to the lack of experience about the “lead bath recycling process” in an industrial scale. The necessary data for the evaluation is provided by the results of the small-scale trials, by the calculated energy balance and by various documented assumptions that are based on existing industrial plants. The expected investment costs, operating costs and operating revenues are calculated for all scenarios and presented in this work. To calculate the total cost, the discounted net present value method is used. In addition to the technical optimization of the process, the assessment of profitability ratios is the second aim of this thesis.

# Kurzfassung

Im Rahmen dieser Diplomarbeit werden die wichtigsten technologischen und ökonomischen Gesichtspunkte des „Bleibad-Recyclingprozesses“ im „Top Blown Rotary Converter“ (TBRC) beleuchtet und präsentiert. Aufgrund der limitierten Bleivorkommen, der immer strenger werdenden Deponievorschriften, sowie aus Umwelt- und Nachhaltigkeitsgründen sollen enthaltene Wertmetalle der Bleischlacke aus der Primärproduktion simultan rückgewonnen werden. Das Ziel dieser Arbeit ist es, den Recyclingprozess in technischer Hinsicht zu optimieren, um ihn effizienter und konkurrenzfähig zu gestalten. Dazu wurden diverse Einflussfaktoren auf die Effizienz der Rückgewinnung identifiziert und im Rahmen von zwei Versuchsreihen im Labormaßstab sowie im technischen Maßstab auf deren Einflüsse hin getestet. Der Fokus lag dabei auf verschiedenen Zuschlagstoffen, die sowohl die Schmelztemperatur, als auch die Viskosität der Schlacke beeinflussen. Damit kann einerseits der Energieaufwand reduziert und andererseits die Wertmetallausbeute erhöht werden. Um die Arbeit zu unterstützen, wurden die vorliegenden Phasen der Wertmetalle im Rasterelektronenmikroskop bestimmt.

Der zweite Teil der Diplomarbeit ist eine wirtschaftliche Evaluierung einer simulierten Anlage im Industriemaßstab. Aufgrund der noch nicht im Großmaßstab etablierten Technik, werden drei Szenarien mit jeweils zwei unterschiedlichen Ausgangsschlacken zur Berechnung herangezogen. Die für die Evaluierung notwendigen Daten stammen aus den zuvor durchgeführten Kleinversuchen, aus einer errechneten Energiebilanz und werden durch diverse dokumentierte Annahmen, die sich an bereits bestehenden Anlagen orientieren, ergänzt. Die zu erwartenden Investitionskosten, Betriebskosten und Betriebserlöse werden für alle Szenarien berechnet und in dieser Arbeit präsentiert. Zur Berechnung der Gesamtwirtschaftlichkeit wird die diskontierte Kapitalwertmethode eingesetzt. Neben der technischen Optimierung des Prozesses ist die Abschätzung von Rentabilitätskennzahlen somit das zweite Ziel dieser Diplomarbeit.

# Table of Contents

# 1 Introduction

Over the last years there was a continuous increase in lead production and lead usage (see also section 2). The main driver for this development is the globally growing automotive industry which uses lead in their lead-acid batteries. The generated slag of the production process is landfilled for the most part, which leads to an increasing demand of landfill sites and high disposal costs. According to the US Geological Survey, published by the US Department of the interior the lead reserves economically extractable to recent prices are used up in the next two decades. Those facts express the need for a more sustainable usage of the metal and higher recycling rates. [1; 2]

The growing legal requirements concerning landfilling, especially towards limiting values for heavy metal contents in disposables is one of the major reasons to comprehensively introduce lead slag recycling throughout Europe. The European Commission puts great efforts into gaining more independence of the large mineral exporting countries by changing the legislation towards a circular economy and a “zero-waste” society. In July 2014 the commission adopted a legislative proposal to review recycling and other waste-related targets. One of the goals is to phase out landfilling for all recyclable metals in 2025, corresponding to a maximum landfilling rate of 25 %. Those goals will pose major challenges for industrial companies. [3; 4]

To comply with all those requirements and future challenges the lead bath recycling process is a well suited option among others. It is a recycling process, which enables the simultaneous recovery of different valuables like zinc, lead and silver in a Top Blown Rotary Converter. This thesis deals with different options to optimize this recycling process. Additionally to theoretical considerations two different trial series were performed to investigate the influence of different fluxes on the recovery rate of the metals.

Experience shows that a process only asserts itself if it can be run profitable or at least cost-covering. An economic calculation is included in the thesis to assess whether a lead bath recycling process could be operated profitable or not. It covers all estimated capital expenditures, operational expenditures and expected revenues. Due to the many uncertainties a new process set up entails, three scenarios (realistic case, best expected case and worst expected case) were developed to comply with those difficult predictions.

# 2 Lead production and usage worldwide

This section deals with the quantities of lead production and recycling worldwide. It gives an overview of the present situation and currently developing trends. It provides data of the global distribution of primary and secondary lead smelters. Furthermore, it presents and describes the shares of different production methods in primary- and secondary production processes.

## 2.1 Primary Production

The world output of refined lead has been significantly increased over the last decade. In 2012, the overall production capacity amounted approximately 10.5 million tonnes. The main application for lead nowadays is the usage in lead-acid batteries of passenger vehicles with almost 80 %. Therefore, the lead industry is highly dependent on the automotive industry. Due to the unbroken sales increase of cars every year, the annual lead production was growing by more than 50 % over the last 9 years and this trend is still expected to continue. The biggest rate of growth can be found in the Eastern countries like China. [1; 5]

The World Directory 2006 of the International Lead and Zinc Study Group counted 243 plants, including 61 primary smelters and refineries and 182 secondary plants, spread in over 57 countries all over the world. It can be assumed that the number of plants has risen over the last 10 years, since the quantity of production increased as well. [6]

In 2004 primary smelting capacity was about 4,000,000 t, spread among 26 countries. As indicated in Figure 2.1 Asia is by far the largest primary lead producer followed by Europe. All the other continents (Africa, America and Oceania) combined represent a share of just over a quarter. The largest producing country is China, which is responsible for 28.8 % of the worldwide primary capacity [6] .

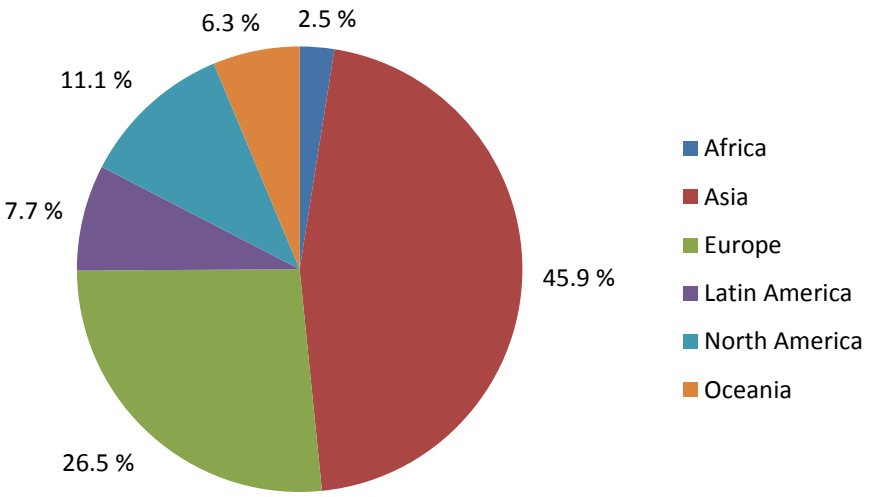


Figure 2.1: The distribution of primary lead production per continent

Figure 2.2 shows the relative importance of the main smelting technologies. Two of them are described in detail in section 3.1.1 and 3.1.2. It can be seen that almost half of the capacity or nearly 2,000,000 of the primary lead is produced by the conventional Blast Furnace. Imperial Smelting Furnaces are used in six countries and have an overall capacity of approximately 320,000 tonnes or 8.2 % of the total. Only three of the 61 primary smelters are designed as QSL reactors having almost the same production quantity. The two Kivcet plants in Canada and Italy produce 220,000 tonnes or 5.6 %. The remaining share consists of less widespread processes like Ausmelt, ISA, or TBRC. [6]

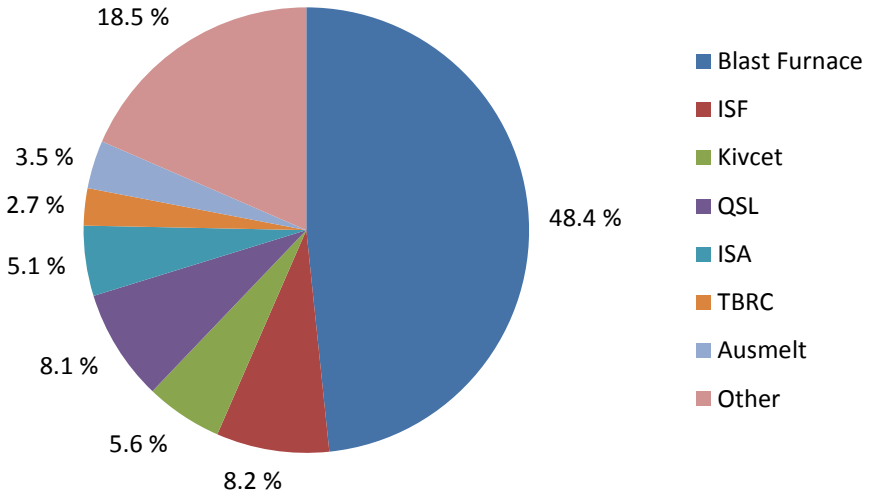


Figure 2.2: The shares of different primary production processes

## 2.2 Secondary Plants

There are approximately three times as many secondary smelters compared to the number of primary plants. The World Directory 2006 lists 182 units in 51 countries throughout the world. Only a few years ago, well developed secondary lead industries operated mainly in the older industrialised countries of Europe, the United States and Japan. Over the last decade many plants have now been established in a wider range of countries, including many developing countries in Asia. As shown in Figure 2.3 the distribution of secondary refining capacities by continent differs considerably from the proportions in primary plants. Especially Northern America has a much larger share in secondary refining, while Africa, Latin America, Asia and Oceania have a smaller one. In Europe the proportion of secondary lead productions is also higher than the primary one. [6]

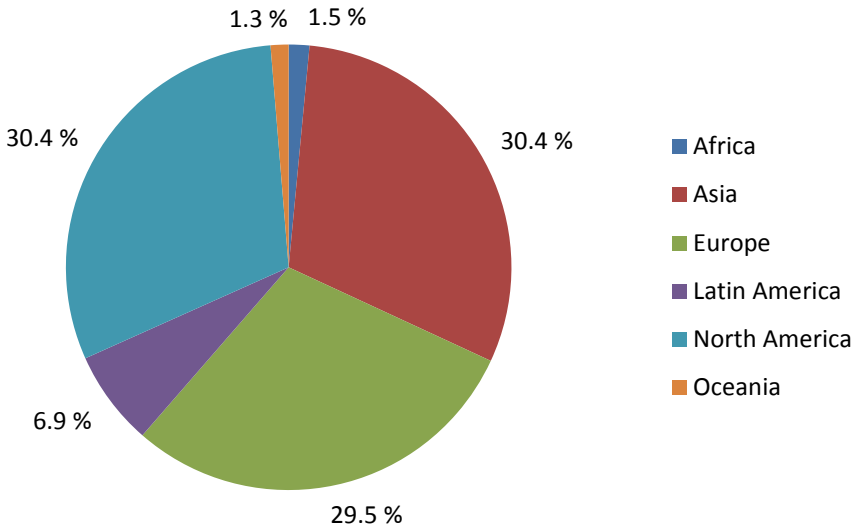


Figure 2.3: The distribution of secondary production quantities per continent [6]

The most common secondary production process is by far the Rotary Reverberatory Furnace in almost all countries. Exceptions to this statement are the countries of Europe, Japan and the United States, where Blast Furnaces or combinations of Blast Furnace and Stationary Reverberatory Furnace are widely used. [6]

# 3 Lead slag recycling

This chapter is dedicated to the two main primary lead production processes where slag is generated and to the procedure of the “lead bath recycling process” in order to recover the maximum amount of valuables out of the slag. The chapter also deals with the characterisation of the investigated residue. Additionally the most important parameters that influence the functionality and efficiency of the process, such as the recovery rate, are introduced in this section.

## 3.1 Primary production processes

As illustrated in Figure 2.2 in section 2.1 the two major production processes are the conventional Blast Furnace and the ISF process. Those two processes are described in this section in order to characterise and fully comprehend the main raw material of the lead bath recycling process. [6]

The most common raw material for primary lead production is sulfidic lead concentrate, which usually contains an average of 50-60 % lead. Oxide lead concentrates are of secondary importance. Prior to the smelting process, the beneficiation takes place. It includes crushing, dense-medium separation, grinding, froth flotation and drying of the concentrate. [3; 7]

### 3.1.1 Conventional Blast Furnace process

The conventional and major process route for the production of primary lead is the sinter oxidation and the subsequent Blast Furnace reduction. The objective of sintering lead concentrates is to produce lump agglomerate of adequate strength combined with porosity for the following reduction in the Blast Furnace. The net reaction of the sinter roasting process is listed in Equation 3.1 underneath. The sulphur from the galena and the accompanying iron, zinc and copper (not shown in the reaction equations) is removed by oxidation and the mineral is converted into an oxide. When common sintering conditions are used, the oxidation starts with the formation of lead sulfate, which reacts with lead sulphide, to increasingly basic sulfates and finally to lead monoxide. Beside the general roasting reaction, several side reactions shown in Equation 3.2-3.4, take place. [7–9]

$$2\,PbS + 3O_2 \leftrightarrow 2\,PbO + 2\,SO_2$$ Equation 3.1

Further possible reactions are:

$$PbS + 2\,PbO \leftrightarrow 3\,Pb + 2\,SO_2 \qquad \text{Equation 3.2}$$

$$PbS + PbSO_4 \leftrightarrow 3\,Pb + 2\,SO_2 \qquad \text{Equation 3.3}$$

$$PbSO_4 + PbS + O_2 \leftrightarrow 2\,PbO + 2\,SO_2 \qquad \text{Equation 3.4}$$

There are two different sinter roasting technologies: the original downdraft sintering, which got replaced by the updraft sintering process. As the names suggest, air is drawn downwards through the charge in the downdraft process, and in the updraft process the air flows upwards through the sinter bed. The changeover of the technology took place because of occuring problems in the original process. The off-gases contain only 1-2 % of sulfur dioxide, which is not enough to produce sulphuric acid in an economic way and too much to be discharged into the atmosphere. [7]

In the improved updraft process the cold air flows into the sinter bed from below. This guarantees that any metallic lead that forms, is cooled down immediately and it solidifies in the sinter bed. This effect ensures a good permeability of the bed, uniform sintering and a lower gas flow, which furthermore leads to higher sulphure dioxide levels. [7]

To achieve the highest possible lead oxide rate while sintering, a temperature beetween 950 °C and 1200 °C and the correct amount of oxygen and sulphur dioxide is necessary. The Pb-S-O system was investigated by Kellogg and Basu and can be seen in Figure 3.1 underneath. [7]

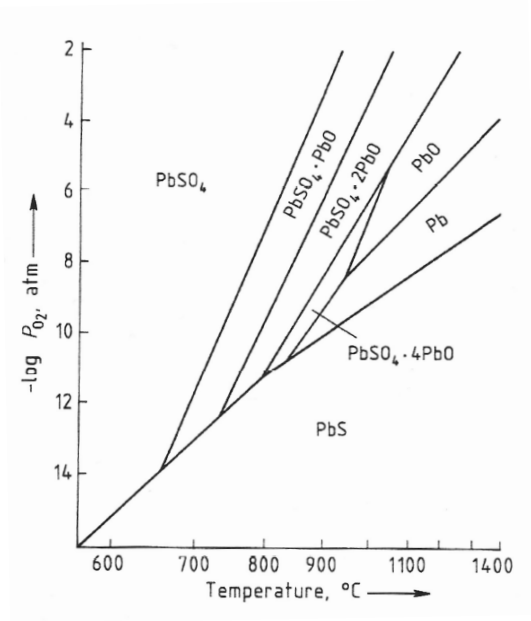


Figure 3.1: Phase diagram of the Pb-S-O system at constant partial sulphur dioxide pressure of 0.2 atm [7]

The second part of the conventional lead production process is carried out in a Blast Furnace. The main function of the furnace is the carbothermic reduction of lead oxide to metallic lead. Additionally other metals such as copper, antimony, arsenic and some noble metals are also produced. All the other constituents (gangues) contained in the sinter are carried off as silicate slag. In contrast to the Imperial Smelting process (see chapter 3.1.2), zinc remains in the slag and cannot be extracted. [7]

The charge to the lead Blast Furnace consists of the following materials:

1. Sinter, which contains the roasted agglomerated concentrate, with fluxes
2. Other oxygen-containing lead materials such as oxides and silicates
3. As reducing agent and energy source, metallurgical lump coke is used

The lead Blast Furnace is a countercurrent reactor. The charge, consisting of sinter, coke and fluxes moves through the vertical shaft from the top to the bottom in countercurrent to the ascending gas flow. Lead Blast Furnaces are classified in two main groups: the round furnaces (Mushroom Furnaces) and the rectangular furnaces (Rachette Furnace). Whereby the second type is the standard one. The typical Rachette Furnace is 6-10 m high (5-8.5 m above the tuyeres) and often has rounded corners. The Chair-Jacket Furnace is a modification of the Rachette design and has two rows of tuyeres. This modification enables a larger width of up to 3.6 m, compared to 1.5 m in the original design. [7; 8]

At the bottom of the furnace is the furnace crucible, which collects the liquid reaction products. Additionally to the lead monoxide reduction all the accompanying elements (such as copper, arsenic, tin, antimony, bismuth) are reduced as well and dissolve together with the noble metals (such as silver and gold) in the liquid lead bullion. When the Blast Furnace is tapped molten metal and hot slag are drawn from the Blast Furnace together and separated from each other. [7]

The tuyere zone is located right above the crucible. This zone is also called combustion zone and blast air enters the furnace through the tuyeres. An enrichment of the blast air with oxygen leads to many positive effects such as a higher combustion temperature, a higher troughput and a reduction of coke demand. On the other hand oxygen enriched air also leads to a higher lead fraction in the slag and a higher zinc fraction in the flue dust, which is of course undesireable. [7; 8]

On top of the tuyere zone is the melting zone with temperatures around 1150 °C and the reduction zone reaching temperatures of approximately 900 °C. Before the descending charge descends trough those two layers, it has to pass the preheating zone at a temperature of roughly 200 °C. The cold sintered material is charged into the mostly open furnace top alternately with the coke. The quantity of the coke is supposed to be between

9-10 wt.-% of the sinter, in order to have the right intensity of the reducing effect. If the quantity of coke exceeds this amount, the temperature rises and zinc oxide of the slag gets reduced to zinc, causing unwanted zinc circulation in the Blast Furnace. [7; 8]

The products of the lead Blast Furnace are:

1. **Lead bullion**, which must be further refined and accompanying elements like copper, arsenic, tin, antimony, silver, gold, zinc, bismuth and other alkali and alkaline-earth metals need to be removed, in order to get pure metallic lead.
2. **Slag**, which contains iron oxide, aluminium oxide, lime, silica, zinc, silver and other oxides. Depending on the composition of the slag it may pay off to be used for further processing.
3. **Flue dust and baghouse dust,** consisting of fumes and dust particles. Often cadmium tends to accumulate in the top gas dust.
4. **Top gas**, is usually discharged into the atmosphere. The small amount of carbon monoxide (3-4 %) is usually not used for further processing and the low temperature of the top gas is too cold for practical heat recovery.
5. **Matte**, is only formed when the burden contains enough sulphur. It is a sulfidic product of Blast Furnace smelting. Usually the charge does not contain too much copper or sulphur, so that matte phase formation can be avoided and the remaining copper remains dissolved in the lead bullion or in the slag.
6. **Speiss**, is only formed when the burden contains very large amounts of arsenic, nickel, cobalt or antimony and cannot be taken up by the matte.

The composition of the two most important products of the lead Blast Furnace is shown in Table 3.1 underneath. [7]

Table 3.1: The chemical composition of the produced lead bullion and the slag [5]

| Lead bullion | | Slag | |
|---|---|---|---|
| Element | [wt.-%] | Compound | [wt.-%] |
| Pb | 92-98 | $SiO_2$ | 20-35 |
| Cu | 0.5-2.5 | FeO | 28-40 |
| Sn | <4 | CaO | 7-25 |
| As | <0.6 | ZnO | 5-22 |
| Sb | <3 | $Al_2O_3$ + MgO | 10 |
| Ag | <1 | | |
| Bi | <0.5 | | |

## 3.1.2 Imperial Smelting Furnace Process

The Imperial Smelting Process (ISF process) is a development out of the coke shaft furnace, which is able to produce crude lead and commercial zinc with a purity of approximately 98.5 %. The goal of the IS process is to prevent the reoxidation of zinc to zinc oxide at the outlet of the furnace. The conventional shaft furnace in a counterflow arrangement shows furnace gas temperatures of approximately 200 °C. In accordance with the Boudouard equilibrium this results in higher $\{CO_2\}$ contents in the top gas. At the Imperial Smelting furnace gas temperatures of 1000 °C are required. To achieve those high temperatures all raw materials and gases are preheated. Therefore, the required heat is generated to a large extent outside the furnace. The used coke and sinter is heated to a temperature over 800 °C and the combustion air is preheated as high as 700-950 °C. The detailed process flow is illustrated in Figure 3.2 below. [10]

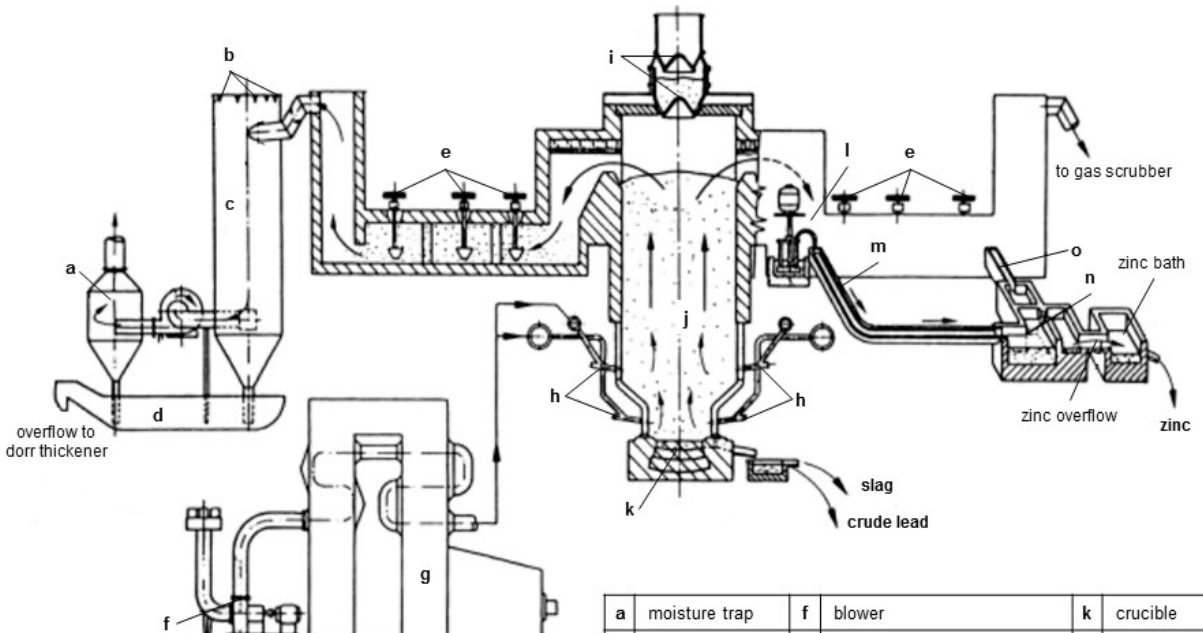


| | | | | | |
|---|---|---|---|---|---|
| **a** | moisture trap | **f** | blower | **k** | crucible |
| **b** | water jets | **g** | air preheater | **l** | lead pump |
| **c** | gas scrubbing | **h** | jets | **m** | condenser |
| **d** | water seal | **i** | feeding vessel hot coke | **n** | cooled weir |
| **e** | stirrers | **j** | furnace | **o** | lead return |

Figure 3.2: Illustration of the Imperial Smelting process [10]

The evaporated zinc gas is collected in a spray condenser, which uses lead at a temperature of approximately 550 °C as a condensing liquid. The solubility of lead is strongly temperature dependent. This effect is used to precipitate the zinc by cooling down the metal to 440 °C, causing the zinc to separate from the lead and float on the surface of the liquid lead stream. It then flows over a weir and gets collected. In practice 400 t of lead are required for every produced tonne of zinc. If the process took place under equilibrium conditions, only 60 t of

lead would be necessary to recover one tonne of zinc. The produced zinc is either used as commercial grade ingots with a purity of 98.5 % or refined to higher grades. [10]

## 3.2 Analysis of the considered slag sample

The residue used in the following trials and investigated in the economic evaluation is a dumped slag out of an Imperial Smelting process. The chemical composition of the slag can be seen in Table 3.2 underneath. The content of valuable metals such as zinc (8.0 %), lead (1.76 %) and silver (0.002 %) is in the expected range of a typical ISF slag. [11]

Table 3.2: Chemical analysis of the examined ISF slag [11]

| Element/ Compound | Concentration by weight [wt.-%] | Analysing Method | Element/ Compound | Concentration by weight [wt.-%] | Analysing Method |
|---|---|---|---|---|---|
| $Fe^{2+}$ | 26.90 | AM_EG.26 | MnO | 1.29 | ISO 11885 |
| $Fe^{3+}$ | 0.90 | calculated | C | 0.13 | ISO 11885 |
| $SiO_2$ | 21.80 | ISO 15350 | Ag | 0.002 | ISO 11885 |
| CaO | 14.00 | ISO 11885 | Cu | 0.50 | ISO 11885 |
| Zn | 8.00 | ISO 11885 | Na | 0.38 | ISO 11885 |
| $Al_2O_3$ | 6.99 | ISO 11885 | Pb | 1.76 | ISO 11885 |
| MgO | 2.07 | ISO 11885 | S | 2.31 | ISO 15350 |

Since many analysed elements, as listed in Table 3.2, exist as oxides, the percentages of the actual chemical compounds were calculated using the molecular weights ratio. After considering the actual structure the percentages by weight add up to 97.35 wt.-%, as seen in Table 3.3.

Table 3.3: Calculation of the actual chemical composition

| Element/ Compound | Concentration by weight [wt.-%] | Element/ Compound | Concentration by weight [wt.-%] |
|---|---|---|---|
| FeO | 34.61 | MnO | 1.29 |
| $Fe_2O_3$ | 1.29 | C | 0.13 |
| $SiO_2$ | 21.80 | Ag | 0.002 |
| CaO | 14.00 | Cu | 0.50 |
| ZnO | 9.96 | $Na_2O$ | 0.51 |
| $Al_2O_3$ | 6.99 | PbO | 1.90 |
| MgO | 2.07 | S | 2.31 |

## 3.3 Characterisation of the slag sample

To characterise a lead slag, one of the options is to calculate the CaO-FeO-$SiO_2$ ratio by weight and draw the result in a ternary system. The most common composition of lead slags

is marked in Figure 3.3 below. All residues, which are pictured with black dots in the red circle have a share of (CaO) between 10-25 wt.-%, an (FeO) content of 35-55 wt.-% and a ($SiO_2$) concentration between 30-45 wt.-%. The investigated slag has a ratio of 20 wt.-% (CaO), 49 wt.-% (FeO) and 31 wt.-% ($SiO_2$) and is marked with a red point within the red circle. As Figure 3.3, suggests the lead slag used in this research, shows a typical CaO-FeO-$SiO_2$ ratio, although it is not the residue of a lead Blast Furnace process. [5; 7]

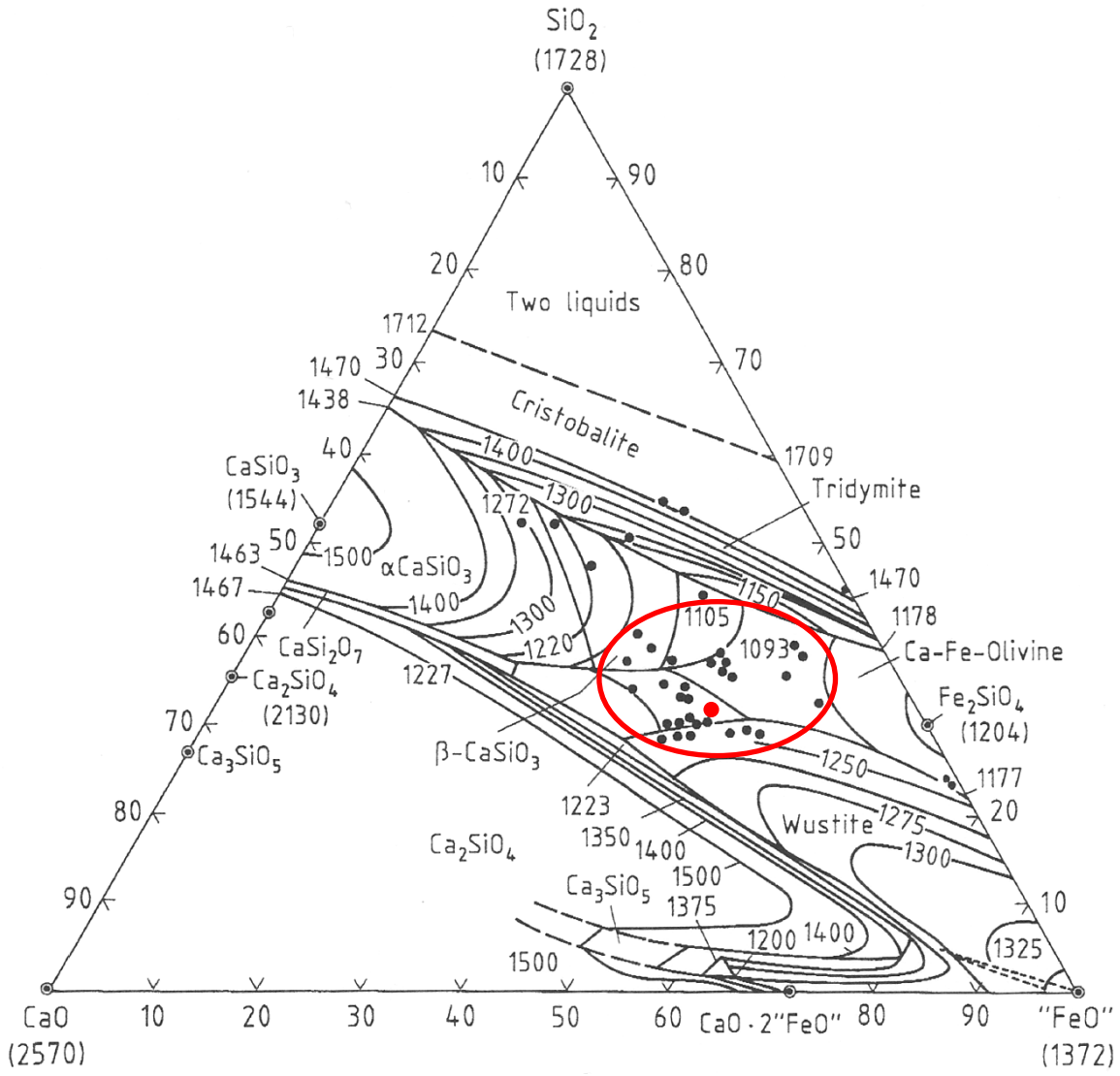


Figure 3.3: : Ternary system, showing compositions of slags from the primary lead production [7]

## 3.4 The lead bath recycling process

The aim of the lead bath recycling process is to recover the valuables like lead, zinc and silver simultaneously from a dumped slag. There are many reasons to change the current situation of depositing the residues on a landfill. Limited resources of primary ore deposits, landfill costs and capacities, increasing regulatory requirements by the legislation and a “greener” image of the companies are some of them. [2; 3]

This process can be operated in different furnaces, like resistance furnaces, Submerged Arc Furnaces (SAF) or Top Blown Rotary Converters (TBRC). A resistance furnace was used for the laboratory scale trials where the industrial scale calculation and economic evaluation were performed using a model of a TBRC. [12]

The first process step is the setup of the lead bath. Solid lead is charged in the furnace where it melts down quickly due to its low melting point with 327.4 °C and the process temperatures between 1200 °C and 1300 °C to guarantee the meltdown of the residue afterwards. The slag is mixed with coke, which serves as reducing agent. Depending on the slag composition and the desired process parameters fluxes like (CaO) or ($SiO_2$) are added as well. The mixture is charged onto the lead bath. [13]

Investigations of previous studies show that the recovery yield of zinc and lead at the Submerged Arc Furnace rises with the process time until 150 minutes, while the recovery rate stops increasing after 75 minutes in the Top Blown Rotary Converter. In this time two main types of reactions take place, which are shown in Figure 3.4. At first, liquid zinc oxide is reduced from the charged residue and the generated zinc evaporates due to the process temperature. The zinc-vapour leaves the furnace through the off-gas system, where it gets post combusted by oxygen or carbon dioxide. The generated zinc oxide is collected in the baghouse filter and represents the first product of the recycling process. The reduction of zinc oxide as well as the oxidation of zinc is shown in the following three equations 3.5, 3.6 and 3.7. [12]

$$ZnO(l) + C \leftrightarrow Zn(g) + CO(g)$$ Equation 3.5

$$2Zn(g) + O_2(g) \leftrightarrow 2ZnO(s)$$ Equation 3.6

$$Zn(g) + CO_2(g) \leftrightarrow ZnO(s) + CO(g)$$ Equation 3.7

At least 80 % of the original zinc oxide content in the slag can be recycled by this process. Unfortunately it is very difficult to introduce a heat recovery system to the off-gas, because zinc oxide tends to attach to surfaces and block the tubes. [12]

The second valuable metal is also reduced by the added carbon, but not evaporated as Equation 3.8 underneath shows. The reduced lead settles to the bottom of the furnace into the original lead bath. [14]

$$PbO(l) + C \leftrightarrow Pb(l) + CO(g)$$ Equation 3.8

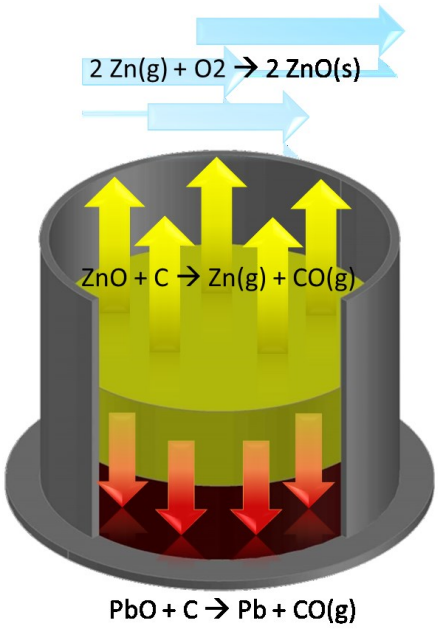


Figure 3.4: Illustration of the chemical reactions in the lead bath recycling process [14]

Usually there is a small freight of silver, copper, antimony, tin or gold in primary lead slags. Especially silver is of particular interest because its content varies between 0.001 wt.-% and 0.1 wt.-% and can add a significant economic benefit to the process. Silver dissolves in lead very well and concentrates in the lead bath at the bottom of the furnace as well. Lead as main phase is chosen because of its function as collector for many relevant metals, its low melting- and high evaporation temperature, the high density and its low heat capacity. The generated lead alloy represents the second product of the lead bath recycling process. [12]

After evaporating zinc and collecting lead and some other metals in the lead bath, a stabilized slag remains, which could be used in construction applications (roads, dykes, etc.) or should at least meet all the requirements for landfill depositing. [12]

## 3.5 Factors of influence on the recovery of valuables

The three most important parameters which influence the efficiency of the pyrometallurgical winning processes are the liquidus temperature, the viscosity of the slag and the solubility of the valuable metals in the slag. The right setup of a recycling process regarding those impact factors can have a tremendous effect on the economic efficiency of the operation. [12]

- Liquidus temperature of the residue

It is self-evident that a lower melting point of the slag reduces the necessary heating energy and reduces the energy intensity of the process. Therefore, mainly ($SiO_2$), alkaline fluxes like ($NaCO_3$), ($Na_2O$), ($K_2O$) or halide substances like ($CaF_2$) are added. A second positive effect

of the alkaline and halide fluxes mentioned above, is their characteristic of reducing the viscosity of the slag. Apart from the positive impacts on the liquidus temperature and the viscosity it needs to be considered that a higher concentration of alkalis and halides reduces the durability of the refractory lining of the furnace and can cause substantial costs. Higher freights of alkalis and halides also influence the quality of the zinc oxide dust and can harm the environment. [12; 15; 16]

- Viscosity of the residue

The material transportation between the metal and the slag as well as the thermal conductivity are highly dependent on the viscosity of the slag. A lower viscosity favours the convective material transport and improves the thermal conductivity. It also enhances the coagulation and separation of the metal droplets from the slag. In addition to the fluxes mentioned in the section above several oxides influence the viscosity in both ways. The Kz-value is linked to the viscosity of the slag and can be calculated with the Equation 3.9 below. [17; 18]

$$Kz = \frac{\%FeO\ (FeO+ZnO+MnO+MgO) + \%CaO}{\%SiO_2+\%Al_2O_3(Al_2O_3+Fe_2O_3)} \qquad \text{Equation 3.9}$$

The Kz-value is indirectly proportional to the viscosity of the slag. Oxides like (FeO), (ZnO), (MnO), (MgO) or (CaO) have a positive effect on the viscosity of the residue, whereas higher contents of ($SiO_2$), ($Al_2O_3$) and ($Fe_2O_3$) increase the viscosity and lower the Kz-value. The correlation between the slag viscosity and the calculated Kz-value can be seen in Figure 3.5. The blue line represents the exponential smoothing of a lead Blast Furnace slag and the red one represents a slag from the copper industry. [17; 18]

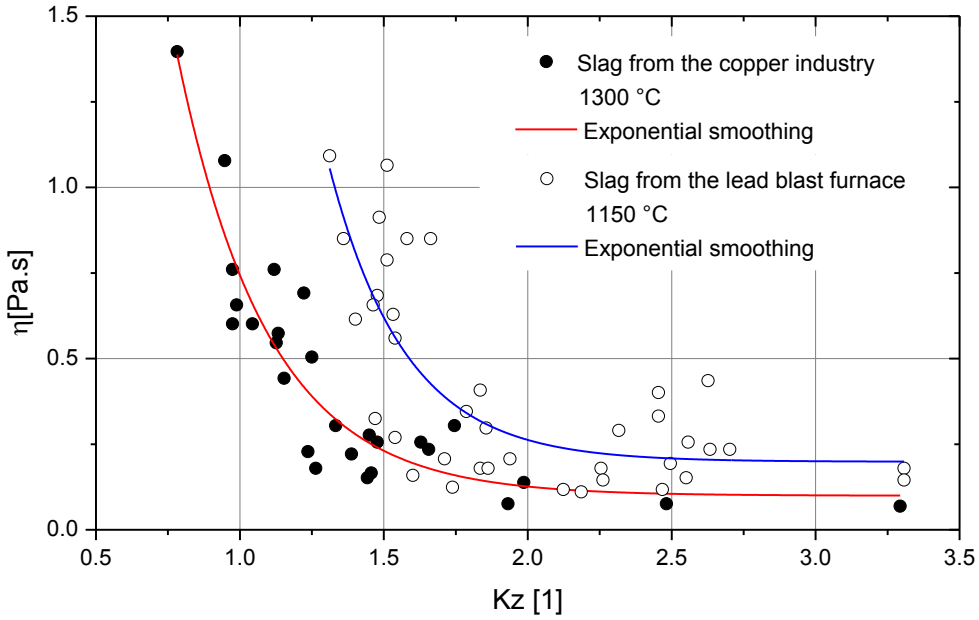


Figure 3.5: Correlation between the viscosity of two slags and their calculated Kz-value [17]

- Solubility of the valuables

The solubility of zinc oxide is described by the Law of Henry, which can be seen in Equation 3.10 underneath. It shows the dependency on the molar concentration and the activity coefficient $\gamma_{ZnO}$, which is related to the concentration of other slag components like (CaO), ($SiO_2$) and ($Al_2O_3$). [17; 18]

$$a_{ZnO}{}^{H} = \gamma_{ZnO}{}^{H} \cdot x_{ZnO}{}^{H} \qquad \text{Equation 3.10}$$

A high activity coefficient indicates a higher separation of (ZnO) from the slag and therefore an increased recovery yield of the valuable metal. [17]

A good summary of the advantages and disadvantages is shown in Figure 3.6 below. It illustrates the dependency of various slag properties of the ($SiO_2$)/(Fe) and ($SiO_2$)/(CaO) ratio. The diagram plots the ($SiO_2$)/(Fe) ratio on the vertical axis and the ($SiO_2$)/(CaO) ratio on the horizontal axis. It is split into four main parts. The characteristic properties for every quarter of the diagram were assigned. [19]

In general ($SiO_2$) and (Fe) are inexpensive fluxes, so the bottom half provides the lowest flux costs. Comparing the zones of different melting points of Figure 3.3 and the plotted ratios of Figure 3.6 it can be seen that a higher ($SiO_2$)/(CaO) ratio goes hand in hand with a lower melting point.[19]

As seen in Equation 3.9, (CaO) and (FeO) contribute to a low viscosity, whereas a higher ($SiO_2$) content shifts the equilibrium towards a higher viscosity. Therefore the upper right

quarter exhibits the highest viscosity, whereas the bottom left quarter shows the lowest possible viscosity. [19]

A lower $(SiO_2)/(CaO)$ ratio influences the lead settling rate as well as the zinc fuming rate in a positive way, due to the fact that higher amounts of (CaO) increase the reducibility of lead and lower the viscosity of the slag, which again influences the zinc evaporation in a favourable way. [19]

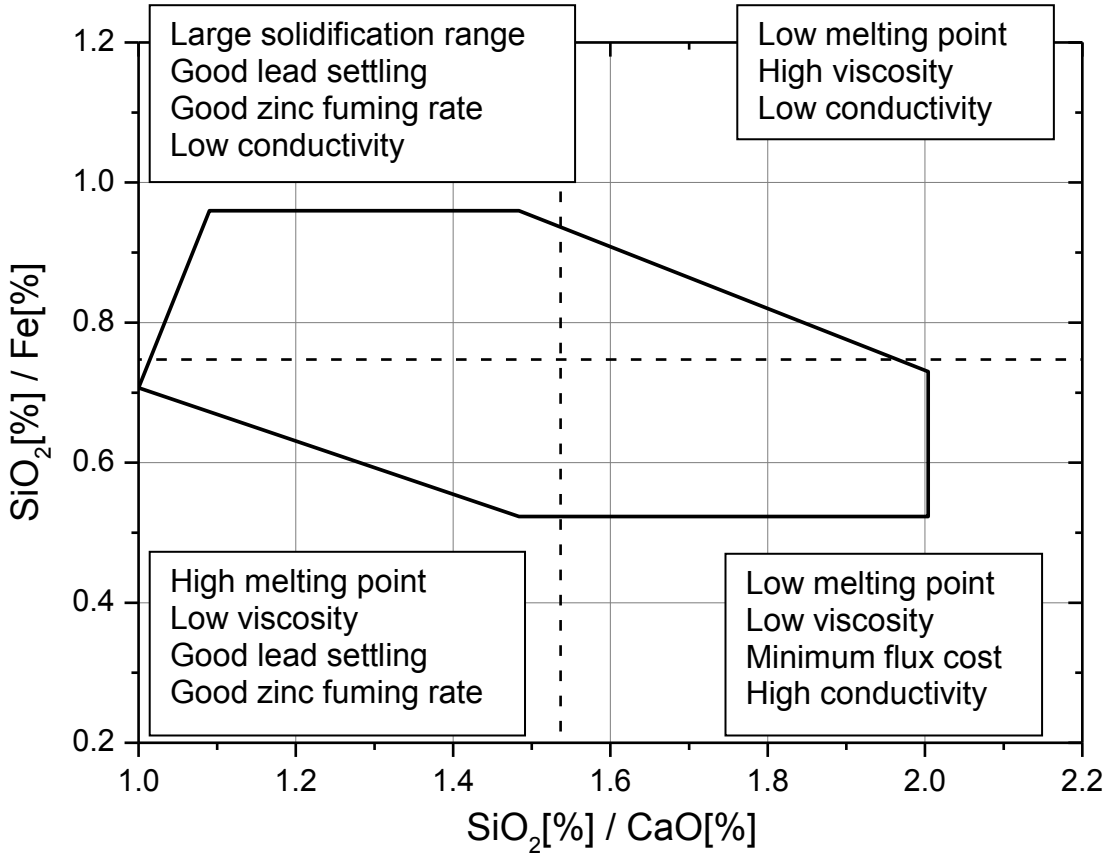


Figure 3.6: Influence of different slag properties on two flux ratios [2]

# 4 Trials in the hot stage microscope

The aim of the trials in the hot stage microscope was the determination of various melting temperatures in the ternary CaO-$SiO_2$-FeO system. The melting temperature zones pictured in Figure 3.3 are only valid for pure mixtures of those three chemical compounds. Other accompanying elements and compounds like (ZnO) or (PbO) have a strong influence on the melting point of the actual slag. As the melting temperature of the residue is of particular significance for the technical process parameters and the economic efficiency, the determination of it is of great importance. It was expected to find the lowest melting point zone around the composition of the investigated slag.

## 4.1 Schematic construction and functionality

The hot stage microscope as seen in Figure 4.1 underneath consists of a heating unit, a lamp and a camera. The test equipment is linked to a computer, which performs a software analysis of the investigated sample. The current temperature of the sample is measured by a thermocouple, on which the sample is placed. Furthermore, an integrated water cooling system and a power supply unit are necessary to run the hot stage microscope.

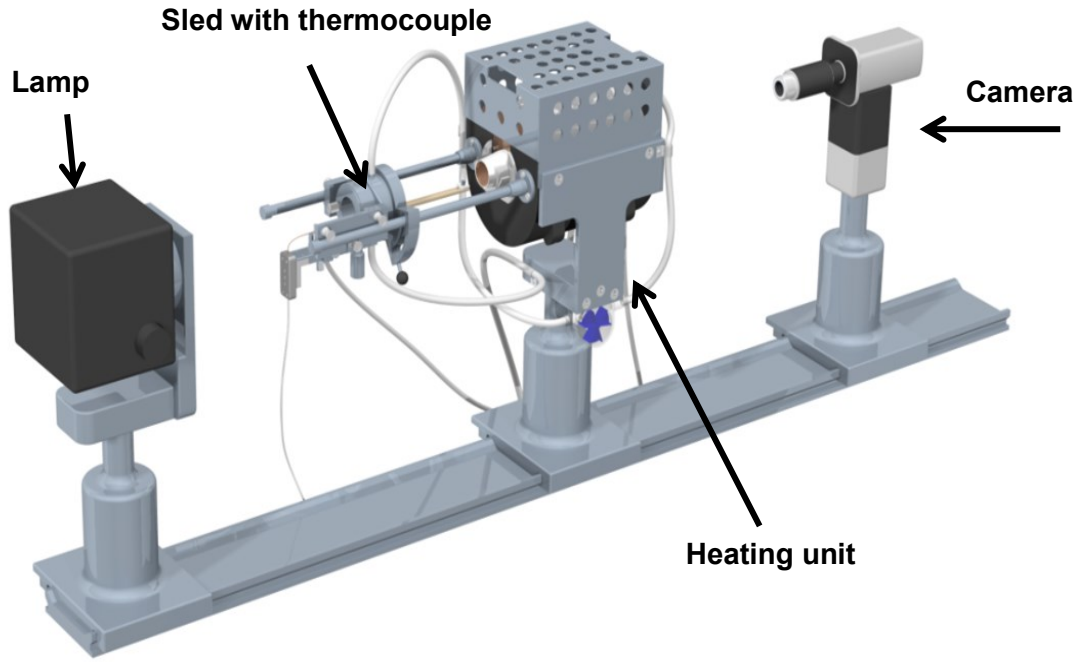


Figure 4.1: Layout of the used hot stage microscope [14]

The camera captures the shadow of the cylindrical sample at given time or temperature intervals, and the computer records all the provided pictures and data. The temperature gradient can be set by the user. The end result of a trial in the hot stage microscope is a high number of pictures of the sample over the entire temperature range, which can be converted to a video as well. An example of three pictures at characteristic sample temperatures can be seen in Figure 4.2.

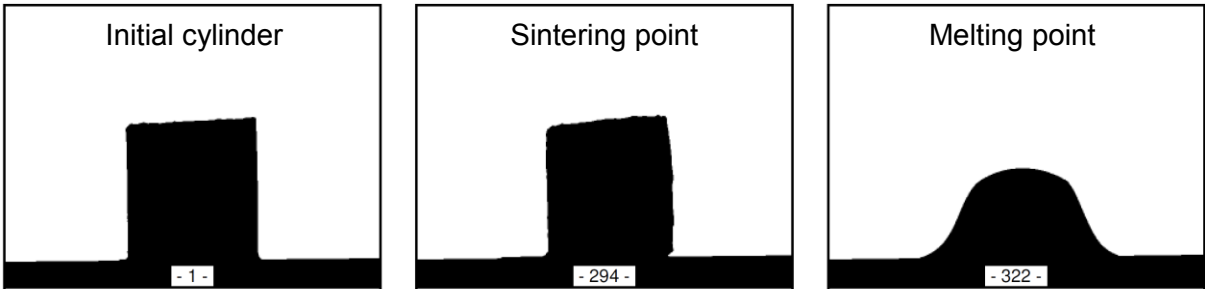


Figure 4.2: Illustration of the sample shape at three characteristic temperatures

Additionally the software records data of the sample like area, corner angles, form factors or the wetting angle. Especially diagrams, which plot the recorded area against the measured temperature have a high significance for the determination of the solidus- and liquidus temperature.

## 4.2 Methodology

To determine the “low-melting zone” in the ternary system, which is shown in Figure 4.3 below a systematic approach was chosen. As one can see an evenly distributed grid with 36 intersections was drawn into the ternary system. Each point represents a different CaO-$SiO_2$-FeO ratio.

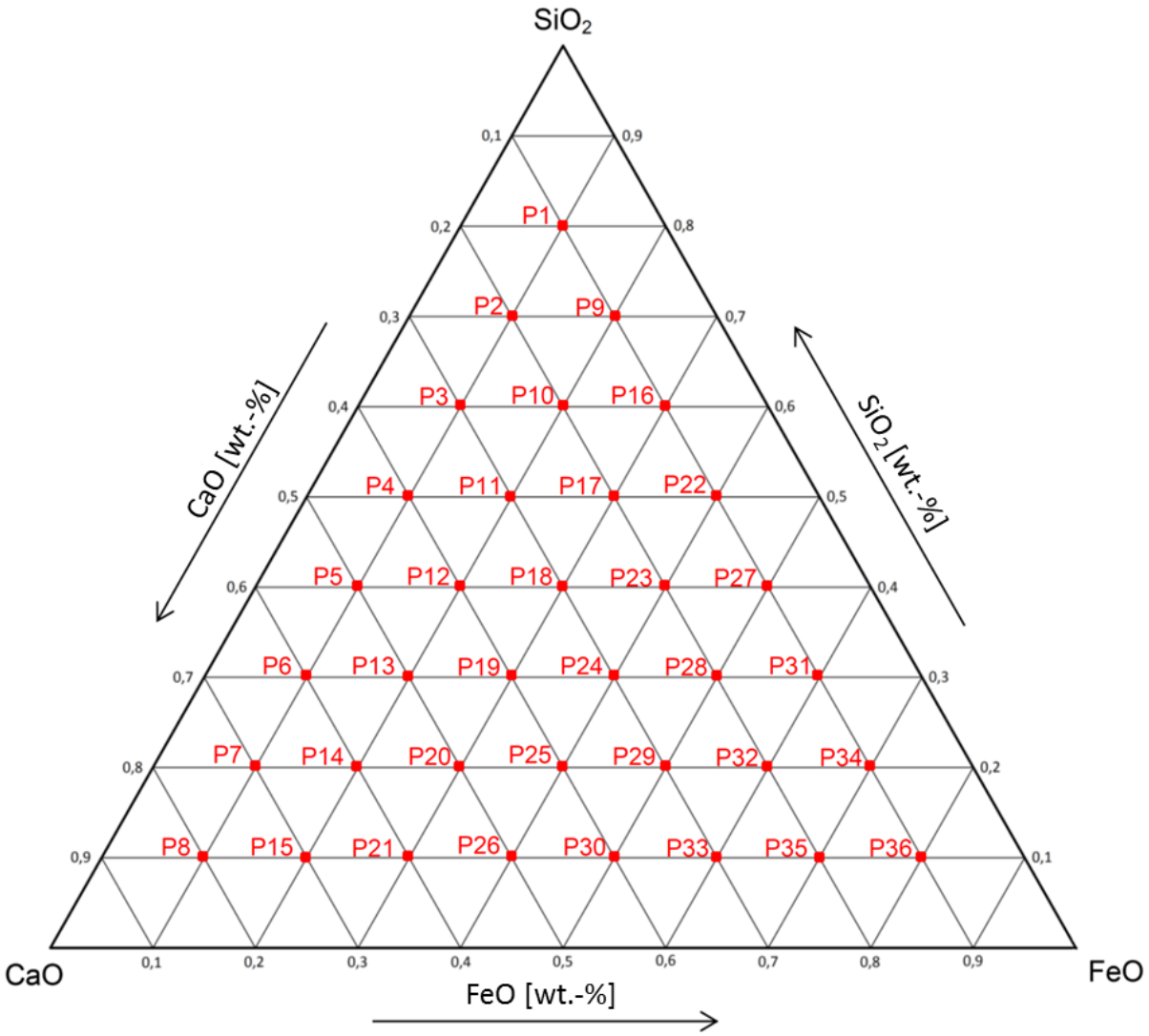


Figure 4.3: Distribution of the tested mixtures in the ternary system

To produce the demanded mixtures P1-P36 the additives lime (CaO), quartz sand ($SiO_2$) and hematite ($Fe_2O_3$) were added to the existing ISF-slag. Trivalent iron oxide had to be used, because of the instability of bivalent iron oxide (FeO) in regular ambient conditions. The weighed in mixtures were grinded together for two minutes in a mill to guarantee a homogenous mixture. The added quantities of the supplements can be seen in the following Table 9.1 in the appendix.

## 4.3 Preparation of the samples and trial procedure

The grinded and mixed powder is carefully added into a cylindric mould, which can be seen in Figure 4.4 below. The sample is then shaped with a special device to compact it. Afterwards the layers of the mould are twisted to enable the user to push the compacted cylinder onto the small platinum plate.

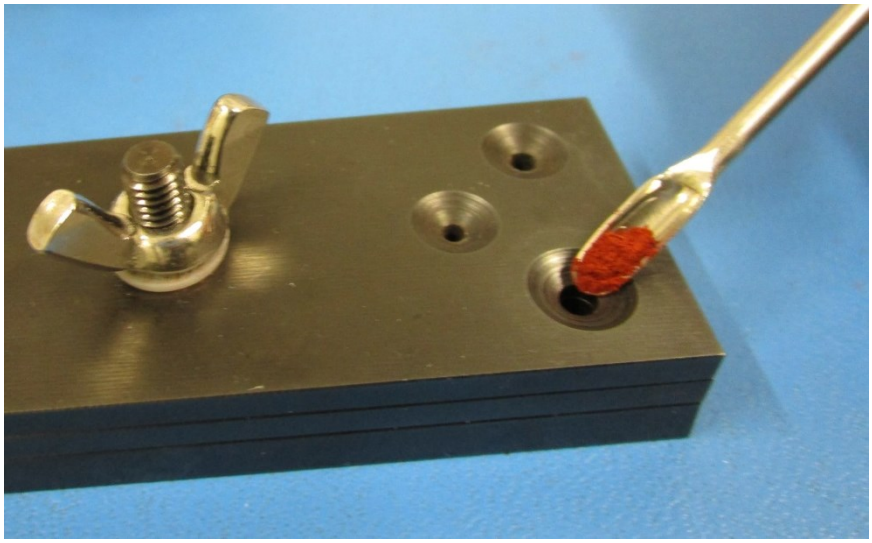

Figure 4.4: A photo showing a sample next to the cylindric mould

This plate is positioned on the thermocouple, which can be moved into the heating unit with the help of the existing sled.

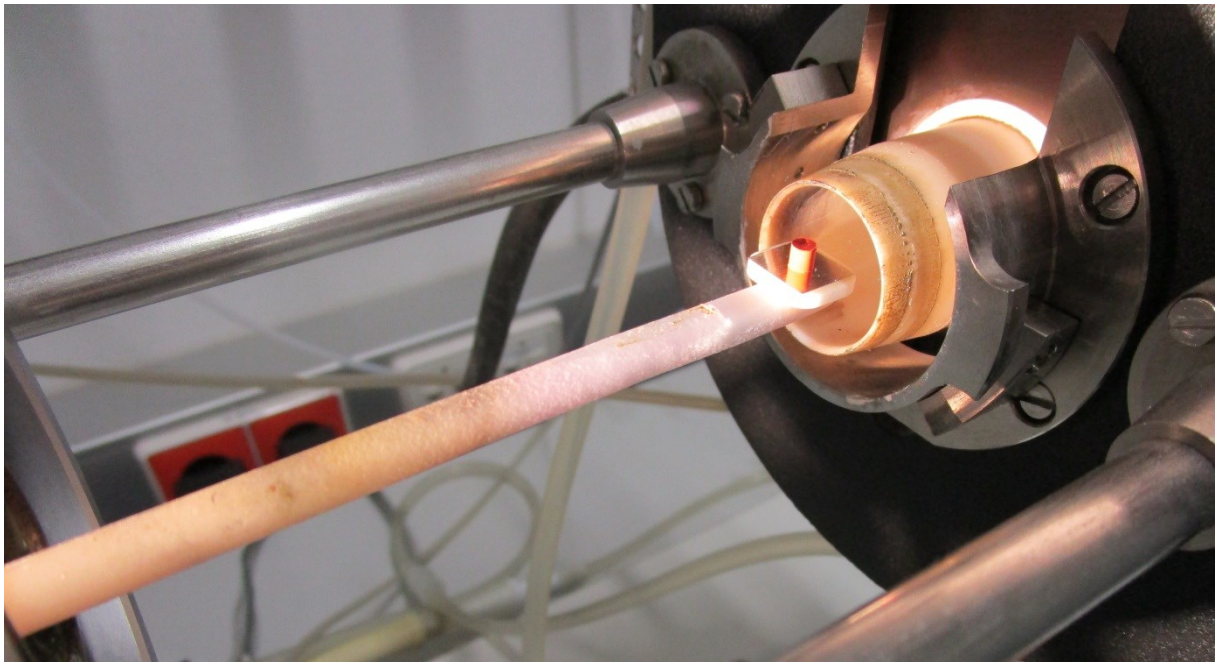

Figure 4.5: The compressed cylindric sample is placed on the thermocouple before getting pushed into the heating unit

## 4.4 Results

This section covers the results of the trials in the hot stage microscope. Shrinkage curves are a very useful tool to determine the liquidus- and solidus temperature. These curves plot the measured area of the sample against the temperature which is continuously increased by the heating unit. 37 of these samples were examined using the described method and due to the large number of samples only a small selection, of three typical shrinkage curves is published in this section of the thesis. The complete set of diagrams and the related description is published in the appendix of this thesis in section 9.

A very simple case of a shrinkage curve is shown in Figure 4.6. The measured area of the sample stays almost constant until the temperature of 700 °C, where the area slightly increases. At a temperature of approximately 1150 °C the area starts to decrease fast and steady until the sample is completely liquefied at just below 1400 °C and only around 25 % of the original area is remaining.

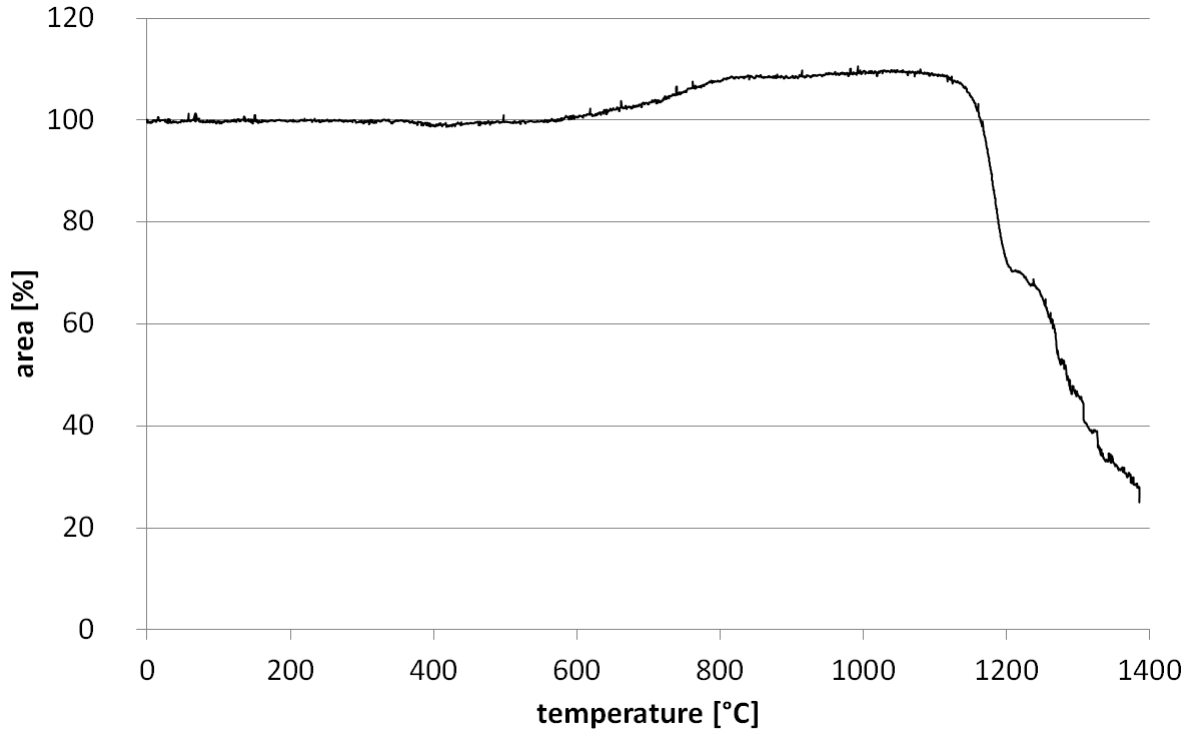


Figure 4.6: Shrinkage curve of sample P29

The taken pictures of the same sample at different temperatures are shown in Figure 4.7. The area is continuously decreasing without any bubble formation or signs of degasification.

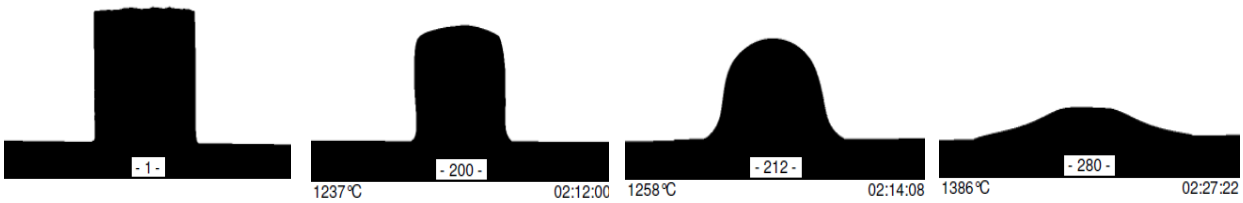


Figure 4.7: Recorded pictures of sample P29 at different temperatures in the hot stage microscope

In some cases the sample showed intense signs of degassing. This phenomenon is expressed in a large increase of the measured area of the samples after starting to melt down. A good example of intense degasification can be seen in Figure 4.8 below. The measured area of the sample is pretty constant at the beginning, before it starts to decrease at the approximate temperature of 1100 °C. In contrary to sample P29 the area is not continuously decreasing to the point of complete liquefaction, but it starts increasing again and due to intense bubble formation it reaches almost 180 % of the original area. A list of all samples showing degassing behaviour can be seen in Table 4.1 further below.

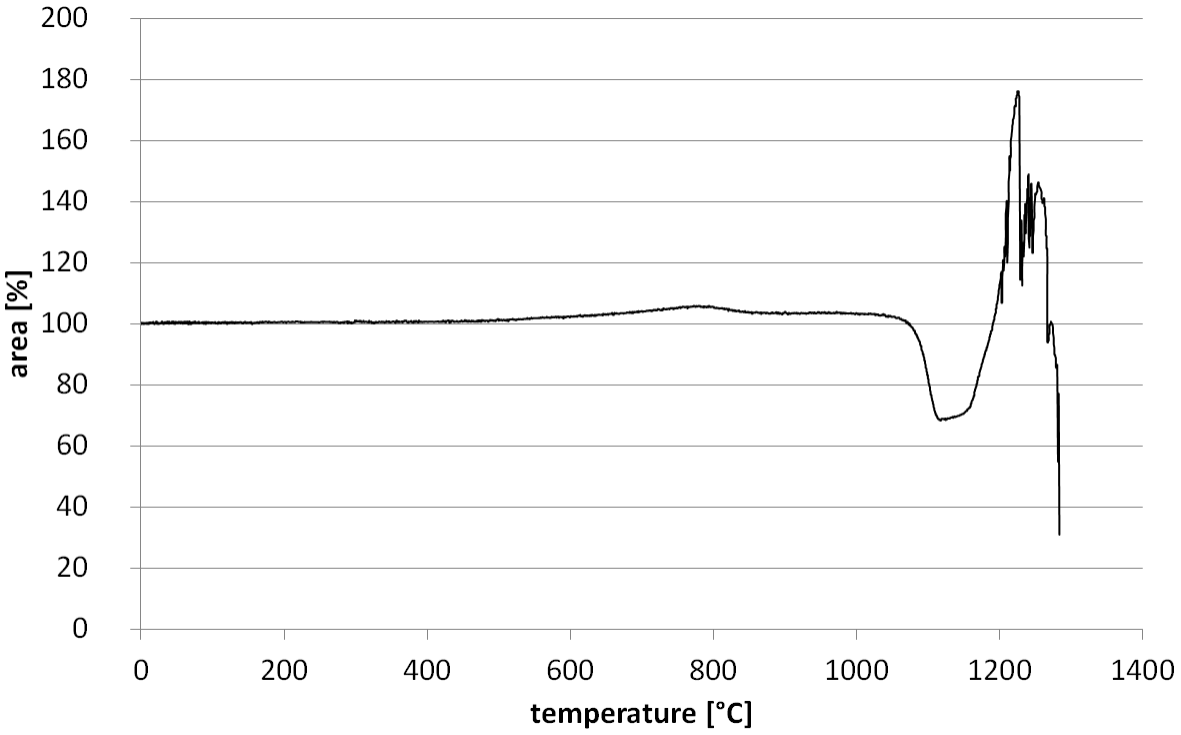


Figure 4.8: Shrinkage curve of sample P22 showing intense degassing behaviour

The taken pictures, as published in Figure 4.9 show the strong increase of the area, especially in the third picture at 1225 °C.

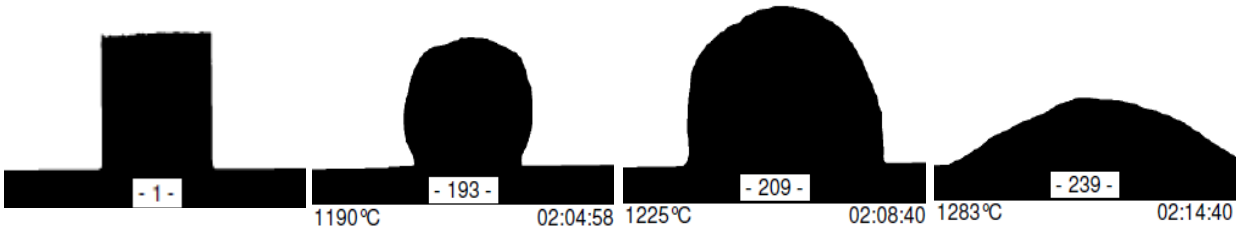


Figure 4.9: Recorded pictures of sample P22, showing intense degassing behaviour

The third common case is shown in Figure 4.10 underneath. The area of the sample remains constant over a long period before the first drop occurs. After this drop, the measured area stays constant for around 150 °C again, followed by a short peak, which doesn't always occur. After the peak the sample melts down continuously until the final state is reached.

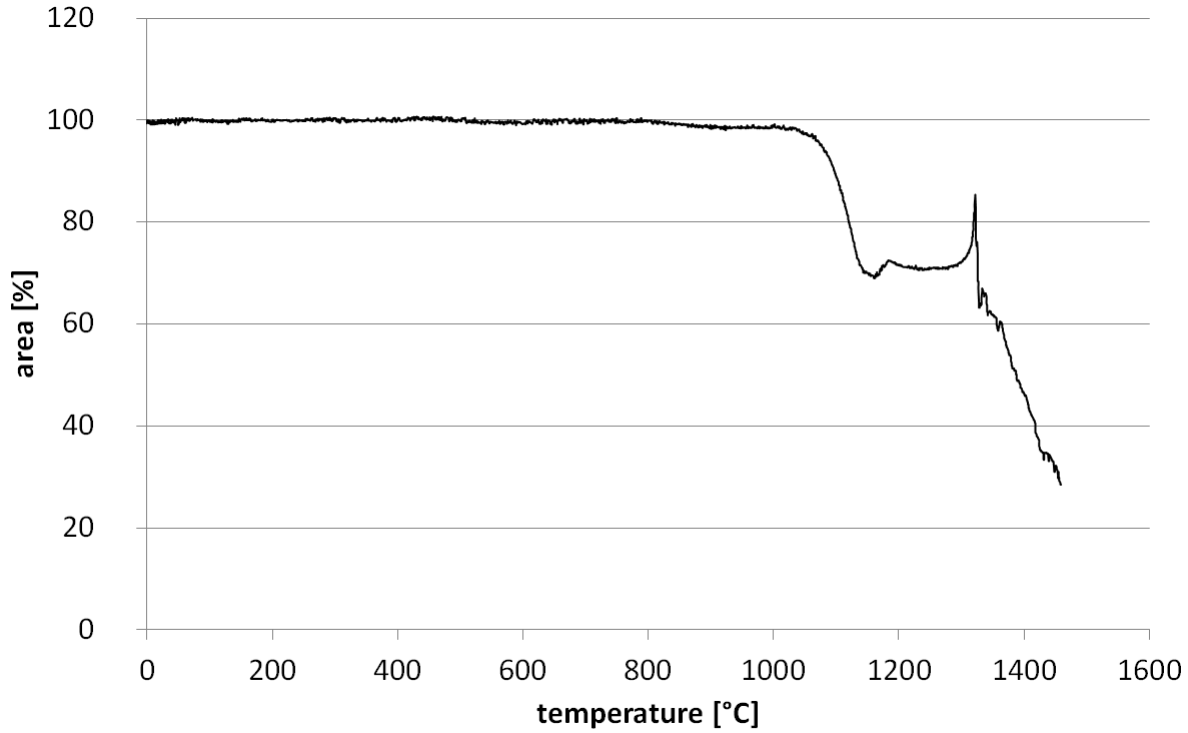


Figure 4.10: Shrinkage curve of the sample P0

This divided decrease in area, as seen in Figure 4.10 often occurs in combination with phase separation. Figure 4.11 below shows an example of a sample after the cooling phase of the trial. It can clearly be seen, that at some point during the trial the phases separated and that the material is inhomogeneous as the colours of the sample changes from the outside to the inside.

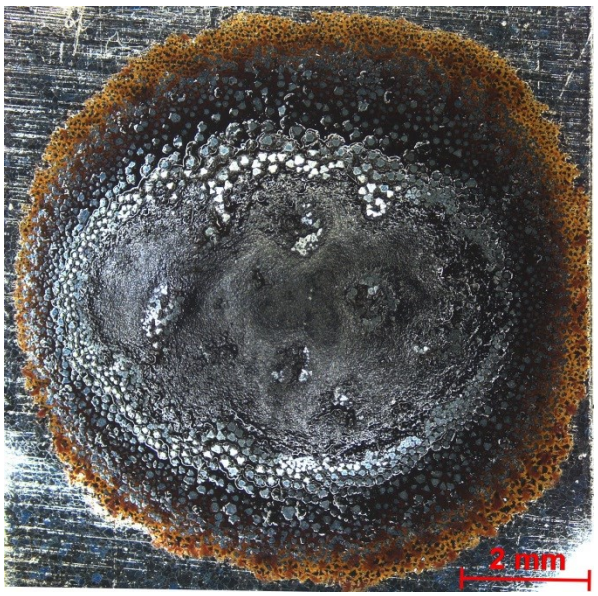


Figure 4.11: Observed phase separation after the trial at sample P0

In contrast to the occurring phase separation of Figure 4.11 most samples remain homogeneous during the trial period and no differences in colour are noticeable. Sample P12 is an example of a homogenous specimen with no phase segregation.

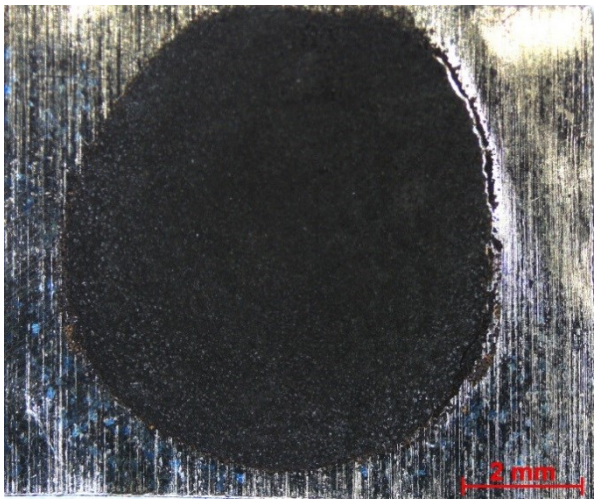


Figure 4.12: Sample P12 after the trial, as an example of a homogeneous sample

As published in the shrinkage curves before, it is not always trivial to define a precise melting temperature. In many samples a significant decrease in area was followed by a longer temperature interval of constant area, before a second drop in area was observed. Also the samples with degassing behaviour are not easy to classify in terms of an exact melting point. This effort to determine the melting points of all mixtures used additional data in the form of the generated pictures. For every sample there are between 260-800 photos of the cylinder. The recorded data and the related shrinking curves can be found in chapter 9 of this thesis. The big amount of generated data adds up to more than 1,200 pages with 24 photos each.

Despite those difficulties, the following Table 4.1 summarizes the melting- and sintering temperatures of all measured samples. The software analysis automatically recognizes the decrease in area, the rounded edges and calculates the sintering temperature. Additionally the collected samples were analysed, if there was any sign of separation or degasification.

Table 4.1: Results of all 37 samples including sintering- and melting temperature as well as degasification and phase separation

| Sample | Sintering temperature [°C] | Melting temperature [°C] | Separation | Degasification |
|---|---|---|---|---|
| P0 | 1190 | 1300 | x | |
| P1 | 1130 | >1600 | | |
| P2 | 1148 | 1540 | | |
| P3 | 1175 | 1220 | x | |
| P4 | 1170 | 1300 | x | |
| P5 | 1220 | 1280 | | |
| P6 | 1250 | 1320 | | |
| P7 | 1280 | >1600 | | |
| P8 | 1300 | >1600 | | |
| P9 | 1300 | 1540 | x | x |
| P10 | 1120 | 1250 | x | |
| P11 | 1180 | 1200 | | |
| P12 | 1150 | 1220 | | |
| P13 | 1200 | 1250 | | |
| P14 | 1300 | 1400 | | |
| P15 | 1350 | 1550 | | |
| P16 | 1320 | 1350 | x | x |
| P17 | 1120 | 1200 | | |
| P18 | 1150 | 1200 | | |
| P19 | 1150 | 1200 | x | |
| P20 | 1200 | 1270 | | |
| P21 | 1250 | 1370 | | |
| P22 | 1200 | 1270 | | x |
| P23 | 1150 | 1260 | x | x |
| P24 | 1150 | 1200 | | |
| P25 | 1150 | 1250 | | |
| P26 | 1280 | 1360 | | |
| P27 | 1200 | 1260 | | x |
| P28 | 1100 | 1300 | x | |
| P29 | 1150 | 1200 | | |
| P30 | 1150 | 1200 | | |
| P31 | 1200 | 1350 | x | x |
| P32 | 1150 | 1320 | | |
| P33 | 1170 | 1200 | | |
| P34 | 1200 | 1400 | x | x |
| P35 | 1200 | 1270 | | |
| P36 | 1380 | 1420 | | |

A visualization of the results in Table 4.1 is illustrated in Figure 4.13 and Figure 4.14 below. The first figure shows the distribution of the samples, which showed degassing behaviour marked with a red circle and the samples, which separated in different phases marked with a blue circle. It is noticeable that degasification only appears at samples with low (CaO) content. The samples where phase separation appeared are also not evenly distributed. The two zones, where separation is observed can be seen in the Figure 4.13 below.

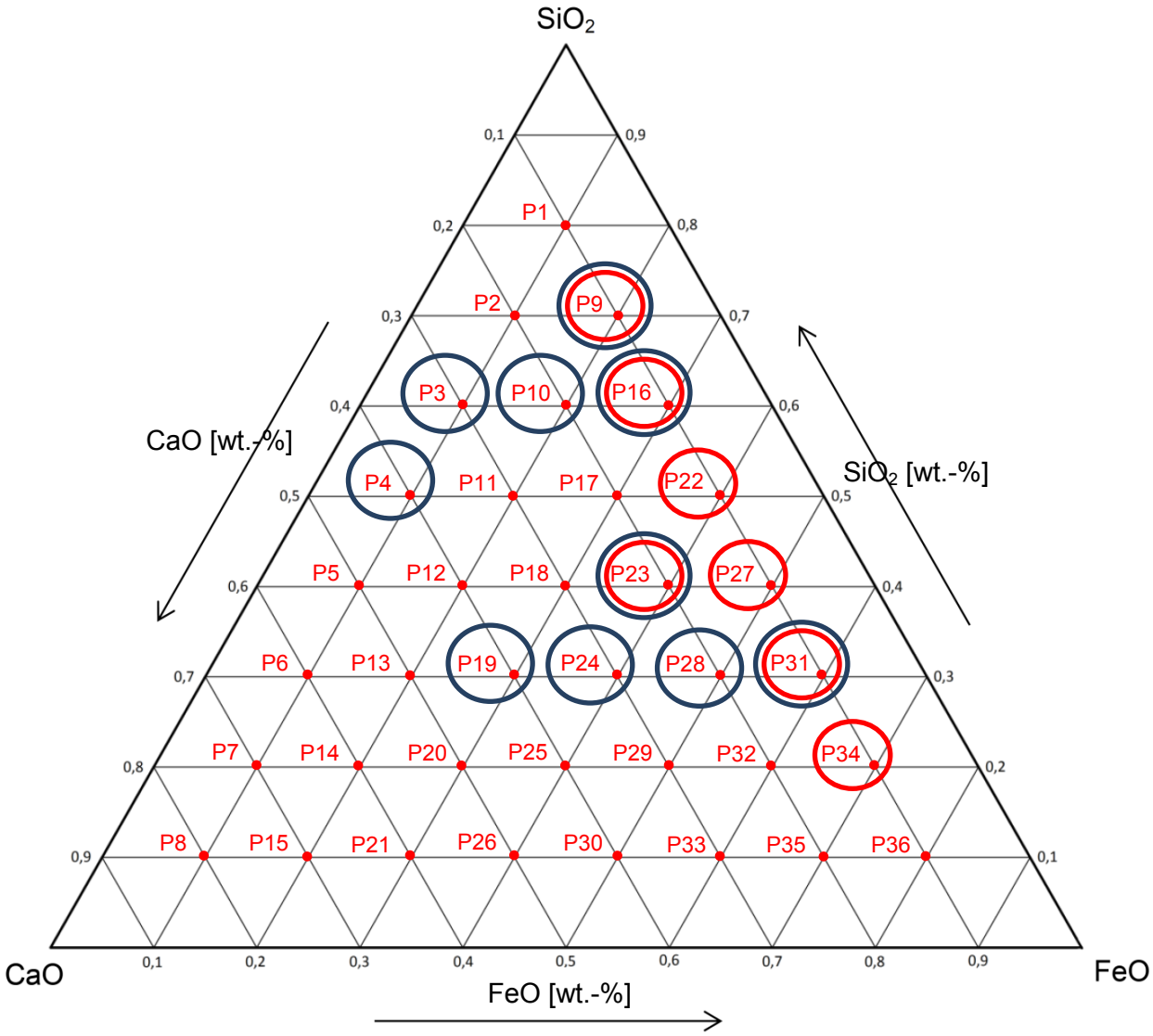


Figure 4.13: Illustration of observed properties including degasification (marked with red circles) and phase separation (marked with blue circles)

A precise statement or explanation of the two observed accumulations cannot be made in this thesis. Further investigations, like scanning electron microscopy of the occurring phases are necessary to make a scientifically objective statement. Since the main target of these trials was the determination of the melting points, no further investigations were conducted.

The zones of different melting temperatures in degrees Celsius were calculated by Origin. The model is illustrated in Figure 4.14 below.

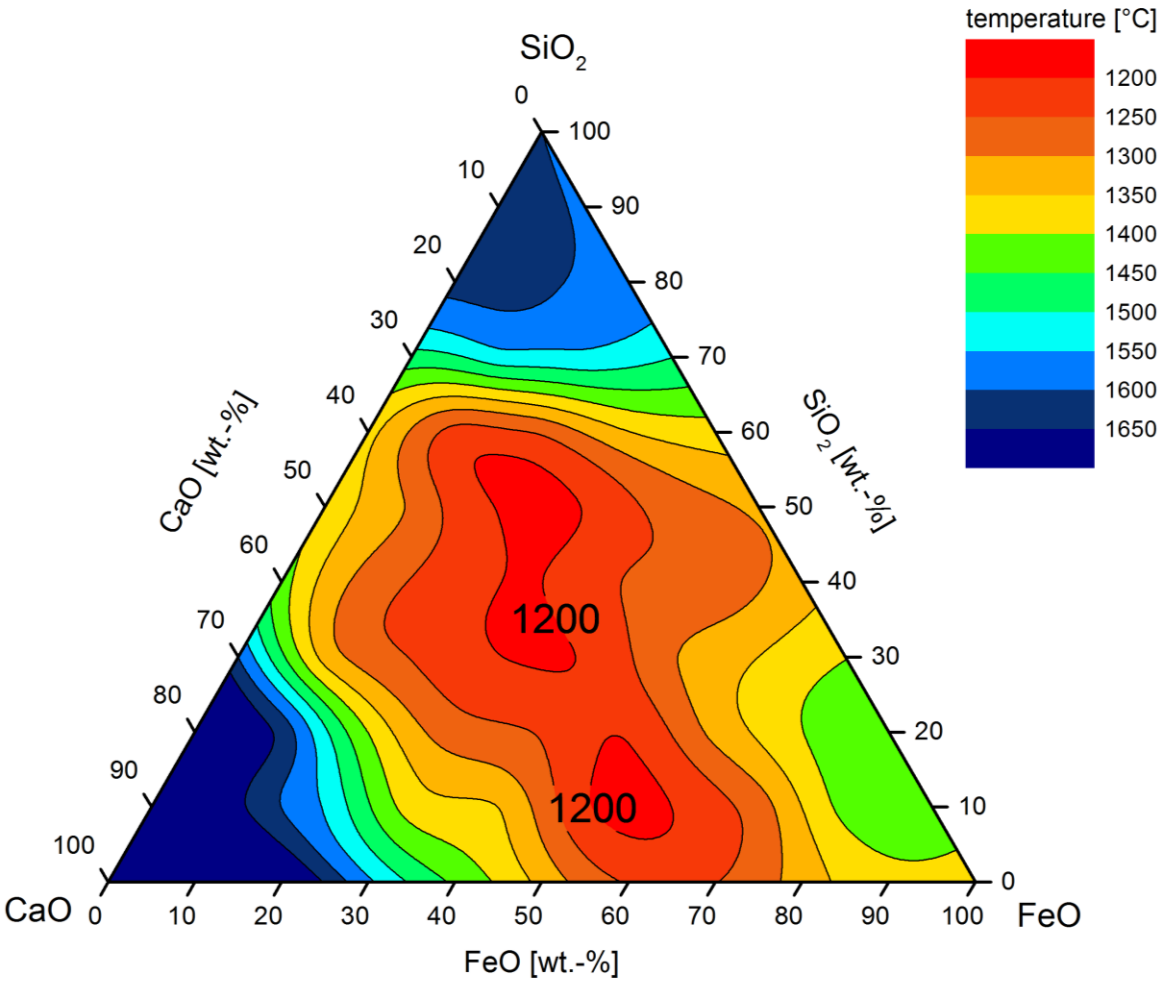


Figure 4.14: Calculated model of melting temperature zones with the data of Table 4.1

The spread-out area in the centre of the ternary system, marked with orange colour is labelling melting points of 1250 °C and below. Towards the corners of (CaO) and ($SiO_2$) the melting points are strongly increasing, which is marked with a blue colour. The comparison between the ternary system published in Figure 3.3 and Figure 4.14 shows a larger area of low melting zones in the area of low ($SiO_2$) concentrations and balanced (CaO)/(FeO) ratios.

# 5 Trials in the resistance furnace

After completing of the first trials in the hot stage microscope solid knowledge about the melting behaviour throughout the ternary system was gained. As mentioned and described before in section 3.5 there are several factors, which influence the recovery of the valuables. According to Figure 3.6 the zinc fuming rate and the lead settling can be increased by shifting the ($SiO_2$)/(CaO) ratio towards more (CaO) and increasing the ($SiO_2$)/(Fe) value. The aim of this trial is to check whether this theoretical thesis can be verified in a practical experiment. Because adding large amounts of fluxes is expensive in an industrial scale process, the ratios have not been shifted too far off the original slag, as it can be seen in Figure 5.1 underneath.

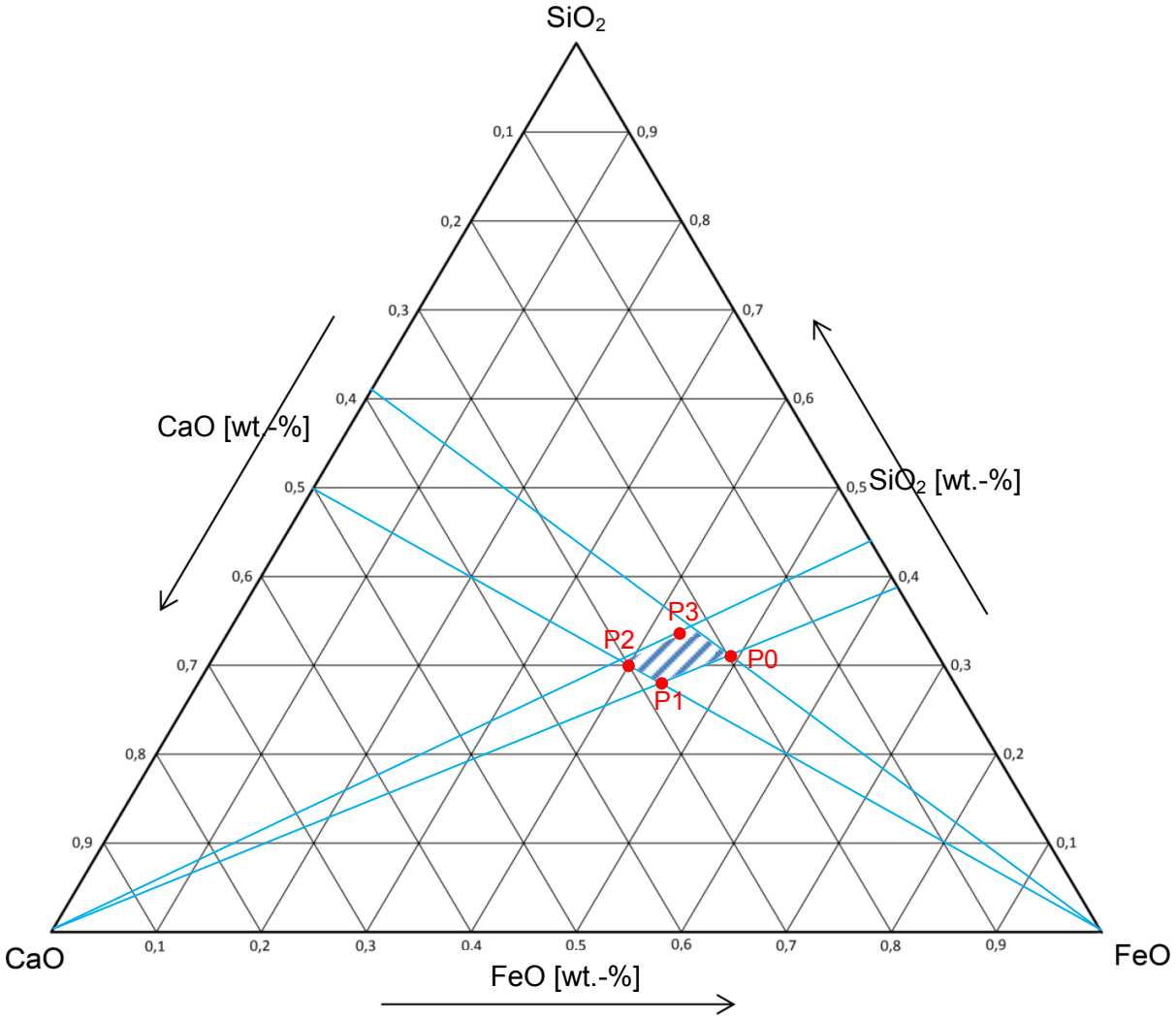


Figure 5.1: Location of the four slag compositions in the ternary system

## 5.1 Preparation of the samples

To produce the mixtures P0-P3, as seen in Figure 5.1 above, the added fluxes (CaO) and ($SiO_2$) had to be weighed and added to the residue. Due to the desired improvement of the zinc fuming rate and the lead settling, there was no (FeO) added in any trial. Each sample consisted of 600 g residue and the added fluxes. An overview of the content of each mixture and its calculated ($SiO_2$)/(CaO) and ($SiO_2$)/(Fe) ratio is published in Table 5.1 underneath.

Table 5.1: Illustration of the target values, the added fluxes and the calculated ratios per mixture

| Samples | Target value | | | Slag | Added fluxes | | mass | Ratios | |
|---|---|---|---|---|---|---|---|---|---|
| | CaO [wt.-%] | $SiO_2$ [wt.-%] | FeO [wt.-%] | [g] | CaO [g] | $SiO_2$ [g] | [g] | $SiO_2$/CaO [1] | $SiO_2$/Fe [1] |
| P0 | 20 | 31 | 49 | 600 | 0.00 | 0.00 | 600.0 | 1.55 | 0.78 |
| P1 | 28 | 28 | 44 | 600 | 66.9 | 0.4 | 667.3 | 0.87 | 0.79 |
| P2 | 30 | 30 | 40 | 600 | 101.9 | 35.4 | 737,3 | 0.89 | 1.00 |
| P3 | 23 | 34 | 43 | 600 | 38.4 | 47.4 | 685.8 | 1.46 | 1.07 |

Since the second experimental campaign should be run closer to industrial conditions already, the weighed in fluxes were not grinded together. Desulco, which is an abbreviation for (desulphurized coke) was used as reducing agent. This is a very pure coke, with low sulphur content (less than 0.05 wt.-%), low ash content and a purity of over 99 wt.-% carbon. In the used ISF-slag there is a zinc content of 8 wt.-% and a lead content of 1.76 wt.-%, as published in Table 3.2. The required reducing agent was identified by the stoichiometric demand to reduce the contained zinc and lead oxide in the slag. The actual added carbon content was 19.2 g per mixture, which equals two times the stoichiometric demand. Additionally to the slag, fluxes and reducing agent the lead had to be prepared. The quantitative ratio between lead bath and residue was specified as 3:1. With the help of a band saw pieces with a weight of 1.8 kg were cut out of a lead ingot.

## 5.2 Furnace, crucible and safety equipment

All trials were performed in a resistance furnace. The exact name is Nabertherm KC 2/15. To enable safe working conditions, safety equipment additionally to heat resistant clothes and safety shoes had to be worn. A special safety mask with external air supply is highly recommended due to the toxicity of lead. This mask was put on every time around the area of the ongoing trials. [20]

The chemical composition of the used crucible from the company Morgan Advanced Materials is listed in Table 5.2 below. The described crucible was coated before usage.

Table 5.2: Chemical composition of the used crucible [21]

| Element/Compound | Content [wt.-%] |
|---|---|
| C | 35-39 |
| SiC | 15-19 |
| $SiO_2$ | 20-24 |
| Si | 4-6 |
| $Al_2O_3$ | 12-16 |
| other oxides | 3-5 |

## 5.3 Trials procedure

At the start of the trial the resistance furnace was heated up to a temperature of 1200 °C. After reaching this temperature the empty crucible was placed in the furnace. It was assumed that thermal equilibrium was reached after 20 minutes. The 1.8 kg of lead were added to the crucible and due to its low melting point (327.4 °C) compared to the process temperature, it got completely liquid within minutes. After 15 minutes the mixture, including fluxes and reducing agent, was charged onto the lead bath. To pour in the mixture, another crucible was used as illustrated in Figure 5.2 below. [13]

Figure 5.2: Picture of charging residue into the preheated crucible onto the lead bath

Regular inspection of the sample conditions showed that the mixture needs between 20-25 minutes to reach a molten state. The time, when the molten residue was first noticed, initiated the “trial start time”. The following 60 minutes were considered as the trial period. Every 15-20 minutes the furnace was reopened to check the sample conditions and to stir up

the molten residue. After the experimental period had expired, the crucible with the sample was carefully removed from the furnace and placed in a safe place on refractory material to cool down. The removal of the crucible can be seen in Figure 5.3 underneath.

Figure 5.3: Removal of the crucible out of the furnace after finishing the trial

The samples were kept overnight on refractory material before the inspection of them began. Because the sample could not be separated from the crucible, the destruction of the crucibles was the only way to get access to the samples. In most of the cases a clear line between the regulus and the slag could be identified as illustrated in Figure 5.4 below.

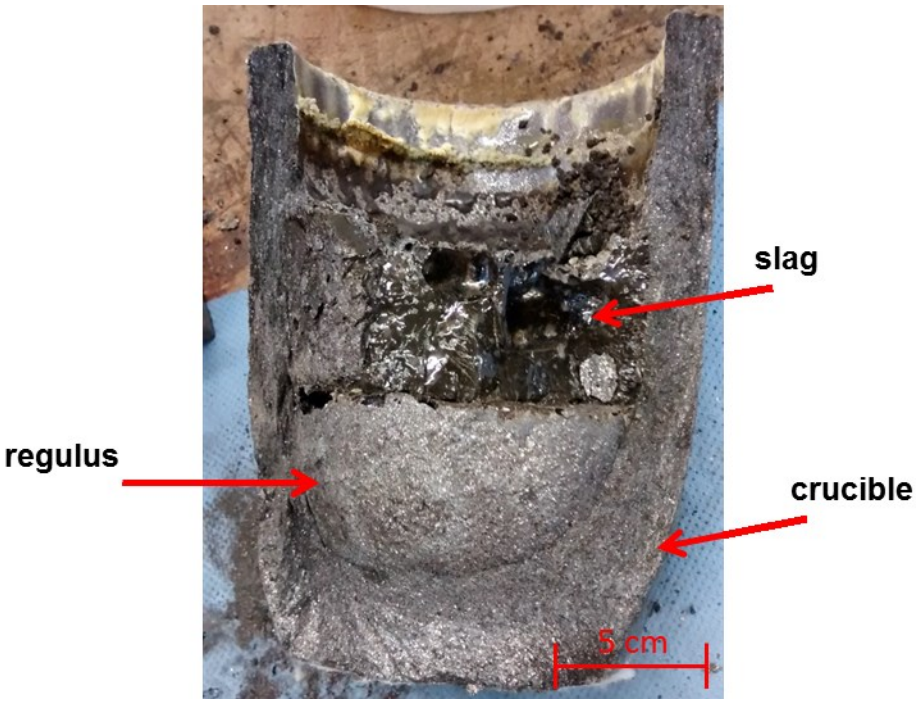


Figure 5.4: Picture of the separated slag and regulus within the destroyed crucible

With the help of hammer and chisel the slag, the regulus and the crucible were separated as good as possible. All above mentioned fractions were weighed and stored for subsequent investigations. Parts of the slag samples were grinded in a swing mill to enable further chemical analysis. All the results of the described process can be reviewed in the following section.

## 5.4 Results of the trials

To perform a mass balance of the trials in the resistance furnace, two sets of data are necessary. First of all, the weight of all raw materials before the trial and the weight of the samples after the trial must be known. The following Table 5.3 lists all the determined masses before and after the trial. The differences between the crucible and the crucible parts can be explained by the difficult separation of the slag and the crucible. The work with the hammer and chisel made it sometimes impossible to separate those parts precisely. Parts of the sample in the crucible (especially the contained zinc) were supposed to evaporate and other valuables like lead and silver were intended to settle in the lead bath. Therefore, it is not surprising that the regulus gained weight compared to the charged lead and the mass of the slag, after the trial decreased compared to the charged mixture prior to the experiment.

Table 5.3: Result of the weighing process before and after the trial

| | Weight before trial | | | Weight after trial | | |
|---|---|---|---|---|---|---|
| Trial-Sample | Crucible [g] | Lead [g] | Sample [g] | Crucible parts [g] | Regulus [g] | Slag [g] |
| T1-P0 | 1340.1 | 1800.1 | 600.0 | 1325.0 | 1836.0 | 548.0 |
| T2-P0 | 1400.0 | 1801.4 | 600.0 | 1408.0 | 1842.1 | 539.3 |
| T3-P1 | 1365.0 | 1794.4 | 667.2 | 1342.0 | 1828.2 | 587.1 |
| T4-P1 | 1365.0 | 1803.0 | 667.2 | 1341.3 | 1834.2 | 608.2 |
| T5-P2 | 1391.2 | 1798.8 | 737.3 | 1352.4 | 1831.9 | 710.5 |
| T6-P2 | 1351.2 | 1802.6 | 737.3 | 1337.5 | 1813.9 | 667.3 |
| T7-P3 | 1337.3 | 1798.6 | 685.8 | 1322.9 | 1835.0 | 618.0 |
| T8-P3 | 1687.7 | 1799.7 | 685.8 | 1662.4 | 1835.8 | 595.4 |

The separated and grinded slag was analysed according to the standard DIN EN ISO 11885, which describes an analytic process to determine the concentration of up to 33 elements via inductive coupled plasma. The result, published in the following Table 5.4 shows that the lead and zinc content of the slag decreases significantly, which is generally consistent with the aims of the process. The silver content is below the level of detection in all slag samples and the iron content decreases slightly as well. The share of (CaO) and ($SiO_2$) is increasing. [22]

Table 5.4: Result of the chemical analysis of the slag samples [23]

| Title of sample | Pb [wt.-%] | Zn [wt.-%] | Ag [wt.-%] | Fe [wt.-%] | CaO [wt.-%] | $SiO_2$ [wt.-%] |
|---|---|---|---|---|---|---|
| Original slag | 1.8 | 8.0 | 0.002 | 27.8 | 14.0 | 21.8 |
| T1-P0 | 0.5 | 4.8 | <LOD | 24.4 | 16.6 | 29.6 |
| T2-P0 | 0.4 | 5.1 | <LOD | 22.1 | 17.8 | 31.4 |
| T3-P1 | 0.1 | 4.5 | <LOD | 21.5 | 25.0 | 26.4 |
| T4-P1 | 0.3 | 4.4 | <LOD | 20.3 | 25.5 | 26.3 |
| T5-P2 | 0.5 | 5.1 | <LOD | 20.9 | 26.7 | 28.5 |
| T6-P2 | 2.4 | 5.0 | <LOD | 20.5 | 27.9 | 26.7 |
| T7-P3 | 0.4 | 4.7 | <LOD | 20.8 | 22.2 | 32.6 |
| T8-P3 | 0.2 | 5.1 | <LOD | 20.8 | 21.0 | 31.4 |

To create a mass balance of the trials in the resistance furnace, the two tables above have to be combined. The following Table 5.5 show the results of the lead settling rate and the zinc fuming rate. Since the silver content is below the detection limit of the chemical analysis it is assumed that about everything contained is dissolved in the lead regulus. The only negative value for the lead settling rate at sample T6-P2 is not included in further calculations. It is assumed that either the sample investigated was not representative in terms of lead content or an error occurred at the chemical analysis.

Table 5.5: Results of the lead and zinc content in the final slag and the calculated lead settling rate and zinc fuming rate

| Sample name | Lead content [g] | Lead settling rate [%] | Zinc content [g] | Zinc fuming rate [%] |
|---|---|---|---|---|
| Original slag | 10.56 | | 48.00 | |
| T1-P0 | 2.96 | 71.98 | 26.30 | 45.20 |
| T2-P0 | 2.16 | 79.57 | 27.50 | 42.70 |
| T3-P1 | 0.82 | 92.22 | 26.42 | 44.96 |
| T4-P1 | 1.58 | 85.03 | 26.76 | 44.25 |
| T5-P2 | 3.55 | 66.36 | 36.24 | 24.51 |
| T6-P2 | 16.02 | -51.66 | 33.37 | 30.49 |
| T7-P3 | 2.47 | 76.59 | 29.05 | 39.49 |
| T8-P3 | 1.19 | 88.72 | 30.37 | 36.74 |

It is noticeable, that the lead settling rate is significantly higher than the zinc fuming rate. It is presumed that the small specific surface due to the geometric form of the crucible and the poor mixing compared to a Top Blown Rotary Converter has negative effects on the zinc fuming rate. The following Figure 5.5 and Figure 5.6 show the average lead settling rate and the average zinc fuming rate per used raw material composition.

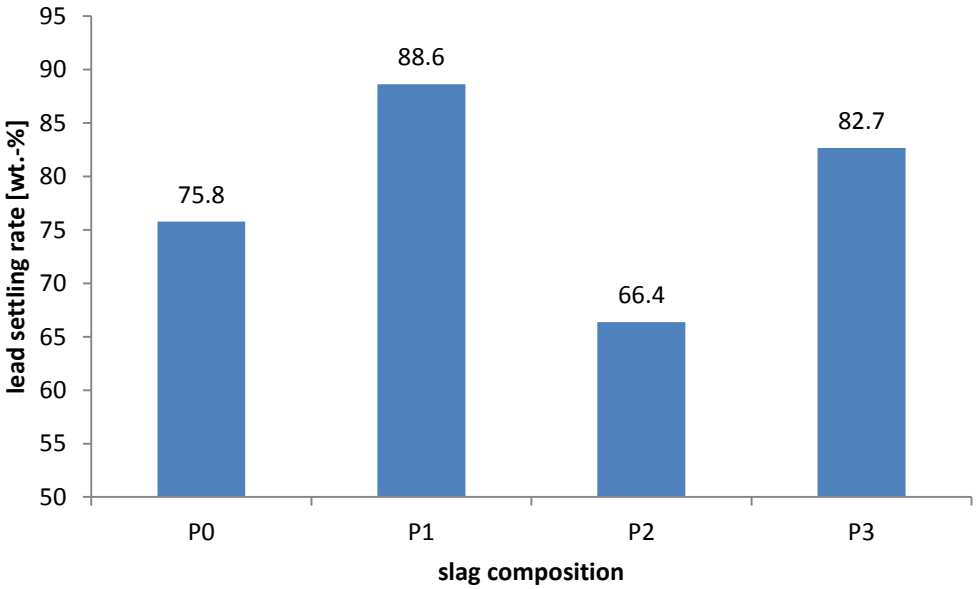


Figure 5.5: Results of the average lead settling rate per sample composition

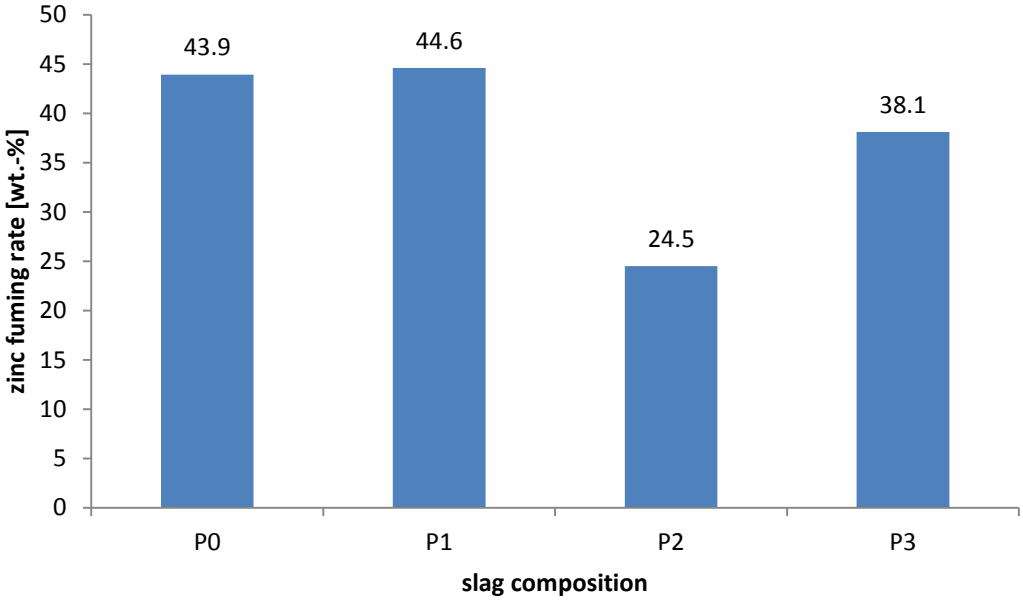


Figure 5.6: Results of the average zinc fuming rate per sample composition

. The theoretical correlation between the output rates of lead and zinc and the varying $(CaO)/(SiO_2)$ and $(SiO_2)/(Fe)$ ratios is shown in section 3.5 in Figure 3.6. The sample compositions were placed around the desired upper left quarter of the diagram. This is the area with good lead settling, a good zinc fuming rate and lower melting temperatures. The experimental results are not in total agreement with the theoretical properties of certain component ratios. The following diagrams show the correlation between the recovery rates of lead and zinc plotted against the $(CaO)/(SiO_2)$ and $(SiO_2)/(Fe)$ ratio.

Figure 5.7 shows the zinc fuming rate of the four different mixtures in red and the associated $(SiO_2)/(CaO)$ ratio. It can be noted that those two curves do not allow the conclusion to be drawn that a lower $(SiO_2)/(CaO)$ ratio leads to a decreased zinc fuming rate and vice versa.

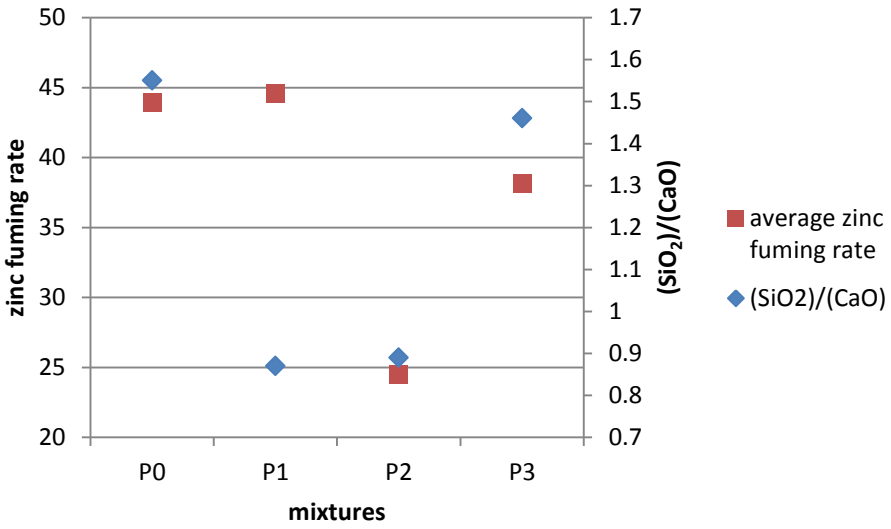


Figure 5.7: Average zinc fuming rate plotted against the $(SiO_2)/(CaO)$ ratio

Also the $(SiO_2)/(Fe)$ ratio plotted against the zinc fuming rate has given no sufficient statement. While the $(SiO_2)/(Fe)$ ratio is steadily increasing the average zinc fuming rate shows no significant correlation, as seen in Figure 5.8 below.

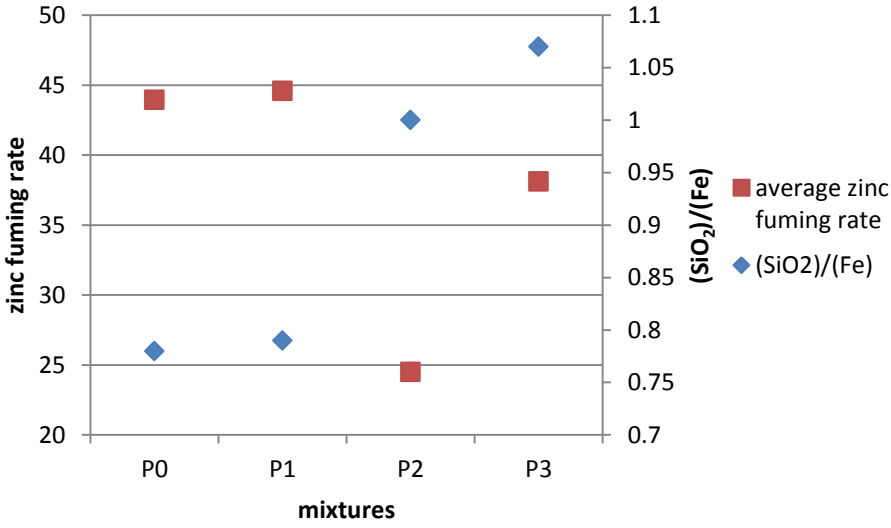


Figure 5.8: Average zinc fuming rate plotted against the $(SiO_2)/(Fe)$ ratio

The results of the lead settling rate in comparison with the component ratios do not allow a general statement either. Figure 5.9 shows the comparison of the average lead settling rate and the calculated $(SiO_2)/(CaO)$ ratio.

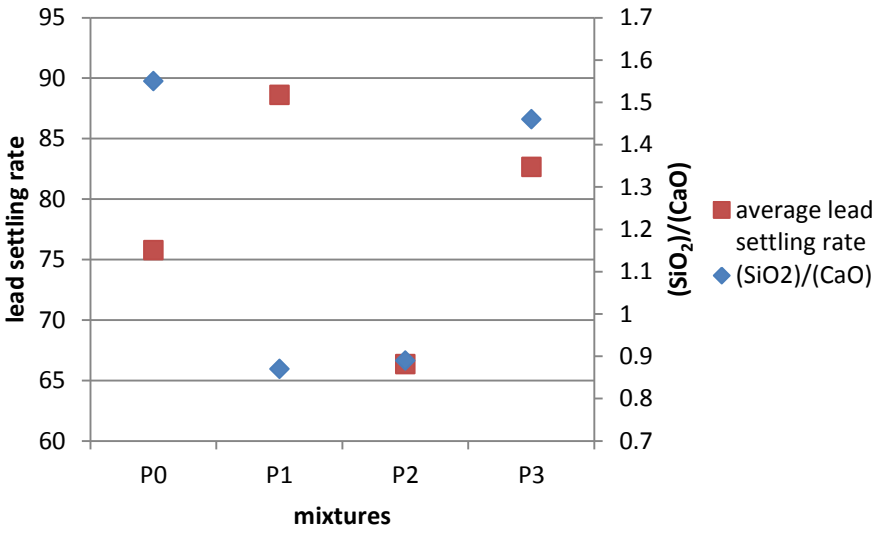


Figure 5.9: Average lead settling rate plotted against the $(SiO_2)/(CaO)$ ratio

Figure 5.10 below shows the average lead settling rate of mixture P0-P3 and their according $(SiO_2)/(Fe)$ value. As seen in the previous figures, no clear correlation was found.

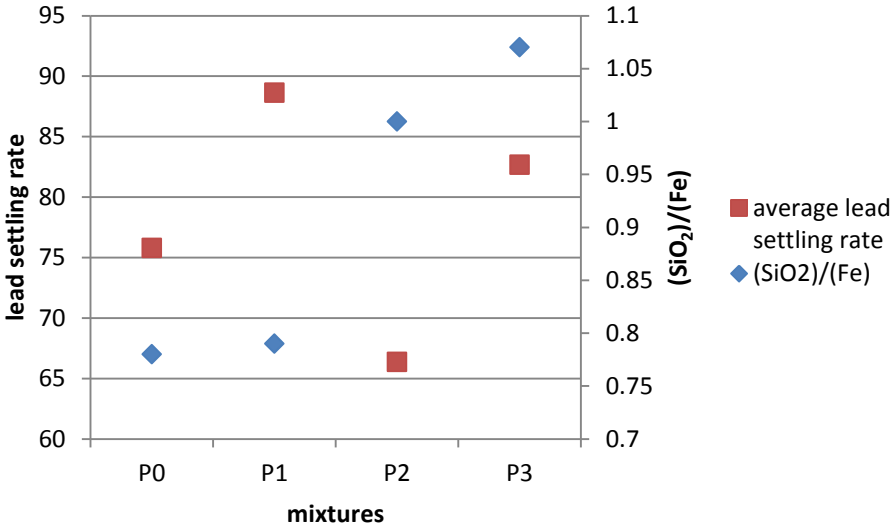


Figure 5.10: Average lead settling rate plotted against the $(SiO_2)/(Fe)$ ratio

Even though no clear direct proportional correlation between the component ratios and the yield rates were discovered, the results of the lead settling rates were strongly improved in mixture P1 and P3. Especially the mixture P1 was tested very successfully. The lead settling rate was improved by 12.8 % and the zinc fuming rate was marginally improved by 0.7 %. The reason for the increase of the settling rate is lowered viscosity of the slag.

Another noticeable result is the unwanted iron reduction of the slag. The trials did not completely succeed in the suppression of iron reduction. This can be explained with the near location of iron oxide in the Richardson-Ellingham diagram compared to zinc at the process

temperature and the high amount of reducing agent (two times the stoichiometric amount). The results of the iron reduction rate can be seen in Table 5.6 underneath and its range lies between 10-30 %. The average iron reduction rate is approximately a quarter of the used quantity.

Table 5.6: Results of the calculated iron reduction rate

| | Original Fe content [wt.-%] | Fe content slag [g] | Fe reduction rate [%] |
|---|---|---|---|
| Original slag | 27.8 | 166.80 | |
| T1-P0 | 24.4 | 133.71 | 19.84 |
| T2-P0 | 22.1 | 119.19 | 28.55 |
| T3-P1 | 21.5 | 126.23 | 24.32 |
| T4-P1 | 20.3 | 123.46 | 25.98 |
| T5-P2 | 20.9 | 148.49 | 10.97 |
| T6-P2 | 20.5 | 136.80 | 17.99 |
| T7-P3 | 20.8 | 128.54 | 22.94 |
| T8-P3 | 20.8 | 123.84 | 25.75 |

The changed (Fe), (CaO) and ($SiO_2$) quantities significantly influence the position of the sample in the ternary system. The effect of the extra amount of (CaO) and ($SiO_2$) affects the (CaO)/($SiO_2$) ratio and the ($SiO_2$)/(Fe) ratio. The deviation from the designed ratios is illustrated in Table 5.7 below.

Table 5.7: Comparison of the initial compound ratio and the actual measured ratio after the trial

| | Original ($SiO_2$)/(CaO) [1] | Original ($SiO_2$)/(Fe) [1] | Actual ($SiO_2$)/(CaO) [1] | Actual ($SiO_2$)/(Fe) [1] |
|---|---|---|---|---|
| P0 average | 1.56 | 0.78 | 1.77 | 1.32 |
| P1 average | 0.87 | 0.79 | 1.04 | 1.26 |
| P2 average | 0.89 | 1.00 | 1.01 | 1.33 |
| P3 average | 1.46 | 1.07 | 1.48 | 1.54 |

Especially the ($SiO_2$)/(Fe) ratio deviates strongly from the initial value. Two effects enhance this change. First of all the analysed ($SiO_2$) value is significantly higher than the input quantity of the slag, which could be explained by dissolved ($SiO_2$) out of the crucible. The second effect is the iron settling. Since 10-30 % of the iron oxide content is reduced, the iron content in the slag decreases. Both effects contribute to a severe change in the ($SiO_2$)/(Fe) ratio.

With the help of the results of the chemical analysis, the viscosity of the different samples was calculated. The significance of the Kz-value and the equation to calculate it is mentioned in section 3.5 in the theoretical part of the thesis. The result of the calculation is presented in Table 5.8 below.

Table 5.8: The result of the calculated Kz-value for every sample composition

| Title of sample | Kz [1] |
|---|---|
| P0 average | 1.51 |
| P1 average | 1.83 |
| P2 average | 1.84 |
| P3 average | 1.48 |

## 5.5 Scanning electron microscope

The following investigations of the slag were performed in the JSM-IT300 scanning electron microscope (SEM) of the brand JEOL. The device is equipped with a stationary energy dispersive X-Ray detector that enables the determination of the chemical composition (mappings and line scans) in realtime and high resolution. The large sample chamber of a diameter up to 200 mm allows the observation of slag samples under a high vacuum down to 650 Pa. The additional feature of a high temperature hot stage was not used to analyse the residue. Apart from performing a determination of the qualitative distribution of chemical compounds of the slag, the structure of formed phases in the slag is observed and described in this section as well. A photo of the SEM is shown in the following Figure 5.11. [24]

Figure 5.11: Picture of the scanning electron microscope

### 5.5.1 Analysis of the utilized slag

This section deals with the characterisation of the utilized slag, which served as raw material for the trials. Especially the individual present phases of the valuable metals are of severe interest, because the chemical analyses in section 3.2 can only provide information concerning the total quantity of a compound or element. Therefore, most following samples contain different spectra, which are analysed by the scanning electron microscope. Usually the first sample is a spectrum to determine the overall quantities in a chosen area, which is called mapping. To perform a mapping with the help of the SEM, an area without any obvious anomalies is chosen and marked with the cursor. The determination of the chemical composition takes between a few minutes and many hours depending on the size of the analysed area and the selected resolution. An example for a selected area is illustrated in spectrum 7 of Figure 5.12.

Additionally to the mapping several eye-catching structures are marked and different spectra are assigned to those structures. The SEM analyses all spectra and determines the chemical composition of all marked spectra. In this case the result of spectrum 7 is quite similar to the chemical analyses. Spectrum 4 is not deviating a lot from spectrum 7. There is a little more calcium and silicon and a little less iron in the matrix compared to the total mapping. The structure of a light needle is analysed as spectrum 5. It is determined as Fe-O compound with 51.6 wt.-% of iron and 36.1 wt.-% of oxygen. Spectrum 6 is a different shaped typical structure, which is rich in iron (34.8 wt.-%), zinc (18.0 wt.-%), sulphur (16.4 wt.-%) and lead (9.5 wt.-%). All detailed results of all published spectra can be found in the appendix section 9.2 of the thesis.

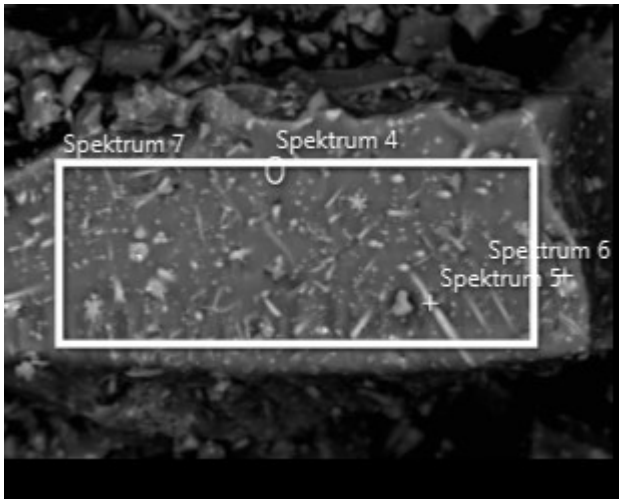


Figure 5.12: Mapping and other spectra of the utilized slag before the trial

## 5.5.2 Analysis of the treated slag

Analogous to the mapping of the used slag before the trial, all treated slags were analysed as well. Figure 5.13 below shows an example of a performed mapping of mixture P1.

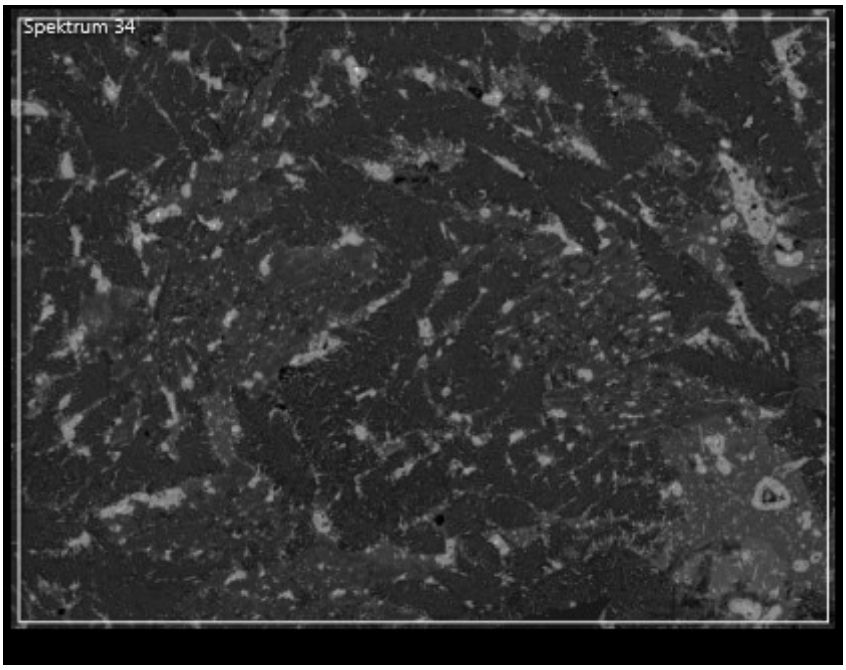


Figure 5.13: Selected area for a mapping of sample P1

The software analysed the chosen sector and displayed the result of the detected element quantity in percent by weight. It has to be pointed out, that all results are only representative for this specific area. Due to the heterogeneous structure of the slag and the very small analysed area (2-3 $mm^2$) compared to the total amount of slag, the results cannot be applied to the total chemical composition.

Additionally to the determination of the chemical distribution of elements and compounds in a selected area, the structure of the contained substances was analysed with the help of the SEM. In the following part observed structures that stand out of the matrix are pictured and analysed.

Figure 5.14, shown below pictures a little hole with an approximate diameter of 80 µm in the treated slag matrix of mixture P3. A structure is located in this hole and was investigated under the name spectrum 8. The concentration in spectrum 8 shows 71.4 wt.-% zinc and 15.3 wt.-% iron. The molar ratio between zinc and iron is almost exactly 1:4.

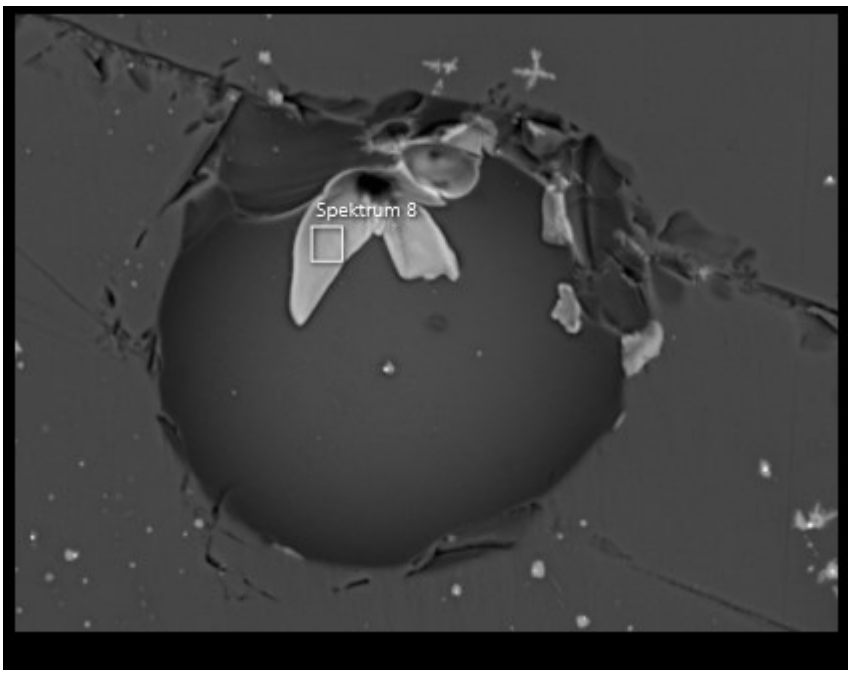


Figure 5.14: Picture of a zinc and iron phase within a discovered hole of the treated slag of P3

In Figure 5.15 one can see an eye-catching rectangular-shaped dark structure and more different shaped lighter structures in and outside the rectangular. The dark matrix that also forms the rectangular (spectrum 12,16 and 18) consists for the most part of (CaO) and ($SiO_2$). Spectrum 14 is recognized as lead sulphide and the spectra 13 and 15 consist of iron oxide. The bright spot on the left of the picture is labelled spectrum 17 and appears to be almost pure reduced iron (97 wt.-%).

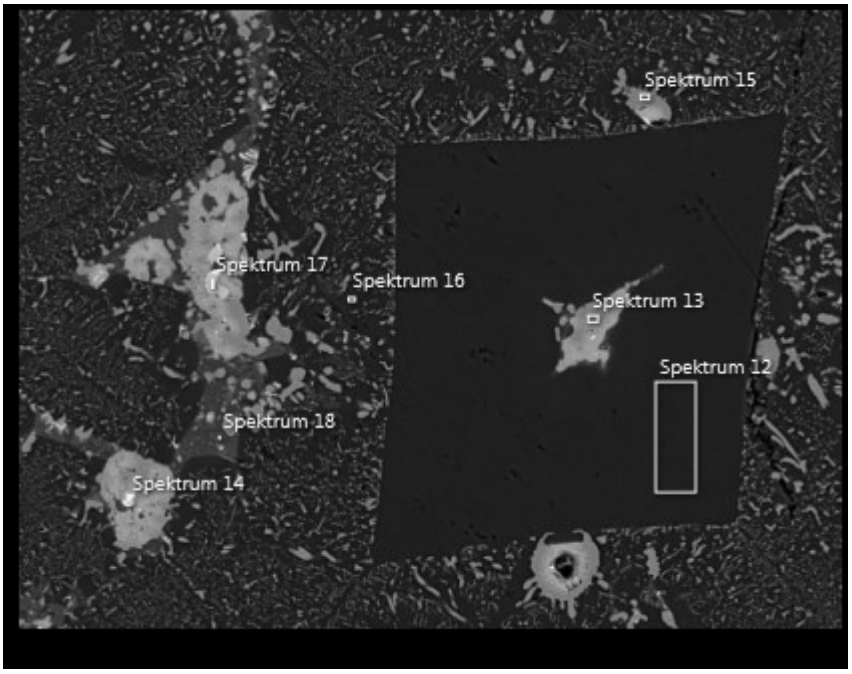


Figure 5.15: Illustration of different analysed spectra within a selected area of mixture P2

The included software analysis of the SEM is also able to determine the phase composition by calculating molar ratios in examined areas. In Figure 5.16 the recognized phases and their location is displayed by different colours.

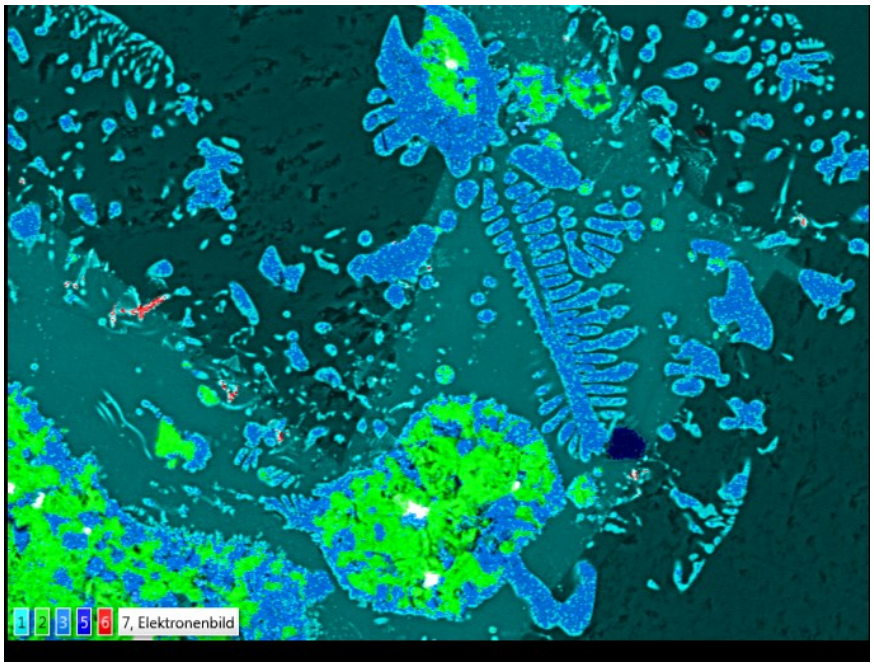


Figure 5.16: Result of a phase recognition in a selected sample area

The same picture split into the most common phases can be seen in Figure 5.17. The above labelled phase is pictured in different colours, whereas all the other existing phases are blinded out. This enables a good overview where the common compounds occur.

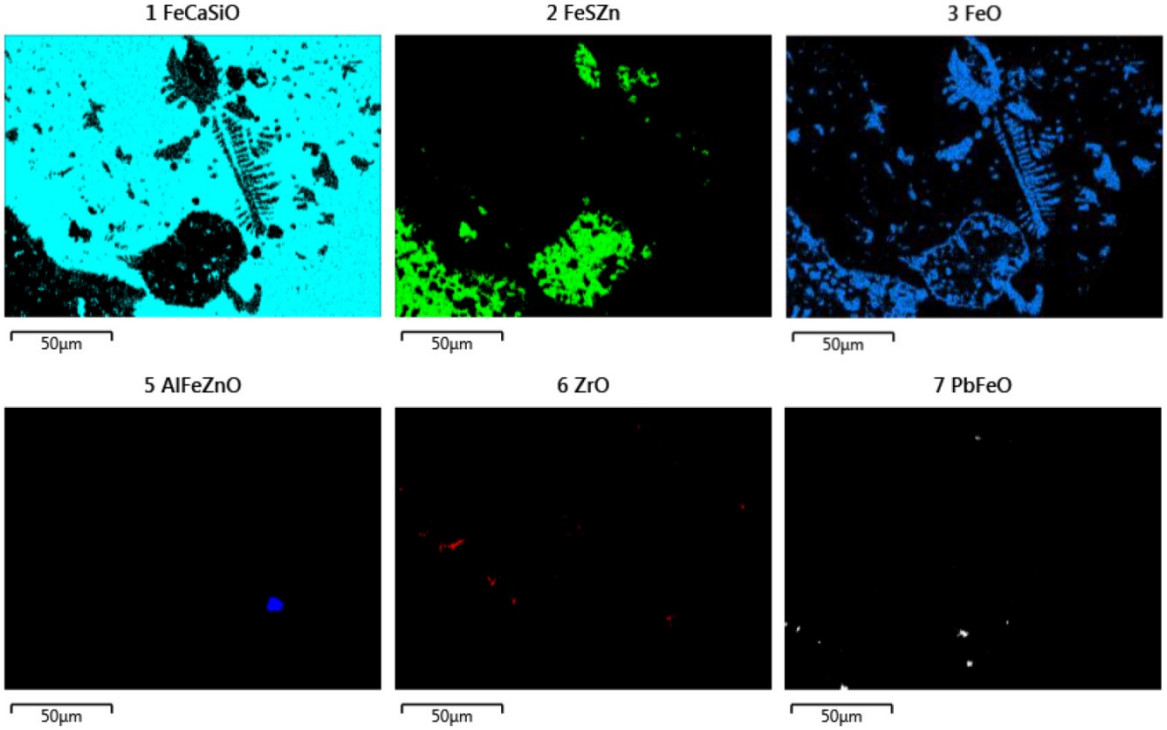


Figure 5.17: Result of the phase recognition, where the above labelled phases are shown in different colours and all other contents are blinded out

### 5.5.3 Analysis of the regulus

Figure 5.18 below is a picture of the regulus. The investigated spectra show different compound contents. Spectrum 13 (the matrix) is identified as lead with a purity of 93.4 wt.-%. The spectrum 14 is a zinc sulphide compound in an eye-catching crystalline structure. Spectrum 16 appears as small black dot in the lead matrix and is identified as a Si-Al-O compound.

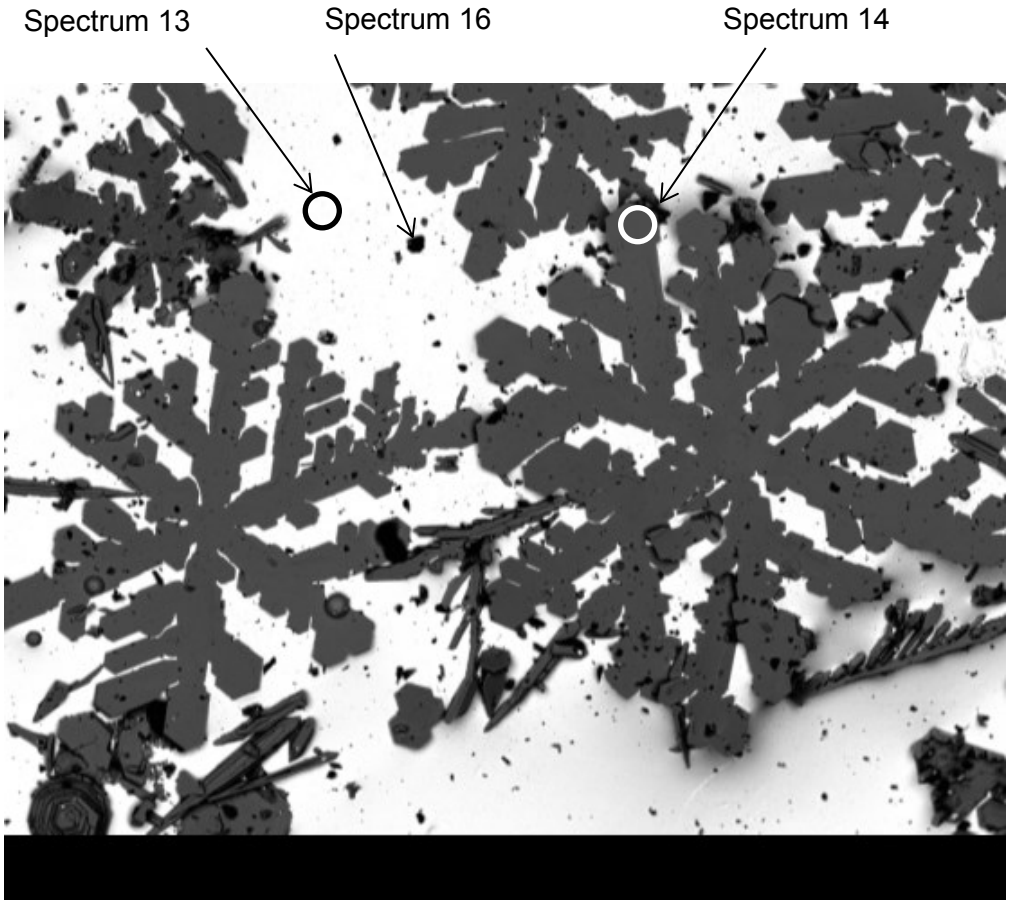


Figure 5.18: Crystalline zinc sulphide structures embedded in a lead matrix

# 6 Mass and energy balance

In order to evaluate the economic feasibility of the lead bath recycling process the following two chapters deal with a technical and economic scenario with the goal of simulating as realistic process conditions as possible. Before any economic calculations can be done, a mass and energy balance is required in order to gain relevant data such as the raw material demand, the heating energy demand or the required size of different aggregates. Therefore, this section deals with the basic process model, all necessary assumptions and the result of the balances.

The aim was to establish a flexible calculation tool, which allows changing different parameters such as residue composition, combustion conditions or different efficiency factors. This enables a quick comparison of different slag compositions and an immediate evaluation of certain process parameters.

The actual planned plant consists of a Top Blown Rotary Converter, which is fired with natural gas and pure oxygen in order to minimize the off-gas quantity. The raw material is the lead slag, which is supposed to be charged onto a liquid lead bath with the goal of recovering the valuables. Lead oxide and zinc oxide needs to be reduced. After reducing lead oxide, it is supposed to settle to the bottom, while the reduced zinc evaporates, reoxidizes and gets collected in a baghouse filter. The utilized reducing agent is coke, which is assumed to serve the reducing process only, while the energy for the heating- and melting process is supplied by natural gas. The silver content of the slag is assumed to dissolve in the lead bath. Baghouse filters allow maximum flue gas temperatures of 250 °C. This means that the exhaust gas of the process, with temperatures around 1200 °C needs to be cooled down in a hot gas quench. [25]

The first step of performing a mass and energy balance is to calculate the input quantities. The input parameter of the slag content is measured in per cent by weight. Those values are transformed into kmol and kg, with the help of the total slag amount and the respective molar masses. The heating demand is then calculated with the enthalpies of the specified streams at the initial temperature and the final temperature. The melting enthalpies (latent heat) of the species have to be considered as well. To calculate the correct value the melting temperature of the residue has to be known. In this case, the determined value of the hot stage microscope of section 4.4 was selected. The total heating demand also includes the necessary energy to heat up the fluxes, the reducing agents and the lead bath.

The result of the total energy demand for heating and melting is shown in Table 6.1 below.

Table 6.1: Calculation of the heating demand of the residue

| Species | H 25°C | H 1200°C | ∆ H1 | ∆ H2 | Latent heat | Total heating | Total energy |
|---|---|---|---|---|---|---|---|
| | [MJ/kmol] | | [MJ/kmol] | | [MJ/kmol] | | [MJ] |
| FeO | -267.5 | -176.2 | 66.3 | 1.8 | 23.1 | 91.3 | 17,171,476 |
| $Fe_2O_3$ | -823.5 | -656.0 | 163.6 | 3.9 | 0.0 | 167.5 | 526,809 |
| $SiO_2$ | -911.1 | -826.7 | 79.4 | 2.3 | 2.6 | 84.3 | 11,943,764 |
| CaO | -635.1 | -499.2 | 58.0 | 1.7 | 76.3 | 136.0 | 13,250,565 |
| ZnO | -350.7 | -238.2 | 58.0 | 1.6 | 52.8 | 112.5 | 5,370,978 |
| $Al_2O_3$ | -1,676.1 | -1,425.3 | 135.8 | 3.9 | 111.1 | 250.8 | 6,710,305 |
| MgO | -601.8 | -482.3 | 56.3 | 1.8 | 61.3 | 119.4 | 2,394,463 |
| MnO | -385.4 | -280.4 | 60.7 | 1.6 | 42.7 | 105.0 | 745,401 |
| Ag | 0.0 | 45.7 | 44.9 | 0.9 | 0.0 | 45.8 | 332 |
| $Na_2O$ | -415.4 | -249.9 | 165.6 | 2.8 | -2.9 | 165.6 | 534,080 |
| PbO | -218.3 | -125.9 | 90.7 | 1.8 | 0.0 | 92.4 | 306,427 |
| Cu | 0.0 | 46.6 | 45.8 | 0.9 | 0.1 | 46.7 | 143,560 |
| C | 0.0 | 22.6 | 22.0 | 0.6 | 0.0 | 22.7 | 1,987,922 |
| CaO | -635.1 | -499.2 | 58.0 | 1.7 | 76.3 | 136.0 | 10,266,214 |
| $SiO_2$ | -911.1 | -826.7 | 79.4 | 2.3 | 2.6 | 84.3 | 24,809 |
| Pb | 0.0 | 38.9 | 8.7 | 25.7 | 4.7 | 39.1 | 438,496 |
| total | -7,831.6 | -6,132.2 | 1,193.3 | 55.4 | 450.7 | 1,699.4 | 71,815,599 |

∆ H1 represents the enthalpy difference between the original input enthalpy and the enthalpy of the residue at melting point. The necessary melting energy is considered in the latent heat. After liquefying the slag it needs to be heated up to its final temperature of 1200 °C. This amount of heat is considered in the column ∆ H2. The sum of both heating energies and the latent heat is multiplied with the compound quantity in kmol to get the total amount of needed energy.

After calculating the heating energy, the necessary amount of natural gas to provide the demand has to be determined. Therefore, the gas needs to be characterized. The assumed composition of the natural gas is shown in Table 6.2 below.

Table 6.2: Assumed composition of natural gas [26]

| Chemical compound | Share [vol.-%] |
|---|---|
| $CH_4$ | 98.13% |
| $C_2H_6$ | 0.64% |
| $C_3H_8$ | 0.20% |
| $C_4H_{10}$ | 0.10% |
| $CO_2$ | 0.09% |
| $N_2$ | 0.84% |

In this scenario the stoichiometric air-fuel ratio is selected as 1. This means that exactly the demanded amount of oxygen needed for a complete combustion is available. The air-fuel ratio is one of the existing input parameters and is adjustable. In a stoichiometric combustion with natural gas and oxygen there are only two reaction products: {$CO_2$} and {$H_2O$}. The oxygen demand is determined with the help of the reaction equations. Afterwards the whole combustion process is regarded as a black box and the enthalpy stream into the black box and out of the black box is compared for 1 kmol natural gas. The determined caloric value per kmol is linked to the demanded energy. This procedure leads to the necessary quantities of natural gas and oxygen, assuming that no heat losses occur. The real lossy process can be determined by using an efficiency factor. Assuming that methane and oxygen are ideal gases, the multiplication with the molar volume leads to the standard cubic metres. The annual methane quantity needed at 80 % efficiency of the process amounts 165,383 kmol or 3,706,896 $Nm^3$. The oxygen amount is approximately two times as high, compared to the natural gas quantity.

The coke demand is determined by the reduction of zinc oxide and lead oxide, described by the reaction Equations 6.1 and 6.2 below. The energy needed for the reactions is calculated with the help of reaction enthalpies, at a temperature of 1200 °C. The necessary energy to reduce the oxides is provided by the natural gas burner.

$$ZnO(l) + C \leftrightarrow Zn(g) + CO(g) \qquad \text{Equation 6.1}$$

$$PbO(l) + C \leftrightarrow Pb(l) + CO(g) \qquad \text{Equation 6.2}$$

The reaction enthalpies of Equation 6.1 and 6.2 amount 297,83 MJ/kmol for the zinc oxide reduction and 69,54 MJ/kmol for the lead oxide reduction. The total energy demand is determined after the multiplication of the quantities of zinc oxide and lead oxide in the residue. The necessary carbon amount is calculated with the help of the reaction equations above. The molar quantity is multiplied by the molar weight of carbon. Assuming that the used coke has a carbon content of 85 wt.-%, the coke demand can be calculated. In this process scenario a stoichiometric factor of 1.5 is applied for coke, which means an extra 50 wt.-% of coke. The result of the annual coke use is therefore 1,054 tonnes.

Another important issue is the design of the hot gas quench and the necessary cooling water. A typical value of the ratio between injected cooling water to air is 10 l/min of water to 42 $Nm^3/h$ of air. The enthalpy difference between the off-gas at 1200 °C and the highest possible temperature for the baghouse filter 250 °C is determined. Additionally the energy difference between air and liquid water at a temperature of 10 °C and air and steam at 250 °C is determined. Regarding the ratio of air to water the demanded amounts to cool 1859 $Nm^3/h$ are determined as 3.35 $m^3$ of liquid water and 226.0 $m^3$ of air per working hour. [25]

Most calculated data is used for the economic evaluation of the process, where further assumptions have to be made. The economic calculation is based on the same developed excel simulation tool, which enables an immediate evaluation of different process conditions. The detailed calculations and results of the economic evaluation are addressed in the following economic part of the thesis.

# 7 Economic part

The technical feasibility and efficiency of the process is just one condition of a successful establishment of the lead bath recycling process. In order to evaluate the economic reasonability of the lead bath recycling process, the following chapter shows and explains the calculations of two scenarios. The applied calculation method for the calculation is the net present value method. Due to fast changing market conditions many necessary parameters for the economic evaluation are hard to predict. To attenuate the effect all costs are calculated three times. The realistic cost scenario represents the actual value at this time or the expected value over the period of time. All future cost calculations relate to an annual slag recycling amount of 38,000 t/year and are indicated as expenditures per year. Additionally a best- and worst case scenario is calculated for all costs.

## 7.1 Assumptions

To calculate the possible economic benefit, a list of assumptions has to be made. The detailed assumptions concerning the individual expenditures and revenues are described in the related sections. A few general assumptions regarding more sections are made in this section of the thesis.

In the scope of this work an Excel tool (as described in section 6) was developed with all technical and economic calculations. All assumptions for economic values are marked as input values of the simulation and can be changed by the user at any time to any possible value. The two further calculations are only case studies performed with the developed tool and can be used and modified at the operators will.

The whole calculation is based on the assumption of establishing the recycling process on a “brown field”. This means that fundamental infrastructure, such as natural gas pipelines, power lines or water pipes exist on the property. It is assumed that the needed land is already available and no further administration buildings have to be built. Additionally all legal costs, all official permit costs or any sort of taxes will not be taken into account.

To be applicable and comparable in an international business environment all costs are calculated in US Dollars, but many costs are stated in Euro as well. The actual value of Euro to US Dollars is approximately 1.05 in March 2015. This is the lowest exchange rate since 2002. In order to adapt to the average exchange rate of the last decade all further calculations are performed with a defined exchange rate of 1.2 €/USD. [27]

Furthermore the depreciation times of all main capital expenditures like the TBRC or the "balance of plant" are 20 years. Only the ground-, and framework have a designated depreciation time of 40 years. The result shows (see section 7.2.5) that this part represents only 0.8 % of the capital expenditures and is therefore neglected. It is assumed that all capital expenditures are depreciated after 20 years.

## 7.2 Capital Expenditures

The following section gives an overview of the different capital expenditures that are necessary to run the lead bath recycling process. As mentioned above all fundamental infrastructure is assumed to exist on the property already.

### 7.2.1 Groundwork, framework and installations

This section covers the necessary groundwork, which is needed to place heavy aggregates like the Top Blown Rotary Converter or prepare access routes for internal transport of the raw material needed. An area of approximately 500 $m^2$ is considered as enough space for the demanded process. On top of the groundwork a framework needs to be built in order to mount different aggregates like the exhaust gas system. The additional installations cover smaller costs like a necessary crane, safety measures, lightning, tools, working space or cleaning equipment.

The expected realistic costs per square meter are 150 € or 180 USD/$m^2$. The additional Installations are specified with 50,000 USD. In the best case model the demanded area is 20 % below the realistic scenario. The lowest possible price per area is assumed with 120 USD, while the best price for the additional installations is expected with 30,000 USD. In the worst case scenario an area of 600 $m^2$ is necessary at a price of 200 €/$m^2$. Table 7.1 shows the expected costs for all three developed models covering all expenses for groundwork, framework and additional installations.

Table 7.1: Expected costs for groundwork, framework and additional installations

| | Unit | Best case | Realistic case | Worst case |
|---|---|---|---|---|
| Required space | [$m^2$] | 400 | 500 | 600 |
| Price per area | [€/$m^2$] | 100 | 150 | 200 |
| Price per area | [USD/$m^2$] | 120 | 180 | 240 |
| Additional Installations | [USD] | 30,000 | 50,000 | 70,000 |
| Expenditure | [USD/$m^2$] | 78,000 | 140,000 | 214,000 |

## 7.2.2 Top Blown Rotary Converter

The TBRC is the main aggregate of the process and its price is strongly dependent on its size. To process 38,000 t/year, 9.05 t per charge (assumption: 300 working days, 7 charges per working day and 2 aggregates) are necessary. The mass ratio of lead to slag is 3:1 and additional fluxes are added to the slag as well. This means around 27 t lead, 9 t of slag and around 1 t of fluxes have to fit into the TBRC. The known density of lead (11,3 g/cm$^3$) and an approximate density of the slag with the fluxes (2,8 g/cm$^3$) adds up to 6 m$^3$ of useable volume. At a filling level of around 45 % the total volume of the TBRC is between 13-15 m$^3$. The following numbers represent an offer of Andritz with a full setup including a methane-oxygen burner and installations.

The expected costs of all three models for the TBRC are illustrated in Table 7.2. The total expenditure for two aggregates adds up to approximately 14 million USD in the realistic case. The left column of the table shows the lowest expected costs of two TBRCs. The best expected price is a discount of 20 % with regard to the realistic case. The highest expected price for the two TBRCs is a raise of 20 % of the realistic costs.

Table 7.2: Expected costs of the Top Blown Rotary Converter

| | Unit | Best case | Realistic case | Worst case |
|---|---|---|---|---|
| Slag amount | [t/year] | 38,000 | 38,000 | 38,000 |
| Size TBRC | [t/charge] | 9.05 | 9.05 | 9.05 |
| Amount TBRC | [units] | 2 | 2 | 2 |
| Price/TBRC | [€/unit] | 4,720,000 | 5,900,000 | 7,080,000 |
| Price/TBRC | [USD/unit] | 5,664,000 | 7,080,000 | 8,496,000 |
| Expenditure | [USD] | 11,028,000 | 13,860,000 | 16,692,000 |

## 7.2.3 Storages, hoppers and internal transport

The expected demand of material storage is geared to the estimated throughput. It is requested, that enough raw material to run the process for 2-3 weeks should be stored in the material storage to prevent downtimes caused by delivery delay. A rough estimation recommends around 1,800 m$^3$ of storage room for slag and coke, 300 m$^3$ room for lime and an additional 10 m$^3$ room for sand. Furthermore, a wheel loader to transport the raw materials to the TBRC is necessary.

The expected costs in all three considered cases are shown in Table 7.3. In the realistic case the material storage is valued with 72,000 USD, the big lime hopper costs 120,000 USD, the small sand hopper is estimated with 18,000 USD and the wheel loader costs 72,000 USD. The left column of Table 7.3 illustrates the best case scenario in this section. The total capital

costs of storage room, hoppers and internal transport add up to 224,000 USD, which is significantly lower than in the realistic case. The right column represents the costs in the worst case scenario. All hopperst cost 165,600 USD, the material storage costs 90,000 USD and the highest expected price for the wheel loader is 84,000 USD. [28; 29]

Table 7.3: Specification of the expected CAPEX concerning storages, hoppers and internal transport

| | Unit | Best case | Realistic case | Worst case |
|---|---|---|---|---|
| Material storage | | | | |
| Area | [$m^2$] | 300 | 300 | 300 |
| Height | [m] | 6 | 6 | 6 |
| Volumina | [$m^3$] | 1,800 | 1,800 | 1,800 |
| Cost/area | [€/$m^2$] | 150 | 200 | 250 |
| Cost/area | [USD/$m^2$] | 180 | 240 | 300 |
| Expenditure storage | [USD] | 54,000 | 72,000 | 90,000 |
| Lime hopper | | | | |
| Size | [$m^3$] | 300 | 300 | 300 |
| Cost/unit | [€/unit] | 80,000 | 100,000 | 120,000 |
| Cost/unit | [USD/unit] | 96,000 | 120,000 | 144,000 |
| Expenditure lime hopper | [USD] | 96,000 | 120,000 | 144,000 |
| Sand hopper | | | | |
| Size | [$m^3$] | 10 | 10 | 10 |
| Cost/unit | [€/unit] | 12,000 | 15,000 | 18,000 |
| Cost/unit | [USD/unit] | 14,400 | 18,000 | 21,600 |
| Expenditure sand hopper | [USD] | 14,400 | 18,000 | 21,600 |
| Wheel loader | | | | |
| Price/unit | [€/unit] | 50,000 | 60,000 | 70,000 |
| Price/unit | [USD/unit] | 60,000 | 72,000 | 84,000 |
| Units | [1] | 1 | 1 | 1 |
| Expenditure wheel loader | [USD] | 60,000 | 72,000 | 84,000 |
| Sum Expenditures | [USD] | 224,400 | 282,000 | 339,600 |

## 7.2.4 Exhaust gas system

The costs of the exhaust gas system are dependent on the composition of the flue gas and its quantity. The composition is rather uncritical and due to the combustion with methane and pure oxygen the quantity of the exhaust gas is minimized as well. As seen in section 6 the approximate exhaust gas flow is 1,859 $Nm^3/h$. To estimate the costs of the exhaust gas system the composition and the quantity was compared to other similar offers. The realistic costs for a whole off-gas treatment including a hot gas quench, a baghouse filter and other cleaning aggregates, is valued with 950,000 USD. To be prepared for any uncertainties the worst case is numbered with 1,080,000 USD and the best case with 820,000 USD.

### 7.2.5 Total Capital Expenditures

The necessary expenditures of the above described categories are summarized in this section. It also includes the category “balance of plant” which covers all system components, not included in the primary system itself. This includes all blowers, compressors, pumps, safety measures or control equipment. It is estimated with an additional 10 % of the calculated capital expenditures. A complete listing of all capital expenditures in all three scenarios is shown in Table 7.4 underneath.

Table 7.4: Listing of all necessary capital expenditures in three simulated scenarios

| | Unit | Best case | Realistic case | Worst case |
|---|---|---|---|---|
| Ground work, frame work and installations | [USD] | 78,000 | 140,000 | 214,000 |
| Top Blown Rotary Converter | [USD] | 11,028,000 | 13,860,000 | 16,692,000 |
| Storages and internal transport | [USD] | 224,400 | 282,000 | 339,600 |
| Exhaust gas system | [USD] | 820,000 | 950,000 | 1,080,000 |
| Sum CAPEX | [USD] | 12,150,400 | 15,232,000 | 18,325,600 |
| Balance of plant | [USD] | 1,215,040 | 1,523,200 | 1,832,560 |
| Total Capital Expenditures | [USD] | 13,365,440 | 16,755,200 | 20,158,160 |

The shares of all categories on the total amount of the capital expenditures are illustrated in Figure 7.1 below. It can be seen that the largest part by far is the expenditure on the Top Blown Rotary Converter with 82.7 %.

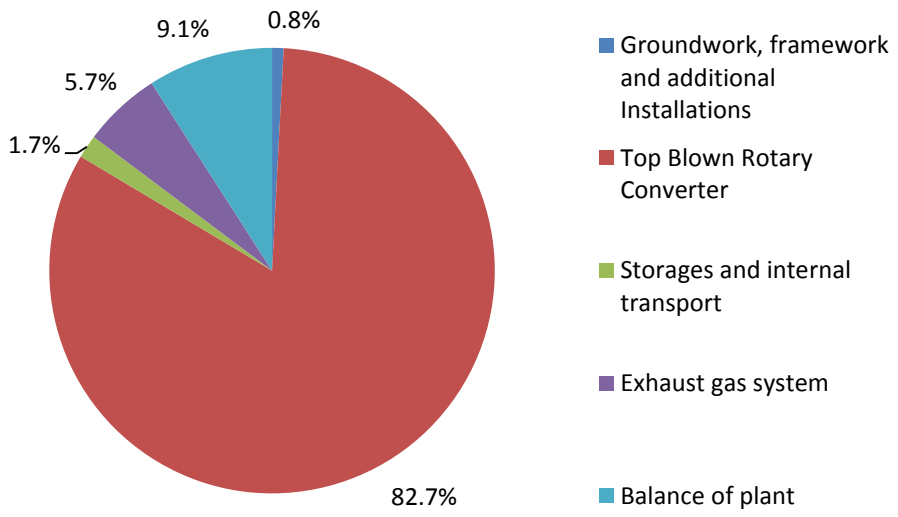


Figure 7.1: Shares of different capital expenditures in the realistic scenario

## 7.3 Operational Expenditures ISF slag

The following section is dedicated to the calculation of all operational expenditures. Since two scenarios are simulated, the first part treats all involved costs of recycling ISF slag with the composition listed in Table 3.2. The ISF slag contains 8.0 wt.-% zinc, 1.76 wt.-% lead and 20 ppm silver. The content of valuables is significantly lower than in the Blast Furnace slag, which is described further on in section 7.6.

### 7.3.1 Raw material

The calculation of the required raw materials uses data of the energy and mass balance. It is assumed that the residue in the form of lead slag is available for free. Coke is only used to reduce zinc oxide and lead oxide. The needed amount of coke is linked to the stoichiometric demand. It is necessary to obtain lead although it is a product, because the silver content of the slag dissolves in the lead bath and the silver enriched lead is the saleable product. Unloaded lead is therefore needed to run the process. It is assumed that the lead bath is completely replaced every seventh working day. The substitution of loaded lead with the unloaded lead is not performed all at once, but batch-wise.

The lead price varies in the three different scenarios. It may irritate that the lead price is assumed higher in the best case scenario and lower in the worst case scenario, causing lower expenditures at the worst case scenario and vice versa. The reason for these assumptions is the overall balance of lead. The amount of sold lead is higher than the purchased amount. At a holistic scenario view the prices of the purchased raw material have to be identical with the price of the products, because of the low period of time between buying and selling. Overall it is advantageous for the economic evaluation of the process, if the lead price is higher. This is the reason for the irritating higher prices at the best price scenarios and vice versa.

Additionally to coke and lead, two different fluxes are added to the feed material. According to the results of section 5.4 concerning the lead settling and zinc fuming rate the optimum composition was chosen for the model in all three scenarios. The prices of those fluxes vary in the three different cases.

In the realistic case a stoichiometric factor of 1.5 is assumed. This means that 50 wt.-% additional coke is introduced to the process, than theoretically needed. The coke price in the realistic scenario is assumed to be 156 USD/t. The lead price in this scenario is 2,100 USD/t, and the prices for sand and lime are 12 USD/t and 132 USD/t. The overall expenditure on raw materials is 5,609,591 USD per year in the realistic scenario, as seen in the central column of Table 7.5 below. [30]

In the best case scenario the stoichiometry factor amounts 1.3. This saves around 140 t coke per year. All other quantities remain unchanged, only the prices vary. Lead costs are assumed to amount 2,400 USD/t and coke prices come to 132 USD/t. The prices of the fluxes are assumed to be 88 €/t for the lime and 8 €/t for the sand. The total raw material expenditures in the best case scenario amount 6,151,584 USD/year and are listed in the left column of Table 7.5 underneath.

Similar to the best case scenario above the stoichiometry factor is changed to 1.7 in the worst case model. This leads to an increased coke amount of 1,194 t/year. The different assumed prices are 168 USD/t for coke, 1,700 USD/t for lead, 14.4 USD/t for sand and 158.4 USD/t for lime. The right column of Table 7.5 shows the calculations of the operational expenditures for the worst case scenario. The total necessary expenditure is 4,826,782 USD/year.

Table 7.5: The expected raw materials expenses of all three scenarios per year

| | Unit | Best case | Realistic case | Worst case |
|---|---|---|---|---|
| Amount lead slag | [t/year] | 38,000.00 | 38,000.00 | 38,000.00 |
| Price lead slag | [€/t] | 0 | 0 | 0 |
| Price lead slag | [USD/t] | 0 | 0 | 0 |
| Expenditure lead slag | [USD/year] | 0 | 0 | 0 |
| Stoichiometric coke demand | [t/year] | 703 | 703 | 703 |
| Stoichiometry factor | [C/red] | 1.3 | 1.5 | 1.7 |
| Actual coke demand | [t/year] | 913 | 1,054 | 1,194 |
| Price coke | [€/t] | 110 | 130 | 140 |
| Price coke | [USD/t] | 132 | 156 | 168 |
| Expenditure coke | [USD/year] | 120,574 | 164,419 | 200,676 |
| Amount lead bath | [t/year] | 2,327 | 2,327 | 2,327 |
| Price lead bath | [€/t] | 2,000 | 1,750 | 1,500 |
| Price lead bath | [USD/t] | 2,400 | 2,100 | 1,700 |
| Expenditure lead bath | [USD/year] | 5,583,673 | 4,885,714 | 3,955,102 |
| Amount sand | [t/year] | 24 | 24 | 24 |
| Price sand | [€/t] | 8 | 10 | 12 |
| Price sand | [USD/t] | 9.6 | 12 | 14.4 |
| Expenditure sand | [USD/year] | 230 | 287 | 345 |
| Amount lime | [t/year] | 4,234 | 4,234 | 4,234 |
| Price lime | [€/t] | 88 | 110 | 132 |
| Price lime | [USD/t] | 105.6 | 132 | 158.4 |
| Expenditure lime | [USD/year] | 447,106 | 558,883 | 670,659 |
| Total expenditure raw materials | [USD/year] | 6,151,584 | 5,609,303 | 4,826,782 |

## 7.3.2 Burning gases

The numbers of the required gas quantity were calculated in the mass and energy balance, in section 6. The calculated values represent the demanded amount of gas without any heat losses and 100 % efficiency. Therefore, the actual required amount of gas is the theoretical quantity, divided by the assumed efficiency of the particular scenario. Additionally to the different quantities of methane and oxygen, the prices of the respective gases vary in each model as well.

In the realistic scenario the prices of methane and oxygen are assumed to be 0.42 USD/$Nm^3$ and 0.20 USD/$Nm^3$. With an overall efficiency of 80 %, a total expenditure on burning gases of 3,068,526 USD/year is necessary, as seen in the middle column of Table 7.6 below. [31]

At the best case scenario the efficiency of the combustion increases to 85 %, which decreases the demanded amount of gas. The prices for methane and oxygen decrease to 0.34 USD/$Nm^3$ and 0.17 USD/$Nm^3$. The sum of expenditures lowers to 2,343,917 USD/year, as stated in the left column of Table 7.6. The right column of Table 7.6 underneath shows the calculation of the expenses for burning gases in the worst case scenario. In this scenario the total efficiency is assumed to be only 75 %. The gas prices are assumed to be 0.54 USD/$Nm^3$ for methane and 0.24 USD/$Nm^3$ for oxygen. These higher prices affect the overall expenditure for burning gases in the worst case scenario. [31]

Table 7.6: Expected expenditures per year on burning gases of all three models [31]

| | Unit | Best case | Realistic case | Worst case |
|---|---|---|---|---|
| Amount natural gas | [$Nm^3$/year] | 3,486,664 | 3,704,580 | 3,951,552 |
| Price natural gas | [€/$Nm^3$] | 0.28 | 0.35 | 0.45 |
| Price natural gas | [USD/$Nm^3$] | 0.34 | 0.42 | 0.54 |
| Total efficiency | [1] | 0.85 | 0.8 | 0.75 |
| Expenditure natural gas | [USD/year] | 1,171,519 | 1,555,924 | 2,133,838 |
| Amount oxygen | [$Nm^3$/year] | 6,978,558 | 7,414,718 | 7,909,032 |
| Price oxygen | [€/$Nm^3$] | 0.14 | 0.17 | 0.2 |
| Price oxygen | [USD/$Nm^3$] | 0.17 | 0.20 | 0.24 |
| Total efficiency | [1] | 0.85 | 0.8 | 0.75 |
| Expenditure oxygen | [USD/year] | 1,172,398 | 1,512,602 | 1,898,168 |
| Total expenditure burning gases | [USD/year] | 2,343,917 | 3,068,526 | 4,032,006 |

## 7.3.3 Refractory material

Refractories are necessary to shield the reaction chamber from the surrounding and to prevent damages on the expensive Top Blown Rotary Converter. As the slag is not particularly aggressive towards the refractory material, a new lining every 8 months seems realistic. The renewal of the refractories is a big cost driver, not because the material is that

expensive, but because of the downtimes it causes. A large part of the 60 days of downtime is scheduled because of the renewal of refractory linings. The stated price for a new refractory lining comes out of an offer of a refractory company called RHI AG and is used in all three scenarios.
As mentioned before, the estimated period of renewal is 8 months in the realistic scenario, which equals 1.5 linings per year and TBRC. The result of the realistic cost estimation per year is 180,000 USD, as illustrated in Table 7.7 below.

In the best case scenario a replacement of the refractory material is only necessary once a year. The left column of Table 7.7 shows the lower estimated expenses in this scenario.

The worst case scenario assumes a necessary renewal period of 6 months. This causes higher costs of 240,000 USD/year, which can be seen in the right column of Table 7.7 underneath.

Table 7.7: Three expenditure models covering expected refractory expenses per year

| | Unit | Best case | Realistic case | Worst case |
|---|---|---|---|---|
| Needed linings | [linings/year] | 1 | 1.5 | 2 |
| Amount TBRC | [units] | 2 | 2 | 2 |
| Price per lining | [€/lining] | 50,000 | 50,000 | 50,000 |
| Price per lining | [USD/lining] | 60,000 | 60,000 | 60,000 |
| Expenditure refractories | [USD/year] | 120,000 | 180,000 | 240,000 |

### 7.3.4 Internal transport

The internal transport costs cover all expenses that are related to moving goods from storages or hoppers to the furnace or the loading process of products on trucks or trains. The amounts of moving goods change slightly in the different models, due to the changing stoichiometric factors of coke and the changing lead settling-, and zinc fuming rate, which influence the quantity of manufactured products.

In the realistic cost model an expenditure of 2 USD per moved good is assumed. Table 7.8 shows the amount of raw material and products needed to transport and the estimated amount of expenditures being 108,219 USD/year.

The best case scenario shows a lower amount of needed raw material, but a higher amount of products paired with lower assumed expenses of 1 USD/t. This leads to lower expenditures of 54,192 USD/year, as stated in the left column of Table 7.8.

In the worst case model, the amount of raw material is slightly higher and the amount of products is marginally lower compared to the realistic scenario. Additionally the estimated

cost of 3 USD per transported ton is higher, which causes costs of 163,725 for internal transport as listed in the right column of Table 7.8 below.

Table 7.8: Expected expenditure on internal transport per year in all three scenarios

| | Unit | Best case | Realistic case | Worst case |
|---|---|---|---|---|
| Amount raw materials | [t/year] | 45,498 | 45,638 | 46,137 |
| Amount products | [t/year] | 8,694 | 8,471 | 8,438 |
| Price per transported mass | [€/t] | 0.83 | 1.67 | 2.50 |
| Price per transported mass | [USD/t] | 1 | 2 | 3 |
| Expenditure internal transport | [USD/year] | 54,192 | 108,219 | 163,725 |

### 7.3.5 Maintenance

The maintenance costs are rather hard to estimate. Prices of service-, maintenance- or repair works can vary and it is also difficult to predict what damages might occur in the future. To be on the safe side a rather conservative method of linking the maintenance costs to the necessary realistic capital expenditures is chosen.

The realistic model assumes annual maintenance costs at an amount of 5 % of the realistic capital expenditures. The central column of Table 7.9 shows the annual maintenance costs in USD/year.

The anticipated annual maintenance costs in the best case scenario are 502,656 USD, which equals 3 % of the realistic capital expenditure, as calculated in the left column of Table 7.9 underneath.

In the worst case scenario 7 % of the expected capital expenditure per year is spent on maintenance costs. The right column of Table 7.9 shows the result of the expected annual maintenance expenditure.

Table 7.9: Estimated expenditure on maintenance in all three scenarios

| | Unit | Best case | Realistic case | Worst case |
|---|---|---|---|---|
| Proportional costs | [% CAPEX/year] | 3 | 5 | 7 |
| Realistic CAPEX | [USD] | 16,755,200 | 16,755,200 | 16,755,200 |
| Expenditure maintenance | [USD/year] | 502,656 | 837,760 | 1,172,864 |

### 7.3.6 Labour

The first step to calculate the labour costs of the process is to develop a shift model, define the downtimes and working days and estimate the need of employees and workers. The experience shows that scheduled and unscheduled downtimes of an industrial operation are often in the range of 60 days per year. It was estimated that there are 300 working days per

year. A two-shift operation was chosen, to avoid a third and expensive night shift. Each shift lasts 8 hours, which equals 4,800 working hours. In this model the TBRC is set on holding mode over the remaining hours. It is assumed that the temperature of the holding mode is approximately 400 °C to keep the lead bath liquid at all times.

One manager is supposed to be in charge over the whole administration of the process, run the organisation and lead the co-workers. Every shift needs one shift leader and two workers to run the process. The shift leader is responsible for a smooth running operation and has to know all procedures in detail. The two workers per shift (one for every TBRC), which are named “Blue colour” need to take care of the charging process and the internal transport of all supplies. The deslagging and charging process takes place every 135 minutes, which gives the workers enough time in between to complete other necessary tasks, like transporting the raw materials and mixing them. There are three shift leaders and six Blue Colours needed to run the process over the whole year. Two shift leaders and four Blue Colours are working every day, while the third team is on their day off. This way a smooth operation can be guaranteed. One additional worker is needed to guard the process in the holding mode overnight. This worker needs to be equipped with a dead man’s switch, in order to be allowed to work alone. The two Blue Colours left are taking turns on the overnight shift. The salaries of the respective employees vary in every case scenario, but the amount of employees stays constant. All salaries include non-wage labour costs and social security contributions. The salary assumptions are based on Central European wages and can be significantly lower in developing countries.

In the realistic case the salary of the manager is 78,000 USD/year, the salaries of the shift leaders are 54,000 USD/year and the salaries of the Blue Colours are 42,000 US/year. Those salaries multiplied with the respective number of employees add up to annual labour costs of 576,000 USD, as listed underneath in the central column of Table 7.10 below.
In the best case scenario the salaries of the workers are assumed lower. The manager receives a salary of 72,000 USD/year, the shift leaders receive 48,000 USD/year and the Blue Colours receive 36,000 USD/year. These measures lower the annual personnel costs to 504,000 USD, as shown in the left column Table 7.10 underneath.

The salaries in the worst case scenario are representing usual labour costs in the metallurgical branch of Central Europe. The manager is paid a salary of 84,000 USD/year, the shift leaders are paid 60,000 USD/year and the Blue Colours receive 48,000 USD/year. The right column of Table 7.10 below shows the calculation of the labour costs with a total amount of 648,000 USD/year.

Table 7.10: Estimated labour costs per year in all three considered scenarios

| | Unit | Best case | Realistic case | Worst case |
|---|---|---|---|---|
| Working days | [days/year] | 300 | 300 | 300 |
| Shifts | [shifts/day] | 2 | 2 | 2 |
| Hours per shift | [hours/shift] | 8 | 8 | 8 |
| Total working hours per year | [hours/year] | 4,800 | 4,800 | 4,800 |
| Needed mangers | [1] | 1 | 1 | 1 |
| Needed shift leaders | [1] | 3 | 3 | 3 |
| Needed Workers | [1] | 8 | 8 | 8 |
| Salary manager | [€/year] | 60,000 | 65,000 | 70,000 |
| Salary manager | [USD/year] | 72,000 | 78,000 | 84,000 |
| Salary shift leader | [€/year] | 40,000 | 45,000 | 50,000 |
| Salary shift leader | [USD/year] | 48,000 | 54,000 | 60,000 |
| Salary blue colour | [€/year] | 30,000 | 35,000 | 40,000 |
| Salary blue colour | [USD/year] | 36,000 | 42,000 | 48,000 |
| Expenditure manager | [€/year] | 60,000 | 65,000 | 70,000 |
| Expenditure manager | [USD/year] | 72,000 | 78,000 | 84,000 |
| Expenditure shift leader | [€/year] | 120,000 | 135,000 | 150,000 |
| Expenditure shift leader | [USD/year] | 144,000 | 162,000 | 180,000 |
| Expenditure blue colour | [€/year] | 240,000 | 280,000 | 320,000 |
| Expenditure blue colour | [USD/year] | 288,000 | 336,000 | 384,000 |
| Total expenditure labour | [USD/year] | 504,000 | 576,000 | 648,000 |

### 7.3.7 Total Operational Expenditures

Table 7.11 lists the annual total operational expenditures of all three calculated scenarios. The difference between the best case- and the worst case scenario is around 1,500,000 USD/year.

Table 7.11: Total operational expenditures in all three scenarios

| | Unit | Best case | Realistic case | Worst case |
|---|---|---|---|---|
| Raw material | [USD/year] | 6,151,584 | 5,609,303 | 4,826,782 |
| Refractory | [USD/year] | 120,000 | 180,000 | 240,000 |
| Burning gases | [USD/year] | 2,343,917 | 3,068,526 | 4,032,006 |
| Labour | [USD/year] | 504,000 | 576,000 | 648,000 |
| Maintenance | [USD/year] | 502,656 | 837,760 | 1,172,864 |
| Internal transport | [USD/year] | 54,192 | 108,219 | 163,725 |
| Total OPEX | [USD/year] | 9,676,348 | 10,379,809 | 11,083,377 |

Figure 7.2 illustrates the share of all individual operational expenditures on the total operational expenditure. Clearly the largest part of the costs are the raw materials (56.4 %) followed by the burning gases (26.5 %). Those two main cost drivers are responsible for more than 80 % of the total operational expenditures. The maintenance costs and the labour

costs are also important for the economic evaluation of the process, whereas internal transport and refractories only play a minor role of the total operational expenses.

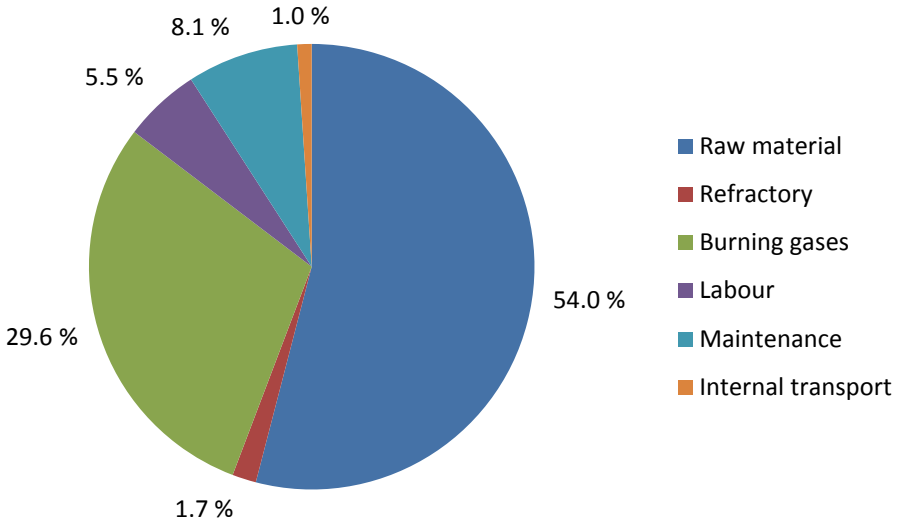


Figure 7.2: The share of different operational expenditures on the total operational expenditure

## 7.4 Revenues ISF slag

The created revenues of the slag split up in three valuables: lead, zinc and silver. The possible lead revenue is dependent on the lead content of the slag, the settling rate and the realized price. Additionally the purchased lead is sold again, to the same price. The zinc revenue is also dependent on the slag content, the fuming rate and the market price. The estimated settling rate of lead and fuming rate of zinc is not consistent to the determined value in the resistance furnace, because of different conditions between the furnaces. Due to the improved mixing and a higher specific surface the values are significantly improved.

In the recycling business it is a frequent practice to sell a precious metal like silver dissolved in a collecting metal. Furthermore, it is common practice not to pay the price for the full silver content dissolved in the lead bath. The sold product is analysed for silver and 50 ppm are not charged and deducted of the original content. Every concentration value beyond 50 ppm is charged to the full silver price. The silver settling rate is assumed to be 95 % in all three scenarios.

In the realistic scenario a lead settling rate of 90 % and a zinc fuming rate of 85 % is assumed. The price for lead is 2,100 USD/t, the zinc oxide price is 1,550 USD/t and the silver price is 20 USD/fine ounce. The valuables content in the slag are equivalent in all three scenarios. The middle column of Table 7.12 shows the calculated expected annual revenues of 11,524,575 USD. [30; 32; 33]

The calculation of the best case scenario is shown in the left column of Table 7.12. In this model the settling rate of lead increases to 95 % and the zinc fuming rate increases to 90 %. In combination with the higher assumed prices for lead (2,400 USD/t), zinc (1,800 USD/t) and silver (25 USD/fine ounce), a significantly higher revenue can be gained. [30; 32; 33]

The lead settling rate, the zinc fuming rate and the prices for all products are decreased in the worst case scenario. This leads to a considerably dropped total revenue of 9,148,931 USD/year. The lead settling rate is 85 % and the zinc fuming rate is 85 %. The lead market price is assumed to amount 1,800 USD/t, the zinc oxide price amounts 1,250 USD/t and the zinc price amounts 15 USD/fine ounce: [30; 32; 33]

Table 7.12: Expected revenues of the valuables in all three scenarios

| | Unit | Best case | Realistic case | Worst case |
|---|---|---|---|---|
| Lead slag content | [t/year] | 669 | 669 | 669 |
| Efficiency | [%] | 95 | 90 | 85 |
| Settled lead | [t/year] | 635 | 602 | 568 |
| Lead bath | [t/year] | 2,327 | 2,327 | 2,327 |
| Total amount of lead | [t/year] | 2,962 | 2,928 | 2,895 |
| Market price | [€/t] | 2,000.00 | 1,750.00 | 1,416.67 |
| Market price | [USD/t] | 2,400 | 2,100 | 1,700 |
| Revenues lead | [USD/year] | 7,108,537 | 6,149,746 | 4,921,518 |
| Zinc oxide slag content | [t/year] | 3,784 | 3,784 | 3,784 |
| Efficiency | [%] | 90 | 85 | 80 |
| Zinc oxide | [t/year] | 3,406 | 3,216 | 3,027 |
| Market price | [€/t] | 1,500 | 1,291.67 | 1,083.33 |
| Market price | [USD/t] | 1,800 | 1,550 | 1,300 |
| Revenues zinc oxide | [USD/year] | 6,129,967 | 4,985,328 | 3,935,288 |
| Silver slag content | [t/year] | 0.76 | 0.76 | 0.76 |
| Settling rate | [%] | 95 | 95 | 95 |
| Silver concentration | [ppm] | 310.33 | 310.33 | 310.33 |
| Saleable silver content | [ppm] | 260.33 | 260.33 | 260.33 |
| Amount saleable | [t/year] | 0.61 | 0.61 | 0.61 |
| Fine ounce/ton | [oz/t] | 32,154.34 | 32,154.34 | 32,154.34 |
| Saleable silver content | [oz/year] | 19,475 | 19,475 | 19,475 |
| Market price | [€/oz] | 20.83 | 16.67 | 12.50 |
| Market price | [USD/oz] | 25 | 20 | 15 |
| Revenues silver | [USD/year] | 486,876 | 389,501 | 292,125 |
| Total revenues | [USD/year] | 13,725,381 | 11,524,575 | 9,148,931 |

The gained revenues of the three valuable metals are shown in Figure 7.3. At the composition of the ISF slag the largest profit is generated by lead. Silver plays a minor role at this composition of the slag.

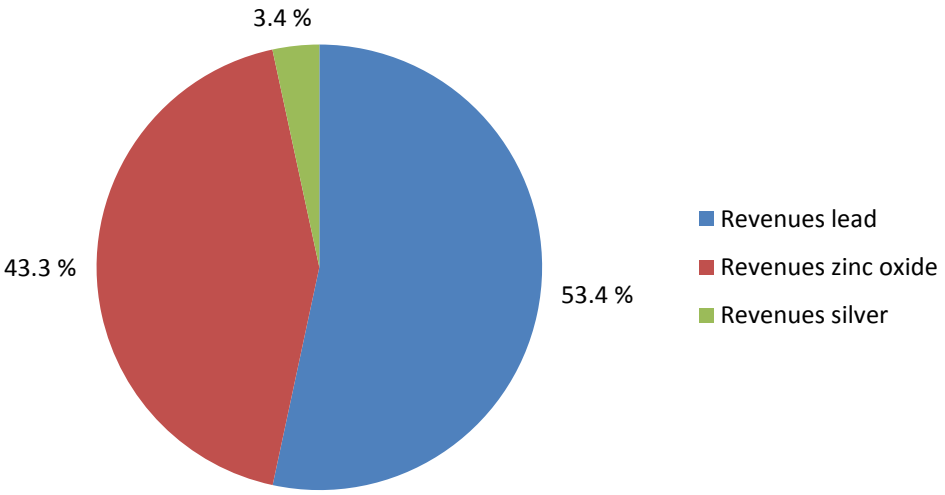


Figure 7.3: The share of revenues of the three valuable metals on the total revenues

Table 7.13 below, summarises all expected revenues of every valuable metal in all three case scenarios.

Table 7.13: Results of the expected revenues per metal in all three case scenarios of the ISF slag

| | Unit | Best case | Realistic case | Worst case |
|---|---|---|---|---|
| Revenues lead | [USD/year] | 7,108,537 | 6,149,746 | 4,921,518 |
| Revenues zinc oxide | [USD/year] | 6,129,967 | 4,985,328 | 3,935,288 |
| Revenues silver | [USD/year] | 486,876 | 389,501 | 292,125 |
| Total revenues | [USD/year] | 13,725,381 | 11,524,575 | 9,148,931 |

## 7.5 Operational Expenditures Blast Furnace slag

Some operational expenses like refractory-, maintenance- or labour expenditures remain unchanged in this new slag. Due to a change of the main raw material (Blast Furnace slag), the slag composition changes and with it some operational expenditures like raw materials, burning gases and internal transport expenditures. All changes are documented and described in this section. All identical costs are listed in section 7.3 above.

### 7.5.1 Raw Materials

All calculations follow the same principle as described in section 7.3.1. The only difference is the significant increase in coke demand, due to the higher amount of zinc oxide and lead oxide in the Blast Furnace slag compared to the ISF slag. The increased demand of coke has impacts on the total expenditures as well. The central column of Table 7.14 shows that the sum of all raw material expenses increases to 5,655,260 USD/year in the realistic scenario.

The left and right column of Table 7.14 list all necessary expenses for raw materials in order to run the process. All assumptions are identical to the best case and worst case scenario of the ISF slag in Table 7.5. [30]

Table 7.14: Raw material expenditures in all three scenarios of the Blast Furnace slag

| | Unit | Best case | Realistic case | Worst case |
|---|---|---|---|---|
| Amount lead slag | [t/year] | 38,000.00 | 38,000.00 | 38,000.00 |
| Price lead slag | [€/t] | 0 | 0 | 0 |
| Price lead slag | [USD/t] | 0 | 0 | 0 |
| Expenditure lead slag | [USD/year] | 0 | 0 | 0 |
| Stoichiometric coke demand | [t/year] | 899 | 899 | 899 |
| Stoichiometry factor | [C/red] | 1.3 | 1.5 | 1.7 |
| Actual coke demand | [t/year] | 1,169 | 1,349 | 1,528 |
| Price coke | [€/t] | 110 | 130 | 140 |
| Price coke | [USD/t] | 132 | 156 | 168 |
| Expenditure coke | [USD/year] | 154,275 | 210,375 | 256,766 |
| Amount lead bath | [t/year] | 2,327 | 2,327 | 2,327 |
| Price lead bath | [€/t] | 2,000 | 1,750 | 1,417 |
| Price lead bath | [USD/t] | 2,400 | 2,100 | 1,700 |
| Expenditure lead bath | [USD/year] | 5,583,673 | 4,885,714 | 3,955,102 |
| Amount sand | [t/year] | 24 | 24 | 24 |
| Price sand | [€/t] | 8 | 10 | 12 |
| Price sand | [USD/t] | 9.6 | 12 | 14.4 |
| Expenditure sand | [USD/year] | 230 | 287 | 345 |
| Amount lime | [t/year] | 4,234 | 4,234 | 4,234 |
| Price lime | [€/t] | 88 | 110 | 132 |
| Price lime | [USD/t] | 105.6 | 132 | 158.4 |
| Expenditure lime | [USD/year] | 447,106 | 558,883 | 670,659 |
| Total expenditure raw materials | [USD/year] | 6,185,285 | 5,655,260 | 5,192,555 |

## 7.5.2 Burning gases

Due to minor changes of the slag composition the demand of burning gases changes slightly as well. The proceeding of the calculations however, is identical to the calculations of section 7.3.2. The calculated demand of burning gases for the Blast Furnace slag in the realistic scenario is shown in the middle column of Table 7.15.

The left and right columns list all necessary expenses for burning gases in order to run the process. All assumptions are identical to the best case and worst case scenario of the ISF slag in Table 7.6.

Table 7.15: Results of the calculated expenditures on burning gases in all three scenarios [31]

| | Unit | Best case | Realistic case | Worst case |
|---|---|---|---|---|
| Amount natural gas | [$Nm^3$/year] | 3,625,888 | 3,852,506 | 4,109,340 |
| Price natural gas | [€/$Nm^3$] | 0.28 | 0.35 | 0.45 |
| Price natural gas | [USD/$Nm^3$] | 0.34 | 0.42 | 0.54 |
| Total efficiency | [1] | 0.85 | 0.8 | 0.75 |
| Expenditure natural gas | [USD/year] | 1,218,298 | 1,618,053 | 2,219,044 |
| Amount oxygen | [$Nm^3$/year] | 7,257,216 | 7,710,792 | 8,224,844 |
| Price oxygen | [€/$Nm^3$] | 0.14 | 0.17 | 0.2 |
| Price oxygen | [USD/$Nm^3$] | 0.17 | 0.20 | 0.24 |
| Total efficiency | [1] | 0.85 | 0.8 | 0.75 |
| Expenditure oxygen | [USD/year] | 1,219,212 | 1,573,001 | 1,973,963 |
| Total expenditure burning gases | [USD/year] | 2,437,511 | 3,191,054 | 4,193,006 |

## 7.5.3 Refractory material

The assumptions of demanded refractory materials are exactly the same as in section 7.3.3. Therefore a new calculation is not necessary and the previous results are applied onto this section as well.

## 7.5.4 Internal transport

Due to a different slag composition and a higher share of valuables the quantities of raw materials and products change, compared to the ISF slag. The calculation method and the assumed prices of transport per model stay the same.
In the realistic approach a total expenditure for internal transport amounts 111,283.96 USD/year, as seen in the middle column of Table 7.16.

The left and right columns show the calculation of the expenditures on internal transport in the best case- and worst case scenario. They result in expenditures of 55,756 USD/year and 168,670 USD/year, as seen in Table 7.16 underneath.

Table 7.16: Expenditures on internal transport in all three scenarios

| | Unit | Best case | Realistic case | Worst case |
|---|---|---|---|---|
| Amount raw materials | [t/year] | 45,753 | 45,933 | 46,571 |
| Amount products | [t/year] | 10,002 | 9,709 | 9,652 |
| Price per transported mass | [€/t] | 0.83 | 1.67 | 2.50 |
| Price per transported mass | [USD/t] | 1 | 2 | 3 |
| Expenditure internal transport | [USD/year] | 55,756 | 111,284 | 168,670 |

### 7.5.5 Maintenance

The assumptions of future maintenance costs are exactly the same as in section 7.3.5. Therefore, a new calculation is not necessary and the previous results of maintenance costs are applied onto this section as well.

### 7.5.6 Labour

The assumptions concerning the demanded workforce and their salary are exactly identical to section 7.3.6. Therefore, a new calculation is not necessary and the previous results are applied onto this section as well.

### 7.5.7 Total Operational Expenditures

Table 7.17 adds up all the operational expenditures for all three scenarios. The difference between the best- and worst case model is with approximately 1,800,000 USD higher than in the operational expenditure calculation of the ISF slag.

Table 7.17: Expected total operational expenditure in all three developed scenarios

| | Unit | Best case | Realistic case | Worst case |
|---|---|---|---|---|
| Raw material | [USD/year] | 6,185,285 | 5,655,260 | 5,192,555 |
| Refractory | [USD/year] | 120,000 | 180,000 | 240,000 |
| Burning gases | [USD/year] | 2,437,511 | 3,191,054 | 4,193,006 |
| Labour | [USD/year] | 504,000 | 576,000 | 648,000 |
| Maintenance | [USD/year] | 502,656 | 837,760 | 1,172,864 |
| Internal transport | [USD/year] | 55,756 | 111,284 | 168,670 |
| Total OPEX | [USD/year] | 9,805,207 | 10,551,358 | 11,615,095 |

Figure 7.4 illustrates the ratios of different costs of the total operational expenditures. The largest parts of the annual operational expenditures are the expenditure on raw materials and the burning gases. The shares of partial costs are only slightly different compared to the ISF slag.

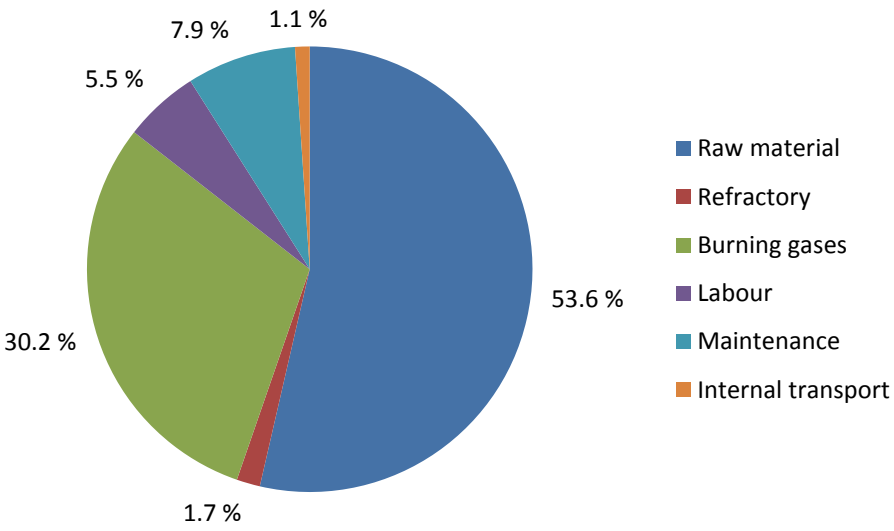


Figure 7.4: The distribution of all expected operational expenses

## 7.6 Revenues Blast Furnace slag

The revenues of the Blast Furnace (BF) slag are calculated analogous to section 7.4. All settling- and fuming rates, as well as the prices in the different scenarios remain unchanged. Due to the large influence of the valuable metal content in the slag, the result differs significantly from the revenues in the ISF slag.

The middle column of Table 7.18 shows the revenues of all three valuables in the realistic scenario. All three metals are expected to bring revenues over 6 million USD. Especially the significantly higher silver content of 300 ppm compared to 20 ppm in the ISF slag shows a huge effect. The expected annual total revenue in this scenario is 20,128,807 USD.

The best case scenario calculates with higher settling- and fuming rates and therefore higher product quantities. The left column of Table 7.18 illustrates the calculation of the expected revenues in the best case scenario. The total annual revenue is expected to amount 24,416,372 USD.

The right column of Table 7.18 lists all revenues of the calculated worst case scenario. The expected total revenue of this scenario is 15,664,135 USD/year.

Table 7.18: The expected revenues of the BF slag per year in all three scenarios [30; 32; 33]

| | Unit | Best case | Realistic case | Worst case |
|---|---|---|---|---|
| Lead slag content | [t/year] | 1,140 | 1,140 | 1,140 |
| Efficiency | [%] | 95 | 90 | 85 |
| Settled lead | [t/year] | 1,083 | 1,026 | 969 |
| Lead bath | [t/year] | 2,327 | 2,327 | 2,327 |
| Total amount of lead | [t/year] | 3,410 | 3,353 | 3,296 |
| Market price | [€/t] | 2,000 | 1,750 | 1,417 |
| Market price | [USD/t] | 2,400 | 2,100 | 1,700 |
| Revenues lead | [USD/year] | 8,182,873 | 7,040,314 | 5,602,402 |
| Zinc oxide slag content | [t/year] | 4,730 | 4,730 | 4,730 |
| Efficiency | [%] | 90 | 85 | 80 |
| Zinc oxide | [t/year] | 4,257 | 4,020 | 3,784 |
| Market price | [€/t] | 1,500 | 1,292 | 1,083 |
| Market price | [USD/t] | 1,800 | 1,550 | 1,300 |
| Revenues zinc oxide | [USD/year] | 7,662,459 | 6,231,661 | 4,919,110 |
| Silver slag content | [t/year] | 11.40 | 11.40 | 11.40 |
| Settling rate | [%] | 95 | 95 | 95 |
| Silver concentration | [ppm] | 3,230.40 | 3,230.40 | 3,230.40 |
| Saleable silver content | [ppm] | 3,180.40 | 3,180.40 | 3,180.40 |
| Amount saleable | [t/year] | 10.66 | 10.66 | 10.66 |
| Fine ounce/ton | [oz/t] | 32,154.34 | 32,154.34 | 32,154.34 |
| Saleable silver content | [oz/year] | 342,842 | 342,842 | 342,842 |
| Market price | [€/oz] | 20.83 | 16.67 | 12.50 |
| Market price | [USD/oz] | 25 | 20 | 15 |
| Revenues silver | [USD/year] | 8,571,040 | 6,856,832 | 5,142,624 |
| Total revenues | [USD/year] | 24,416,372 | 20,128,807 | 15,664,135 |

The shares of the three valuables on the revenue are evenly balanced. Figure 7.5 shows the distribution of the expected incomes in the realistic case scenario. The lead-, zinc oxide- and silver revenue are very balanced and each valuable metal represents approximately a third of the total expected revenue.

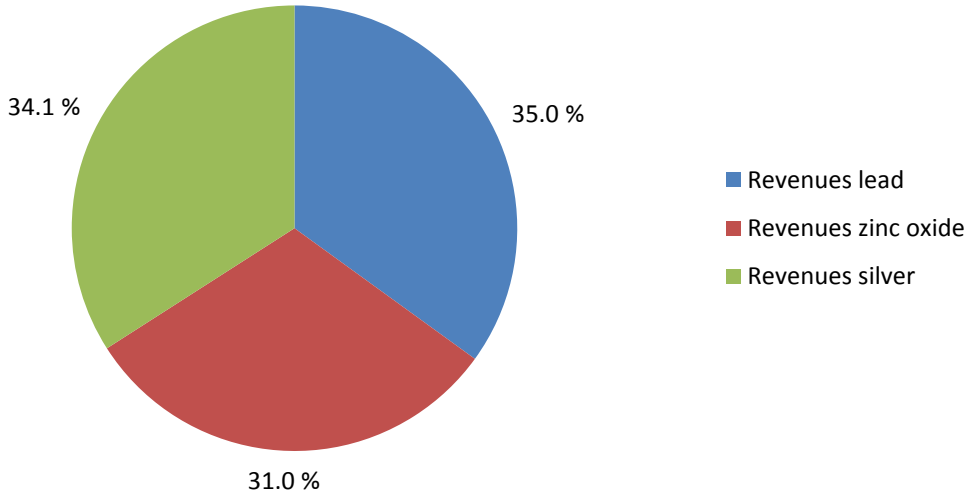


Figure 7.5: Distribution of the revenue in the realistic case scenario

A summary of all gained revenues in all three cases is published in Table 7.19 below.

Table 7.19: Result of the expected revenues per valuable metal in all three case scenarios of the Blast Furnace residue

| | Unit | Best case | Realistic case | Worst case |
|---|---|---|---|---|
| Revenues lead | [USD/year] | 8,182,873 | 7,040,314 | 5,602,402 |
| Revenues zinc oxide | [USD/year] | 7,662,459 | 6,231,661 | 4,919,110 |
| Revenues silver | [USD/year] | 8,571,040 | 6,856,832 | 5,142,624 |
| Total revenues | [USD/year] | 24,416,372 | 20,128,807 | 15,664,135 |

## 7.7 Net present value ISF slag

The following section deals with the economic evaluation of the process. According to the introduction in section 7 the projects lifetime is assume to be 20 years. The results of the calculated capital expenditures, operational expenditures and the expected revenues in all three scenarios are summarised in Table 7.20 below.

Table 7.20: Summary of the CAPEX, OPEX and the expected revenues in all three scenarios

| | Unit | Best case | Realistic case | Worst case |
|---|---|---|---|---|
| Total CAPEX | [USD] | 13,365,440 | 16,755,200 | 20,158,160 |
| Total OPEX | [USD/year] | 9,676,348 | 10,379,809 | 11,083,377 |
| Total revenues | [USD/year] | 13,725,381 | 11,524,575 | 9,148,931 |

The chosen capital budgeting method is the net present value method. In this method the expenses are deducted of the necessary expenses. The result is referred to as cash flow. Before calculating the free cash flow the expenditures and the revenues are inflation

adjusted. The future inflation rate is assumed to be 2 %. To calculate the net present value the cash flow has to be discounted to its present value. The net present value represents the net worth of the capital after the required rate of return has been subtracted. In the following calculations the discount rate is assumed to be 10 %. The following three tables show the calculation and result of the net present value at every year of the operation.

Table 7.21: The calculation of the net present value for every operation year in the realistic scenario

| Operation year | Calculated CAPEX/OPEX | Calculated revenues | Inflation rate | Cumulated inflation rate | Inflation adj. cost | Inflation adj. revenues | Annual cash flow | Discount rate | Discount factor | Discounted cash flow | Realistic case NPV |
|---|---|---|---|---|---|---|---|---|---|---|---|
| 0 | 16,755,200 | 0 | 2% | 1.00 | 16,755,200 | 0 | -16,755,200 | 10% | 1.00 | -16,755,200 | -16,755,200 |
| 1 | 10,379,809 | 11,524,575 | 2% | 1.02 | 10,587,405 | 11,755,067 | 1,167,662 | 10% | 1.10 | 1,061,510 | -15,693,690 |
| 2 | 10,379,809 | 11,524,575 | 2% | 1.04 | 10,799,153 | 11,990,168 | 1,191,015 | 10% | 1.21 | 984,310 | -14,709,380 |
| 3 | 10,379,809 | 11,524,575 | 2% | 1.06 | 11,015,136 | 12,229,971 | 1,214,835 | 10% | 1.33 | 912,724 | -13,796,656 |
| 4 | 10,379,809 | 11,524,575 | 2% | 1.08 | 11,235,439 | 12,474,571 | 1,239,132 | 10% | 1.46 | 846,344 | -12,950,313 |
| 5 | 10,379,809 | 11,524,575 | 2% | 1.10 | 11,460,148 | 12,724,062 | 1,263,914 | 10% | 1.61 | 784,791 | -12,165,521 |
| 6 | 10,379,809 | 11,524,575 | 2% | 1.13 | 11,689,351 | 12,978,544 | 1,289,193 | 10% | 1.77 | 727,716 | -11,437,806 |
| 7 | 10,379,809 | 11,524,575 | 2% | 1.15 | 11,923,138 | 13,238,114 | 1,314,977 | 10% | 1.95 | 674,791 | -10,763,015 |
| 8 | 10,379,809 | 11,524,575 | 2% | 1.17 | 12,161,601 | 13,502,877 | 1,341,276 | 10% | 2.14 | 625,715 | -10,137,299 |
| 9 | 10,379,809 | 11,524,575 | 2% | 1.20 | 12,404,833 | 13,772,934 | 1,368,102 | 10% | 2.36 | 580,209 | -9,557,091 |
| 10 | 10,379,809 | 11,524,575 | 2% | 1.22 | 12,652,929 | 14,048,393 | 1,395,464 | 10% | 2.59 | 538,012 | -9,019,079 |
| 11 | 10,379,809 | 11,524,575 | 2% | 1.24 | 12,905,988 | 14,329,361 | 1,423,373 | 10% | 2.85 | 498,884 | -8,520,196 |
| 12 | 10,379,809 | 11,524,575 | 2% | 1.27 | 13,164,108 | 14,615,948 | 1,451,840 | 10% | 3.14 | 462,601 | -8,057,595 |
| 13 | 10,379,809 | 11,524,575 | 2% | 1.29 | 13,427,390 | 14,908,267 | 1,480,877 | 10% | 3.45 | 428,957 | -7,628,637 |
| 14 | 10,379,809 | 11,524,575 | 2% | 1.32 | 13,695,938 | 15,206,432 | 1,510,495 | 10% | 3.80 | 397,760 | -7,230,877 |
| 15 | 10,379,809 | 11,524,575 | 2% | 1.35 | 13,969,856 | 15,510,561 | 1,540,705 | 10% | 4.18 | 368,832 | -6,862,044 |
| 16 | 10,379,809 | 11,524,575 | 2% | 1.37 | 14,249,254 | 15,820,772 | 1,571,519 | 10% | 4.59 | 342,008 | -6,520,036 |
| 17 | 10,379,809 | 11,524,575 | 2% | 1.40 | 14,534,239 | 16,137,188 | 1,602,949 | 10% | 5.05 | 317,135 | -6,202,901 |
| 18 | 10,379,809 | 11,524,575 | 2% | 1.43 | 14,824,923 | 16,459,931 | 1,635,008 | 10% | 5.56 | 294,071 | -5,908,831 |
| 19 | 10,379,809 | 11,524,575 | 2% | 1.46 | 15,121,422 | 16,789,130 | 1,667,708 | 10% | 6.12 | 272,684 | -5,636,147 |
| 20 | 10,379,809 | 11,524,575 | 2% | 1.49 | 15,423,850 | 17,124,913 | 1,701,062 | 10% | 6.73 | 252,852 | -5,383,295 |

Table 7.22: The calculation of the net present value for every operation year in the best case scenario

| Operation year | Calculated CAPEX/OPEX | Calculated revenues | Inflation rate | Cumulated inflation rate | Inflation adj. cost | Inflation adj. revenues | Annual cash flow | Discount rate | Discount factor | Discounted cash flow | Best case NPV |
|---|---|---|---|---|---|---|---|---|---|---|---|
| 0 | 13,365,440 | 0 | 2% | 1.00 | 13,365,440 | 0 | -13,365,440 | 10% | 1.00 | -13,365,440 | -13,365,440 |
| 1 | 9,676,348 | 13,725,381 | 2% | 1.02 | 9,869,875 | 13,999,888 | 4,130,013 | 10% | 1.10 | 3,754,557 | -9,610,883 |
| 2 | 9,676,348 | 13,725,381 | 2% | 1.04 | 10,067,273 | 14,279,886 | 4,212,613 | 10% | 1.21 | 3,481,499 | -6,129,384 |
| 3 | 9,676,348 | 13,725,381 | 2% | 1.06 | 10,268,618 | 14,565,484 | 4,296,866 | 10% | 1.33 | 3,228,299 | -2,901,085 |
| 4 | 9,676,348 | 13,725,381 | 2% | 1.08 | 10,473,990 | 14,856,793 | 4,382,803 | 10% | 1.46 | 2,993,513 | 92,428 |
| 5 | 9,676,348 | 13,725,381 | 2% | 1.10 | 10,683,470 | 15,153,929 | 4,470,459 | 10% | 1.61 | 2,775,803 | 2,868,231 |
| 6 | 9,676,348 | 13,725,381 | 2% | 1.13 | 10,897,140 | 15,457,008 | 4,559,868 | 10% | 1.77 | 2,573,927 | 5,442,158 |
| 7 | 9,676,348 | 13,725,381 | 2% | 1.15 | 11,115,082 | 15,766,148 | 4,651,066 | 10% | 1.95 | 2,386,732 | 7,828,890 |
| 8 | 9,676,348 | 13,725,381 | 2% | 1.17 | 11,337,384 | 16,081,471 | 4,744,087 | 10% | 2.14 | 2,213,152 | 10,042,042 |
| 9 | 9,676,348 | 13,725,381 | 2% | 1.20 | 11,564,132 | 16,403,100 | 4,838,969 | 10% | 2.36 | 2,052,195 | 12,094,237 |
| 10 | 9,676,348 | 13,725,381 | 2% | 1.22 | 11,795,414 | 16,731,162 | 4,935,748 | 10% | 2.59 | 1,902,945 | 13,997,181 |
| 11 | 9,676,348 | 13,725,381 | 2% | 1.24 | 12,031,323 | 17,065,786 | 5,034,463 | 10% | 2.85 | 1,764,549 | 15,761,730 |
| 12 | 9,676,348 | 13,725,381 | 2% | 1.27 | 12,271,949 | 17,407,101 | 5,135,152 | 10% | 3.14 | 1,636,218 | 17,397,948 |
| 13 | 9,676,348 | 13,725,381 | 2% | 1.29 | 12,517,388 | 17,755,243 | 5,237,855 | 10% | 3.45 | 1,517,220 | 18,915,168 |
| 14 | 9,676,348 | 13,725,381 | 2% | 1.32 | 12,767,736 | 18,110,348 | 5,342,612 | 10% | 3.80 | 1,406,877 | 20,322,044 |
| 15 | 9,676,348 | 13,725,381 | 2% | 1.35 | 13,023,091 | 18,472,555 | 5,449,465 | 10% | 4.18 | 1,304,558 | 21,626,603 |
| 16 | 9,676,348 | 13,725,381 | 2% | 1.37 | 13,283,552 | 18,842,006 | 5,558,454 | 10% | 4.59 | 1,209,682 | 22,836,284 |
| 17 | 9,676,348 | 13,725,381 | 2% | 1.40 | 13,549,223 | 19,218,846 | 5,669,623 | 10% | 5.05 | 1,121,705 | 23,957,989 |
| 18 | 9,676,348 | 13,725,381 | 2% | 1.43 | 13,820,208 | 19,603,223 | 5,783,015 | 10% | 5.56 | 1,040,126 | 24,998,115 |
| 19 | 9,676,348 | 13,725,381 | 2% | 1.46 | 14,096,612 | 19,995,288 | 5,898,676 | 10% | 6.12 | 964,481 | 25,962,596 |
| 20 | 9,676,348 | 13,725,381 | 2% | 1.49 | 14,378,544 | 20,395,194 | 6,016,649 | 10% | 6.73 | 894,337 | 26,856,932 |

Table 7.23: The calculation of the net present value for every operation year in the worst case scenario

| Operation year | Calculated CAPEX/OPEX | Calculated revenues | Inflation rate | Cumulated inflation rate | Inflation adj. cost | Inflation adj. revenues | Annual cash flow | Discount rate | Discount factor | Discounted cash flow | Worst case NPV |
|---|---|---|---|---|---|---|---|---|---|---|---|
| 0 | 20,158,160 | 0 | 2% | 1.00 | 20,158,160 | 0 | -20,158,160 | 10% | 1.00 | -20,158,160 | -20,158,160 |
| 1 | 11,083,377 | 9,148,931 | 2% | 1.02 | 11,305,045 | 9,331,910 | -1,973,135 | 10% | 1.10 | -1,793,759 | -21,951,919 |
| 2 | 11,083,377 | 9,148,931 | 2% | 1.04 | 11,531,146 | 9,518,548 | -2,012,598 | 10% | 1.21 | -1,663,304 | -23,615,223 |
| 3 | 11,083,377 | 9,148,931 | 2% | 1.06 | 11,761,769 | 9,708,919 | -2,052,850 | 10% | 1.33 | -1,542,336 | -25,157,559 |
| 4 | 11,083,377 | 9,148,931 | 2% | 1.08 | 11,997,004 | 9,903,097 | -2,093,907 | 10% | 1.46 | -1,430,166 | -26,587,726 |
| 5 | 11,083,377 | 9,148,931 | 2% | 1.10 | 12,236,944 | 10,101,159 | -2,135,785 | 10% | 1.61 | -1,326,154 | -27,913,880 |
| 6 | 11,083,377 | 9,148,931 | 2% | 1.13 | 12,481,683 | 10,303,182 | -2,178,500 | 10% | 1.77 | -1,229,707 | -29,143,587 |
| 7 | 11,083,377 | 9,148,931 | 2% | 1.15 | 12,731,317 | 10,509,246 | -2,222,071 | 10% | 1.95 | -1,140,274 | -30,283,860 |
| 8 | 11,083,377 | 9,148,931 | 2% | 1.17 | 12,985,943 | 10,719,431 | -2,266,512 | 10% | 2.14 | -1,057,345 | -31,341,205 |
| 9 | 11,083,377 | 9,148,931 | 2% | 1.20 | 13,245,662 | 10,933,820 | -2,311,842 | 10% | 2.36 | -980,447 | -32,321,652 |
| 10 | 11,083,377 | 9,148,931 | 2% | 1.22 | 13,510,575 | 11,152,496 | -2,358,079 | 10% | 2.59 | -909,142 | -33,230,793 |
| 11 | 11,083,377 | 9,148,931 | 2% | 1.24 | 13,780,787 | 11,375,546 | -2,405,241 | 10% | 2.85 | -843,022 | -34,073,815 |
| 12 | 11,083,377 | 9,148,931 | 2% | 1.27 | 14,056,402 | 11,603,057 | -2,453,345 | 10% | 3.14 | -781,711 | -34,855,527 |
| 13 | 11,083,377 | 9,148,931 | 2% | 1.29 | 14,337,530 | 11,835,118 | -2,502,412 | 10% | 3.45 | -724,860 | -35,580,386 |
| 14 | 11,083,377 | 9,148,931 | 2% | 1.32 | 14,624,281 | 12,071,820 | -2,552,461 | 10% | 3.80 | -672,143 | -36,252,529 |
| 15 | 11,083,377 | 9,148,931 | 2% | 1.35 | 14,916,767 | 12,313,257 | -2,603,510 | 10% | 4.18 | -623,260 | -36,875,789 |
| 16 | 11,083,377 | 9,148,931 | 2% | 1.37 | 15,215,102 | 12,559,522 | -2,655,580 | 10% | 4.59 | -577,932 | -37,453,720 |
| 17 | 11,083,377 | 9,148,931 | 2% | 1.40 | 15,519,404 | 12,810,712 | -2,708,692 | 10% | 5.05 | -535,900 | -37,989,620 |
| 18 | 11,083,377 | 9,148,931 | 2% | 1.43 | 15,829,792 | 13,066,927 | -2,762,865 | 10% | 5.56 | -496,926 | -38,486,546 |
| 19 | 11,083,377 | 9,148,931 | 2% | 1.46 | 16,146,388 | 13,328,265 | -2,818,123 | 10% | 6.12 | -460,786 | -38,947,332 |
| 20 | 11,083,377 | 9,148,931 | 2% | 1.49 | 16,469,316 | 13,594,830 | -2,874,485 | 10% | 6.73 | -427,274 | -39,374,606 |

The results of the net present value in all three scenarios are illustrated in Figure 7.6. While the best case scenario seems to be reasonable in economic terms, the realistic scenario and the worst case scenario are not profitable after 20 years. Since the realistic case scenario is not profitable, it can be stated that the recycling process of an ISF slag with the given composition is not economically feasible at current prices.

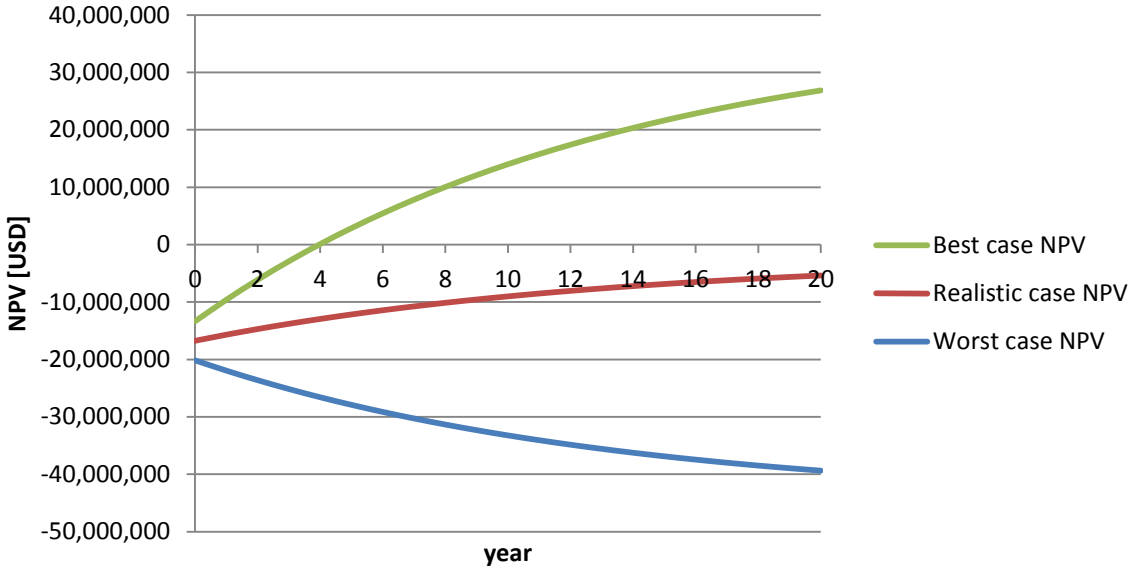


Figure 7.6: The net present value of all three scenarios over the project lifetime of 20 years

## 7.8 Net present value Blast Furnace slag

The same calculation method is used on the Blast Furnace slag in this section. The results of the calculated operational-, capital expenditures and the revenues can be seen in Table 7.24 below.

Table 7.24: Summary of the CAPEX, OPEX and the expected revenues in all three scenarios

| | Unit | Best case | Realistic case | Worst case |
|---|---|---|---|---|
| Total CAPEX | [USD] | 13,365,440 | 16,755,200 | 20,158,160 |
| Total OPEX | [USD/year] | 9,805,207 | 10,551,358 | 11,615,095 |
| Total revenues | [USD/year] | 24,416,372 | 20,128,807 | 15,664,135 |

Table 7.25: The calculation of the net present value for every operation year in the realistic scenario

| Operation year | Calculated CAPEX/OPEX | Calculated revenues | Inflation rate | Cumulated inflation rate | Inflation adj. cost | Inflation adj. revenues | Annual cash flow | Discount rate | Discount factor | Discounted cash flow | Realistic case NPV |
|---|---|---|---|---|---|---|---|---|---|---|---|
| 0 | 16,755,200 | 0 | 2% | 1.00 | 16,755,200 | 0 | -16,755,200 | 10% | 1.00 | -16,755,200 | -16,755,200 |
| 1 | 10,551,358 | 20,128,807 | 2% | 1.02 | 10,762,385 | 20,531,383 | 9,768,998 | 10% | 1.10 | 8,880,907 | -7,874,293 |
| 2 | 10,551,358 | 20,128,807 | 2% | 1.04 | 10,977,633 | 20,942,010 | 9,964,378 | 10% | 1.21 | 8,235,023 | 360,730 |
| 3 | 10,551,358 | 20,128,807 | 2% | 1.06 | 11,197,185 | 21,360,851 | 10,163,665 | 10% | 1.33 | 7,636,112 | 7,996,842 |
| 4 | 10,551,358 | 20,128,807 | 2% | 1.08 | 11,421,129 | 21,788,068 | 10,366,939 | 10% | 1.46 | 7,080,759 | 15,077,601 |
| 5 | 10,551,358 | 20,128,807 | 2% | 1.10 | 11,649,552 | 22,223,829 | 10,574,277 | 10% | 1.61 | 6,565,794 | 21,643,395 |
| 6 | 10,551,358 | 20,128,807 | 2% | 1.13 | 11,882,543 | 22,668,305 | 10,785,763 | 10% | 1.77 | 6,088,282 | 27,731,677 |
| 7 | 10,551,358 | 20,128,807 | 2% | 1.15 | 12,120,193 | 23,121,672 | 11,001,478 | 10% | 1.95 | 5,645,498 | 33,377,175 |
| 8 | 10,551,358 | 20,128,807 | 2% | 1.17 | 12,362,597 | 23,584,105 | 11,221,508 | 10% | 2.14 | 5,234,916 | 38,612,091 |
| 9 | 10,551,358 | 20,128,807 | 2% | 1.20 | 12,609,849 | 24,055,787 | 11,445,938 | 10% | 2.36 | 4,854,195 | 43,466,286 |
| 10 | 10,551,358 | 20,128,807 | 2% | 1.22 | 12,862,046 | 24,536,903 | 11,674,857 | 10% | 2.59 | 4,501,163 | 47,967,449 |
| 11 | 10,551,358 | 20,128,807 | 2% | 1.24 | 13,119,287 | 25,027,641 | 11,908,354 | 10% | 2.85 | 4,173,805 | 52,141,254 |
| 12 | 10,551,358 | 20,128,807 | 2% | 1.27 | 13,381,673 | 25,528,194 | 12,146,521 | 10% | 3.14 | 3,870,256 | 56,011,510 |
| 13 | 10,551,358 | 20,128,807 | 2% | 1.29 | 13,649,306 | 26,038,758 | 12,389,451 | 10% | 3.45 | 3,588,783 | 59,600,293 |
| 14 | 10,551,358 | 20,128,807 | 2% | 1.32 | 13,922,292 | 26,559,533 | 12,637,240 | 10% | 3.80 | 3,327,780 | 62,928,073 |
| 15 | 10,551,358 | 20,128,807 | 2% | 1.35 | 14,200,738 | 27,090,723 | 12,889,985 | 10% | 4.18 | 3,085,760 | 66,013,833 |
| 16 | 10,551,358 | 20,128,807 | 2% | 1.37 | 14,484,753 | 27,632,538 | 13,147,785 | 10% | 4.59 | 2,861,341 | 68,875,174 |
| 17 | 10,551,358 | 20,128,807 | 2% | 1.40 | 14,774,448 | 28,185,189 | 13,410,741 | 10% | 5.05 | 2,653,244 | 71,528,417 |
| 18 | 10,551,358 | 20,128,807 | 2% | 1.43 | 15,069,937 | 28,748,892 | 13,678,955 | 10% | 5.56 | 2,460,280 | 73,988,698 |
| 19 | 10,551,358 | 20,128,807 | 2% | 1.46 | 15,371,336 | 29,323,870 | 13,952,534 | 10% | 6.12 | 2,281,351 | 76,270,049 |
| 20 | 10,551,358 | 20,128,807 | 2% | 1.49 | 15,678,763 | 29,910,348 | 14,231,585 | 10% | 6.73 | 2,115,434 | 78,385,483 |

Table 7.26: The calculation of the net present value for every operation year in the best case scenario

| Operation year | Calculated CAPEX/OPEX | Calculated revenues | Inflation rate | Cumulated inflation rate | Inflation adj. cost | Inflation adj. revenues | Annual cash flow | Discount rate | Discount factor | Discounted cash flow | Best case NPV |
|---|---|---|---|---|---|---|---|---|---|---|---|
| 0 | 13,365,440 | 0 | 2% | 1.00 | 13,365,440 | 0 | -13,365,440 | 10% | 1.00 | -13,365,440 | -13,365,440 |
| 1 | 9,805,207 | 24,416,372 | 2% | 1.02 | 10,001,311 | 24,904,700 | 14,903,389 | 10% | 1.10 | 13,548,535 | 183,095 |
| 2 | 9,805,207 | 24,416,372 | 2% | 1.04 | 10,201,337 | 25,402,794 | 15,201,456 | 10% | 1.21 | 12,563,187 | 12,746,282 |
| 3 | 9,805,207 | 24,416,372 | 2% | 1.06 | 10,405,364 | 25,910,850 | 15,505,486 | 10% | 1.33 | 11,649,501 | 24,395,783 |
| 4 | 9,805,207 | 24,416,372 | 2% | 1.08 | 10,613,471 | 26,429,067 | 15,815,595 | 10% | 1.46 | 10,802,264 | 35,198,047 |
| 5 | 9,805,207 | 24,416,372 | 2% | 1.10 | 10,825,741 | 26,957,648 | 16,131,907 | 10% | 1.61 | 10,016,645 | 45,214,692 |
| 6 | 9,805,207 | 24,416,372 | 2% | 1.13 | 11,042,256 | 27,496,801 | 16,454,545 | 10% | 1.77 | 9,288,162 | 54,502,854 |
| 7 | 9,805,207 | 24,416,372 | 2% | 1.15 | 11,263,101 | 28,046,737 | 16,783,636 | 10% | 1.95 | 8,612,659 | 63,115,513 |
| 8 | 9,805,207 | 24,416,372 | 2% | 1.17 | 11,488,363 | 28,607,672 | 17,119,309 | 10% | 2.14 | 7,986,284 | 71,101,797 |
| 9 | 9,805,207 | 24,416,372 | 2% | 1.20 | 11,718,130 | 29,179,825 | 17,461,695 | 10% | 2.36 | 7,405,463 | 78,507,261 |
| 10 | 9,805,207 | 24,416,372 | 2% | 1.22 | 11,952,493 | 29,763,422 | 17,810,929 | 10% | 2.59 | 6,866,884 | 85,374,145 |
| 11 | 9,805,207 | 24,416,372 | 2% | 1.24 | 12,191,543 | 30,358,690 | 18,167,148 | 10% | 2.85 | 6,367,474 | 91,741,619 |
| 12 | 9,805,207 | 24,416,372 | 2% | 1.27 | 12,435,373 | 30,965,864 | 18,530,490 | 10% | 3.14 | 5,904,385 | 97,646,004 |
| 13 | 9,805,207 | 24,416,372 | 2% | 1.29 | 12,684,081 | 31,585,181 | 18,901,100 | 10% | 3.45 | 5,474,975 | 103,120,980 |
| 14 | 9,805,207 | 24,416,372 | 2% | 1.32 | 12,937,762 | 32,216,885 | 19,279,122 | 10% | 3.80 | 5,076,795 | 108,197,775 |
| 15 | 9,805,207 | 24,416,372 | 2% | 1.35 | 13,196,518 | 32,861,223 | 19,664,705 | 10% | 4.18 | 4,707,574 | 112,905,349 |
| 16 | 9,805,207 | 24,416,372 | 2% | 1.37 | 13,460,448 | 33,518,447 | 20,057,999 | 10% | 4.59 | 4,365,205 | 117,270,554 |
| 17 | 9,805,207 | 24,416,372 | 2% | 1.40 | 13,729,657 | 34,188,816 | 20,459,159 | 10% | 5.05 | 4,047,736 | 121,318,290 |
| 18 | 9,805,207 | 24,416,372 | 2% | 1.43 | 14,004,250 | 34,872,592 | 20,868,342 | 10% | 5.56 | 3,753,355 | 125,071,645 |
| 19 | 9,805,207 | 24,416,372 | 2% | 1.46 | 14,284,335 | 35,570,044 | 21,285,709 | 10% | 6.12 | 3,480,383 | 128,552,028 |
| 20 | 9,805,207 | 24,416,372 | 2% | 1.49 | 14,570,022 | 36,281,445 | 21,711,423 | 10% | 6.73 | 3,227,265 | 131,779,293 |

Table 7.27: The calculation of the net present value for every operation year in the worst case scenario

| Operation year | Calculated CAPEX/OPEX | Calculated revenues | Inflation rate | Cumulated inflation rate | Inflation adj. cost | Inflation adj. revenues | Annual cash flow | Discount rate | Discount factor | Discounted cash flow | Worst case NPV |
|---|---|---|---|---|---|---|---|---|---|---|---|
| 0 | 20,158,160 | 0 | 2% | 1.00 | 20,158,160 | 0 | -20,158,160 | 10% | 1.00 | -20,158,160 | -20,158,160 |
| 1 | 11,615,095 | 15,664,135 | 2% | 1.02 | 11,847,397 | 15,977,418 | 4,130,021 | 10% | 1.10 | 3,754,565 | -16,403,595 |
| 2 | 11,615,095 | 15,664,135 | 2% | 1.04 | 12,084,345 | 16,296,967 | 4,212,622 | 10% | 1.21 | 3,481,506 | -12,922,089 |
| 3 | 11,615,095 | 15,664,135 | 2% | 1.06 | 12,326,032 | 16,622,906 | 4,296,874 | 10% | 1.33 | 3,228,305 | -9,693,784 |
| 4 | 11,615,095 | 15,664,135 | 2% | 1.08 | 12,572,552 | 16,955,364 | 4,382,812 | 10% | 1.46 | 2,993,519 | -6,700,265 |
| 5 | 11,615,095 | 15,664,135 | 2% | 1.10 | 12,824,003 | 17,294,471 | 4,470,468 | 10% | 1.61 | 2,775,809 | -3,924,456 |
| 6 | 11,615,095 | 15,664,135 | 2% | 1.13 | 13,080,483 | 17,640,361 | 4,559,877 | 10% | 1.77 | 2,573,932 | -1,350,524 |
| 7 | 11,615,095 | 15,664,135 | 2% | 1.15 | 13,342,093 | 17,993,168 | 4,651,075 | 10% | 1.95 | 2,386,737 | 1,036,213 |
| 8 | 11,615,095 | 15,664,135 | 2% | 1.17 | 13,608,935 | 18,353,031 | 4,744,096 | 10% | 2.14 | 2,213,156 | 3,249,369 |
| 9 | 11,615,095 | 15,664,135 | 2% | 1.20 | 13,881,114 | 18,720,092 | 4,838,978 | 10% | 2.36 | 2,052,199 | 5,301,568 |
| 10 | 11,615,095 | 15,664,135 | 2% | 1.22 | 14,158,736 | 19,094,494 | 4,935,758 | 10% | 2.59 | 1,902,948 | 7,204,516 |
| 11 | 11,615,095 | 15,664,135 | 2% | 1.24 | 14,441,911 | 19,476,384 | 5,034,473 | 10% | 2.85 | 1,764,552 | 8,969,069 |
| 12 | 11,615,095 | 15,664,135 | 2% | 1.27 | 14,730,749 | 19,865,911 | 5,135,163 | 10% | 3.14 | 1,636,221 | 10,605,290 |
| 13 | 11,615,095 | 15,664,135 | 2% | 1.29 | 15,025,364 | 20,263,229 | 5,237,866 | 10% | 3.45 | 1,517,223 | 12,122,513 |
| 14 | 11,615,095 | 15,664,135 | 2% | 1.32 | 15,325,871 | 20,668,494 | 5,342,623 | 10% | 3.80 | 1,406,880 | 13,529,392 |
| 15 | 11,615,095 | 15,664,135 | 2% | 1.35 | 15,632,388 | 21,081,864 | 5,449,476 | 10% | 4.18 | 1,304,561 | 14,833,954 |
| 16 | 11,615,095 | 15,664,135 | 2% | 1.37 | 15,945,036 | 21,503,501 | 5,558,465 | 10% | 4.59 | 1,209,684 | 16,043,638 |
| 17 | 11,615,095 | 15,664,135 | 2% | 1.40 | 16,263,937 | 21,933,571 | 5,669,634 | 10% | 5.05 | 1,121,707 | 17,165,344 |
| 18 | 11,615,095 | 15,664,135 | 2% | 1.43 | 16,589,216 | 22,372,243 | 5,783,027 | 10% | 5.56 | 1,040,128 | 18,205,473 |
| 19 | 11,615,095 | 15,664,135 | 2% | 1.46 | 16,921,000 | 22,819,688 | 5,898,688 | 10% | 6.12 | 964,483 | 19,169,955 |
| 20 | 11,615,095 | 15,664,135 | 2% | 1.49 | 17,259,420 | 23,276,081 | 6,016,661 | 10% | 6.73 | 894,338 | 20,064,294 |

The results of the NPV of the Blast Furnace recycling process are highly promising concerning the profitability. The higher contents of the valuables have a tremendous effect on the NPV, as pictured in Figure 7.7.

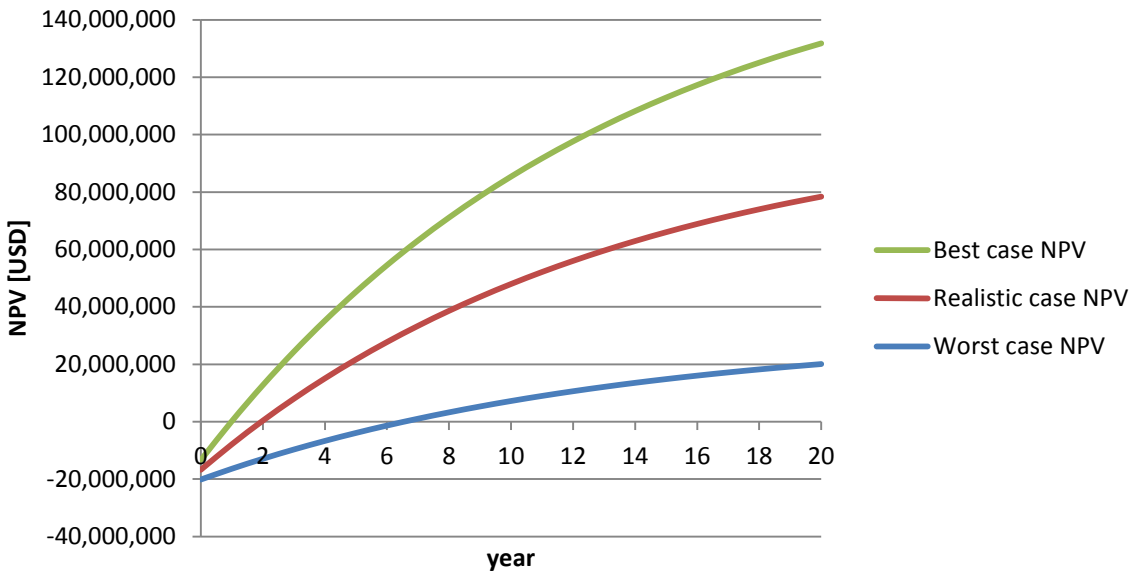


Figure 7.7: Net present value of all scenarios plotted against the project time

# 8 Conclusion and Outlook

The most important objective of the thesis, to find technical measures, to optimize the recycling process and run it more efficiently was achieved. The focus on the fluxes (CaO), ($SiO_2$) and (FeO) turned out to be a reasonable approach. The trials in the hot stage microscope provide information regarding the distribution of melting points in the whole ternary system. This allows the operation of the process at the lowest possible melting point, which is very decisive for the efficiency of the process in technical and economic terms, because a very high share of the operating costs are burning gases.

Additionally to the influence of the melting point of the slag, the addition of fluxes affects the recovery rates of the valuable metals. The lead recovery rate was increased from 75.8 % to 88.6 %, which is almost a 13 % increase. At the same time the zinc fuming rate was slightly raised from 43.9 % to 44.6 %. Only four different sample mixtures were tested in the resistance furnace and it is very likely that this increase is not the absolute optimum and there is still potential to improve the recovery yields.

Furthermore, it should be noted, that the main aim of the trial in the resistance furnace was the comprehension of the correlation between the addition of fluxes and the valuable recovery rates. In spite of all the improvements no clear correlation was found between the zinc fuming-, or lead settling rate and the investigated (CaO)/($SiO_2$) or ($SiO_2$)/(Fe) ratio. Also the approach to predict the behaviour of the valuable metals with the help of a calculated Kz-value, which is a measurement of the viscosity of the slag, has to be treated with caution. Due to the changes in the sample composition during the trial and the low number of sample mixtures, no explicit and reliable correlation was found.

The second aim of the master thesis was the economic evaluation of the lead bath recycling process at an industrial scale. Two different typical slag compositions, a Blast Furnace slag and an ISF slag, have been the subject to the evaluation. As expected, the major contributing factor was the concentration of valuable metals in the slag. This explains the completely different result of the two slags in the economic calculation. While there is a small expected loss of 1,095,421 USD after 20 years of recycling the ISF slag, the expected profit of the Blast Furnace slag recycling sums up to 83,987,944 USD.

This result shows that a typical Blast Furnace slag can be recycled with profit already, while other slags with lower concentrations of valuables won't be treated for economic reasons in the near future. Only if the circumstances change substantially, for example a change in legal landfilling regulations or a significant increase of metal prices could force companies to reconsider.

# 9 Appendix

The following chapter covers additional figures, information and results, which are not essential for the understanding and the conclusion of the thesis, but still important for the reproducibility of the trials. Additionally some previously published results are shown in greater detail in this section and presented with graphics.

## 9.1 Additional information to chapter 4

To produce the necessary samples for the trials in the hot stage microscope the following mixtures were produced. The supplements CaO, $Fe_2O_3$ and $SiO_2$ were added to 20 g of ISF residue to reach the wanted sample composition according to section 4.2. Due to the fact that FeO is not stable at ambient conditions, $Fe_2O_3$ was added to the mixture instead. [34]

Table 9.1: Calculations of the necessary quantities of the supplements for mixture P21-P23

| | target values | | | residue | supplements | | | total |
|---|---|---|---|---|---|---|---|---|
| | FeO [wt.-%] | CaO [wt.-%] | $SiO_2$ [wt.-%] | [g] | $Fe_2O_3$ [g] | CaO [g] | $SiO_2$ [g] | sample [g] |
| P1 | 10 | 10 | 80 | 20 | 0.00 | 5.85 | 72.45 | 98.30 |
| P2 | 10 | 20 | 70 | 20 | 0.00 | 15.68 | 62.62 | 98.30 |
| P3 | 10 | 30 | 60 | 20 | 0.00 | 25.51 | 52.79 | 98.30 |
| P4 | 10 | 40 | 50 | 20 | 0.00 | 35.35 | 42.96 | 98.30 |
| P5 | 10 | 50 | 40 | 20 | 0.00 | 45.18 | 33.13 | 98.30 |
| P6 | 10 | 60 | 30 | 20 | 0.00 | 55.01 | 23.30 | 98.30 |
| P7 | 10 | 70 | 20 | 20 | 0.00 | 64.84 | 13.47 | 98.30 |
| P8 | 10 | 80 | 10 | 20 | 0.00 | 74.67 | 3.64 | 98.30 |
| P9 | 20 | 10 | 70 | 20 | 0.00 | 0.94 | 28.21 | 49.15 |
| P10 | 20 | 20 | 60 | 20 | 0.00 | 5.85 | 23.30 | 49.15 |
| P11 | 20 | 30 | 50 | 20 | 0.00 | 10.77 | 18.38 | 49.15 |
| P12 | 20 | 40 | 40 | 20 | 0.00 | 15.68 | 13.47 | 49.15 |
| P13 | 20 | 50 | 30 | 20 | 0.00 | 20.60 | 8.55 | 49.15 |
| P14 | 20 | 60 | 20 | 20 | 0.00 | 25.51 | 3.64 | 49.15 |
| P15 | 20 | 70 | 10 | 20 | 2.84 | 39.37 | 0.00 | 62.21 |
| P16 | 30 | 10 | 60 | 20 | 2.33 | 0.00 | 17.67 | 40.00 |
| P17 | 30 | 20 | 50 | 20 | 0.00 | 2.58 | 10.19 | 32.77 |
| P18 | 30 | 30 | 40 | 20 | 0.00 | 5.85 | 6.91 | 32.77 |
| P19 | 30 | 40 | 30 | 20 | 0.00 | 9.13 | 3.64 | 32.77 |
| P20 | 30 | 50 | 20 | 20 | 0.00 | 12.41 | 0.36 | 32.77 |
| P21 | 30 | 60 | 10 | 20 | 9.72 | 33.18 | 0.00 | 62.90 |
| P22 | 40 | 10 | 50 | 20 | 6.75 | 0.00 | 13.69 | 40.45 |
| P23 | 40 | 20 | 40 | 20 | 0.00 | 0.94 | 3.64 | 24.58 |

Table 9.2: Calculations of the necessary quantities of the supplements for mixture P24-P36

| | target values | | | residue | supplements | | | total |
|---|---|---|---|---|---|---|---|---|
| | FeO | CaO | $SiO_2$ | | $Fe_2O_3$ | CaO | $SiO_2$ | sample |
| | [wt.-%] | [wt.-%] | [wt.-%] | [g] | [g] | [g] | [g] | [g] |
| P24 | 40 | 30 | 30 | 20 | 0.00 | 3.40 | 1.18 | 24.58 |
| P25 | 40 | 40 | 20 | 20 | 2.84 | 8.41 | 0.00 | 31.25 |
| P26 | 40 | 50 | 10 | 20 | 16.60 | 26.99 | 0.00 | 63.59 |
| P27 | 50 | 10 | 40 | 20 | 11.17 | 0.00 | 9.72 | 40.89 |
| P28 | 50 | 20 | 30 | 20 | 0.55 | 0.15 | 0.00 | 20.70 |
| P29 | 50 | 30 | 20 | 20 | 6.28 | 5.31 | 0.00 | 31.59 |
| P30 | 50 | 40 | 10 | 20 | 23.49 | 20.79 | 0.00 | 64.28 |
| P31 | 60 | 10 | 30 | 20 | 15.59 | 0.00 | 5.74 | 41.33 |
| P32 | 60 | 20 | 20 | 20 | 9.72 | 2.22 | 0.00 | 31.94 |
| P33 | 60 | 30 | 10 | 20 | 30.37 | 14.60 | 0.00 | 64.97 |
| P34 | 70 | 10 | 20 | 20 | 20.01 | 0.00 | 1.76 | 41.77 |
| P35 | 70 | 20 | 10 | 20 | 37.25 | 8.41 | 0.00 | 65.66 |
| P36 | 80 | 10 | 10 | 20 | 44.13 | 2.22 | 0.00 | 66.35 |
| | | | | 720 | 239.65 | 597.39 | 474.41 | 2031.45 |

The following results are divided into six diagrams, plotting temperature against the percentage of the initial measured area. As shown in Figure 9.1 the samples P0-P6 melt at different temperatures. P1 is not melting down at all, but the other samples P2-P6 have melting points between 1250-1570 °C. It can be seen that the mixtures placed in the middle of the corners of the ternary system (CaO and $SiO_2$) are showing lower melting points than the ones closer to the corners. The pure slag (P0) starts decreasing in area already before 1100 °C and it stops when reaching a remaining area of 70 % until 1300 °C, afterwards the sample totally melts down. This behaviour of the pure IS-slag is due to separate melting phases, which can be seen in Figure 4.11.

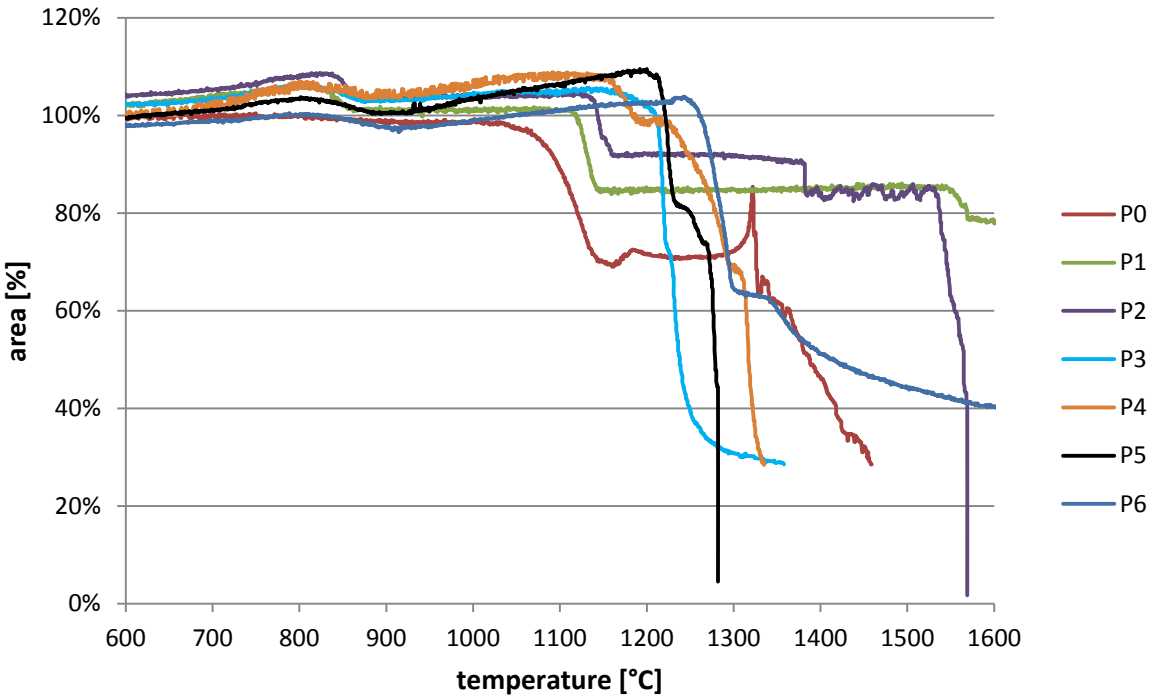


Figure 9.1: Shrinkages of the pure slag (P0) and the samples P1-P6

The shrinkages of the samples P7-P12 are shown in Figure 9.2. It can clearly be seen that the two samples with a very high (CaO) content have a higher melting point than 1600 °C. P9 is showing highly intense degasification behaviour and reaches 150 % of its original area. P10-P12 are showing quite similar characteristics with low melting points between 1200-1250 °C.

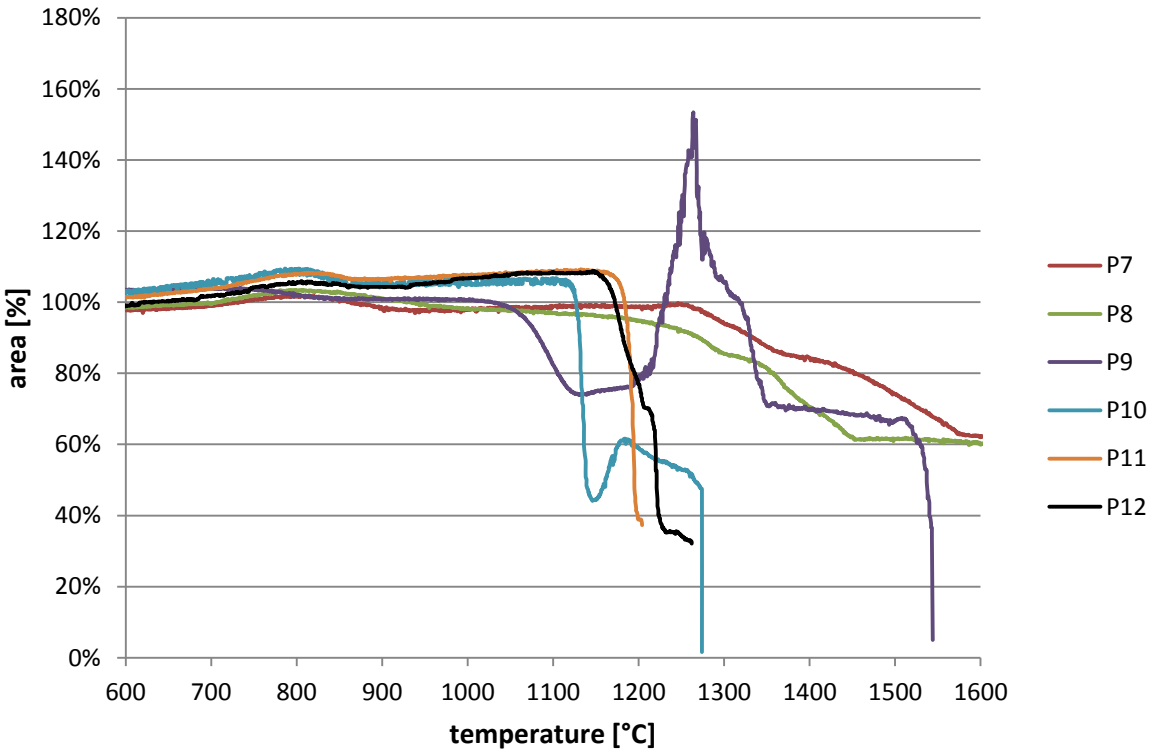


Figure 9.2: Shrinkages of the samples P7-P12

The samples P13-P15 are showing constantly increasing melting points, due to the increasing (CaO) ratio of the samples. P16 is showing degassing behaviour again, where P17 and P18 exhibit similar melting temperatures, as shown in Figure 9.3 underneath.

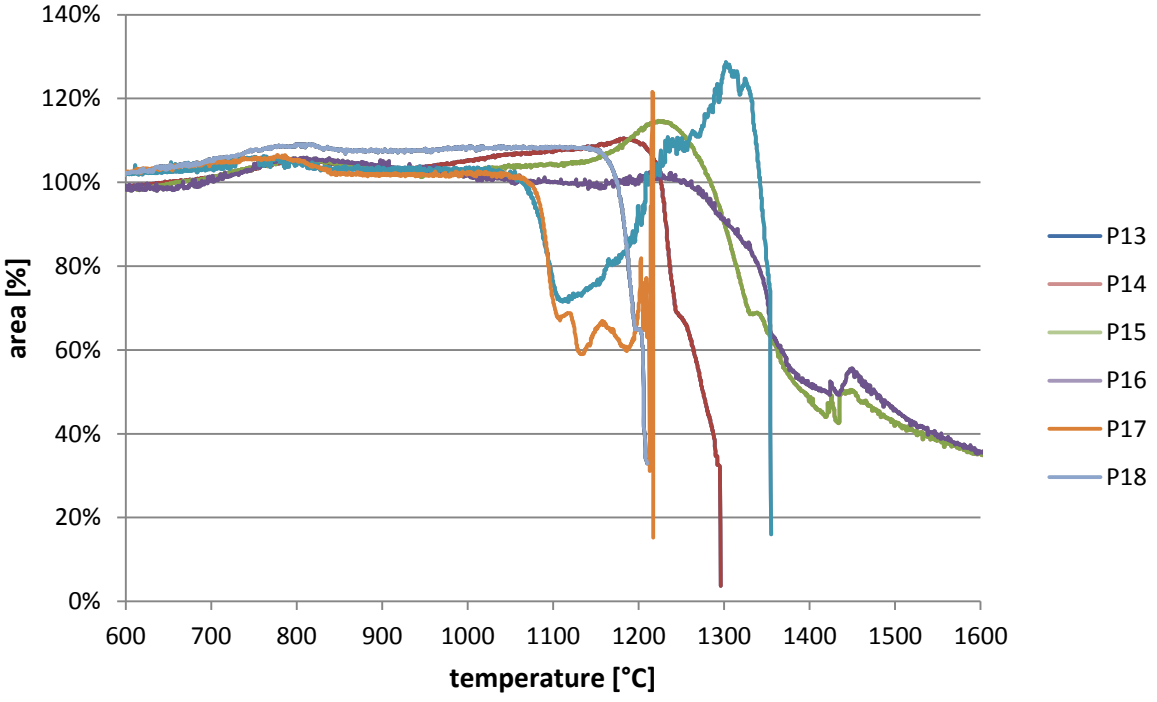


Figure 9.3: Shrinkages of the samples P13-P18

As previously described the melting points of the mixtures P19-P21 are steadily rising with

their increasing (CaO) concentration towards the corner. P22 and P23 show intense degasification again with measured areas of up to almost 180 % of the initial cylindrical area, as presented in the accompanying Figure 9.4 below. The melting temperature of P24 is similar to P19.

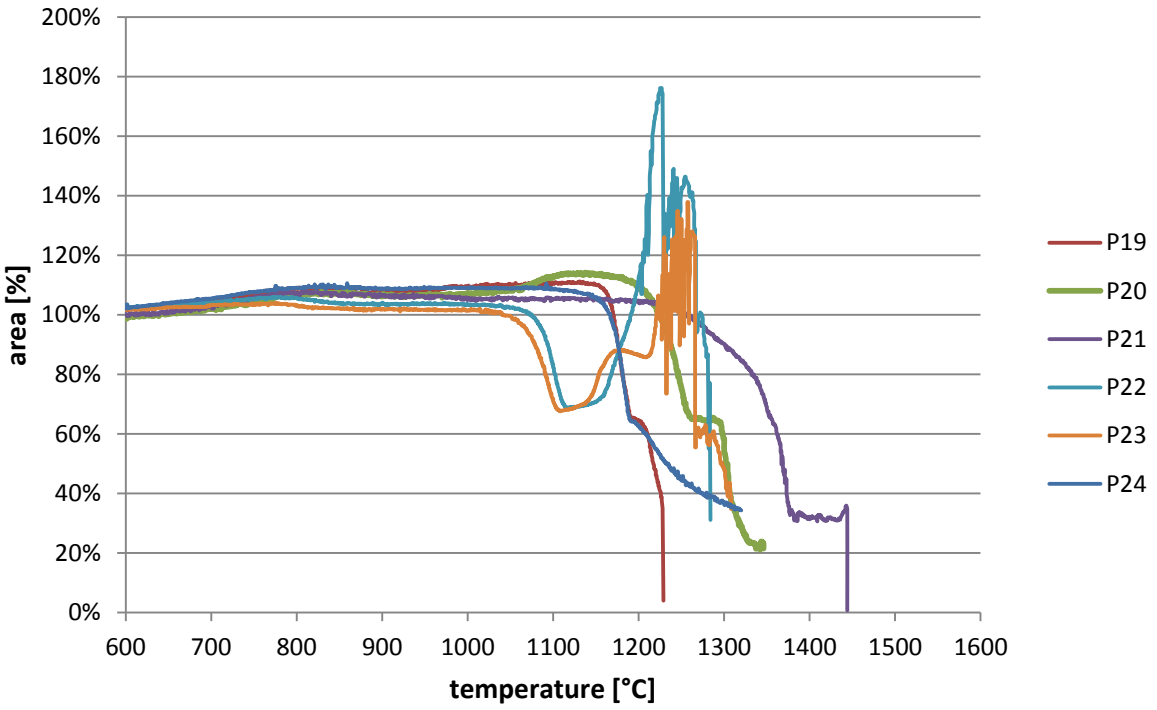


Figure 9.4: Shrinkages of the samples P19-P24

In Figure 9.5 below, the samples P25-P30 are pictured. Only P27 shows degassing behaviour. The other samples have melting points between 1200-1360 °C.

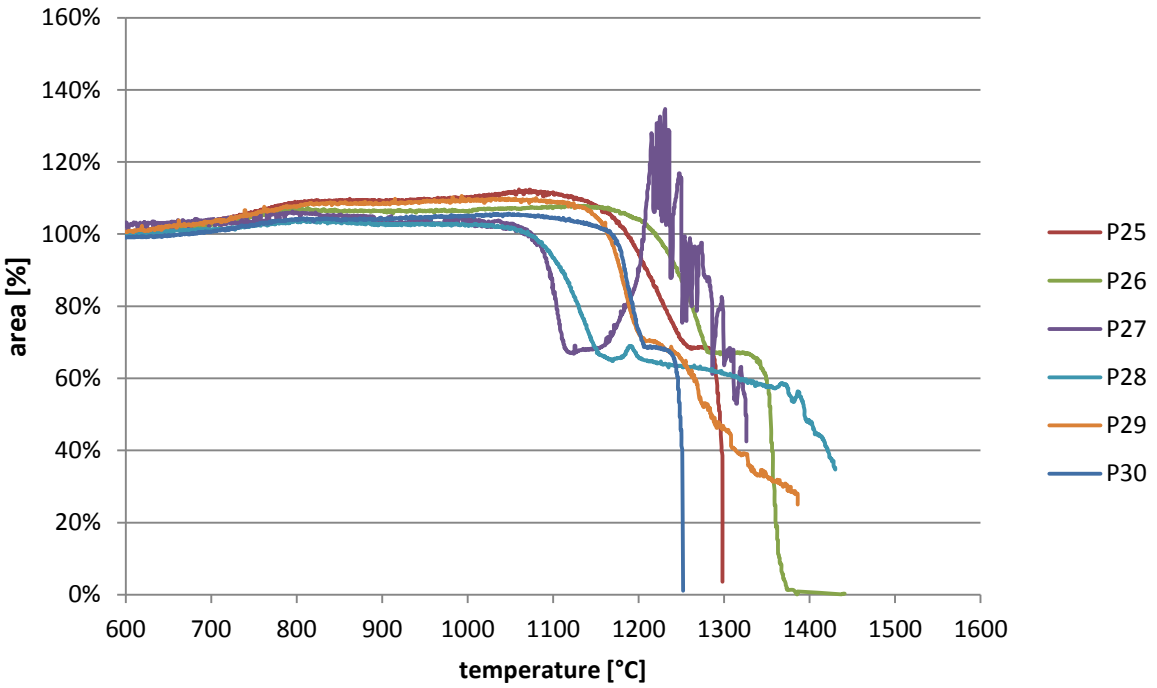


Figure 9.5: Shrinkages of the samples P25-P30

The shrinkages of the last group of samples P31-P36 is depicted in Figure 9.6. Two samples (P31 and P34) show signs of degasification. P36 starts losing volume at low temperatures between 900-1200 °C. After a temperature zone with constant area, the cross section is increasing until just over 1400 °C before it starts decreasing again. Therefore it shows change in the recorded area over a very long temperature interval.

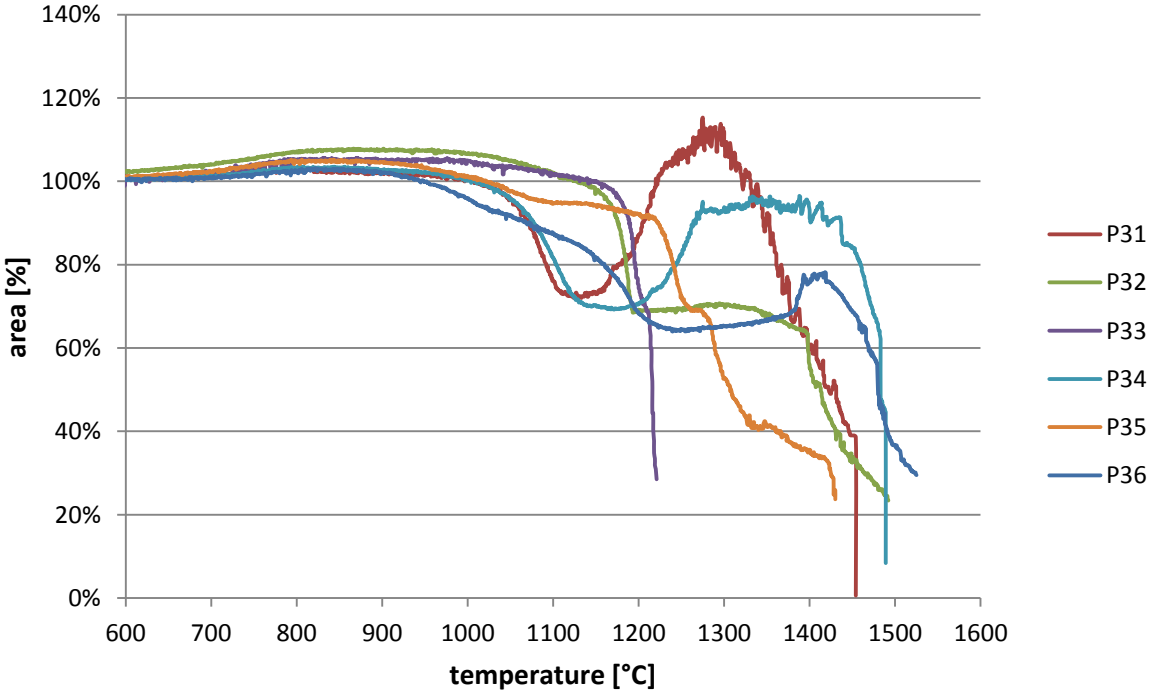


Figure 9.6: Shrinkages of the samples P31-P36

## 9.2 Additional information to chapter 5

This section covers additional information to the performed analyses by the SEM. Comments on the element- and compound concentration of the published spectra can be found in section 5 of the thesis. The published diagrams and pictures in this chapter are only considered additional information.

Figure 9.7 shows the utilized slag before the trial and the marked spectra, that were analysed by the SEM. All results are published below

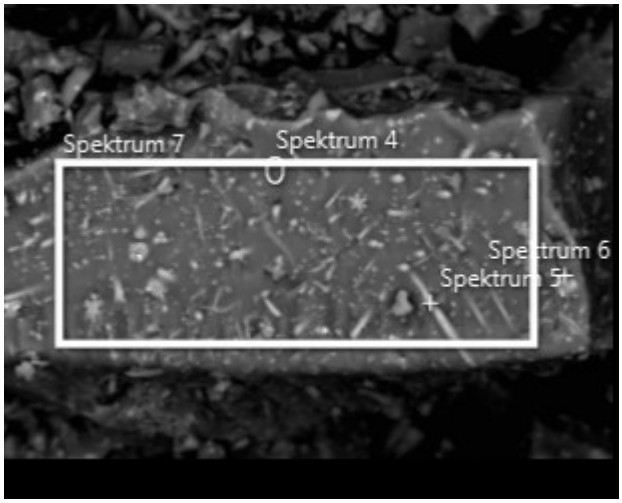


Figure 9.7: Different analysed spectra of the utilized slag before the trial

Spectrum 4 consists mainly of the three components (CaO), (FeO)and ($SiO_2$).as seen in Figure 9.8 below.

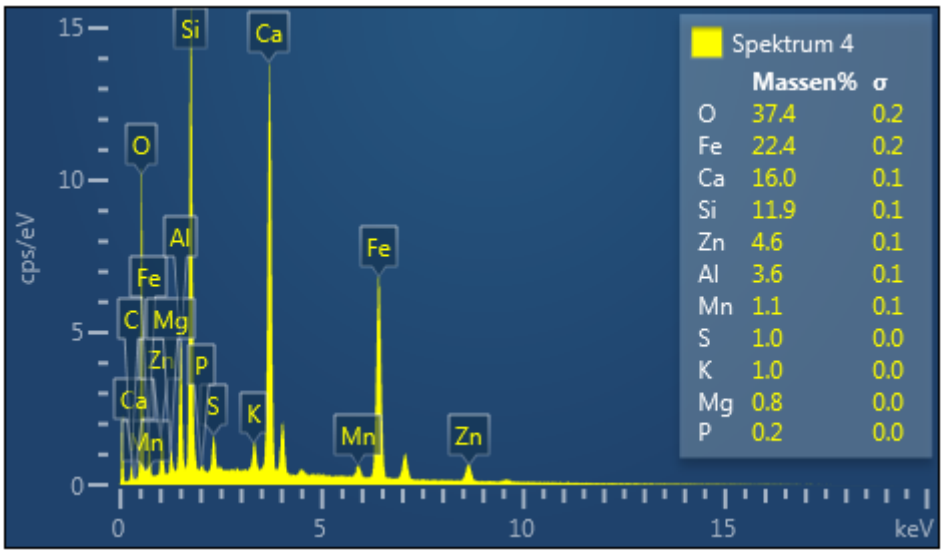


Figure 9.8: Element concentration of spectrum 4 of the utilized slag

The needle shaped structure in the utilized slag consists for the biggest part of iron oxide, as published in Figure 9.9 below.

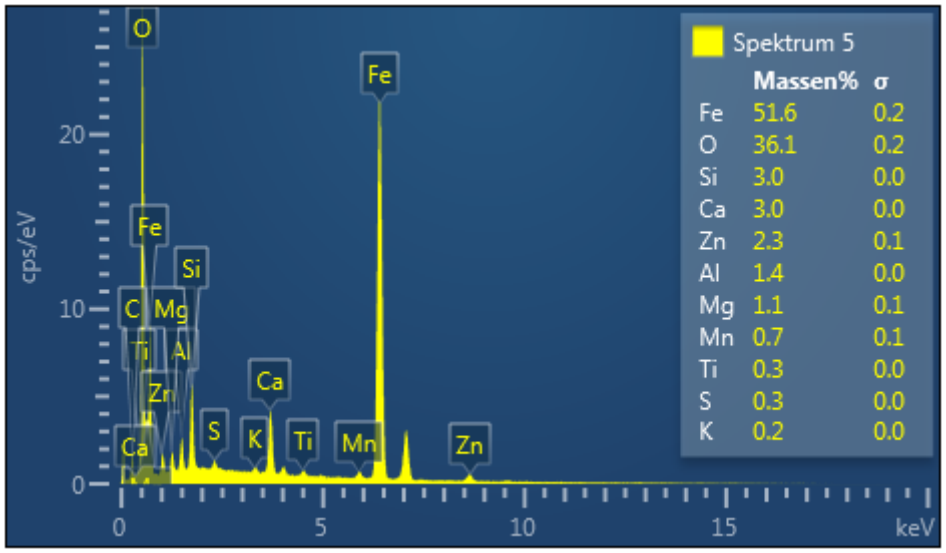


Figure 9.9: Element concentration of spectrum 5 of the utilized slag

The result of the analysis of the structure at the far right side of Figure 9.7 is published in Figure 9.10 below. It is rich in iron, zinc, sulphur and lead. Most metals do not exist as oxides in this spectrum, because the oxygen share is rather low compared to spectrum 4 or 5 of the utilized slag.

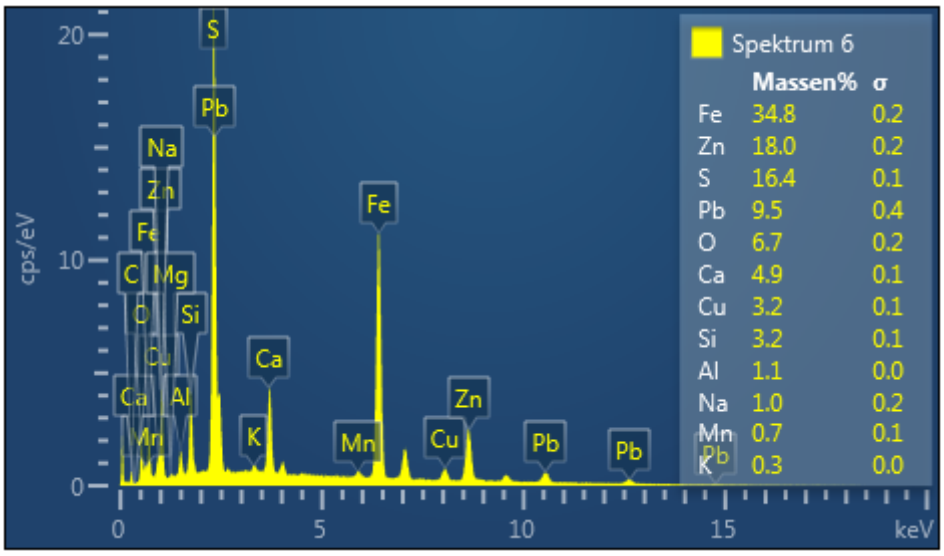


Figure 9.10: Element concentration of spectrum 6 of the utilized slag

The utilized slag consists mainly of three components (CaO), (FeO)and ($SiO_2$). The result of the mapping is published in Figure 9.11 below.

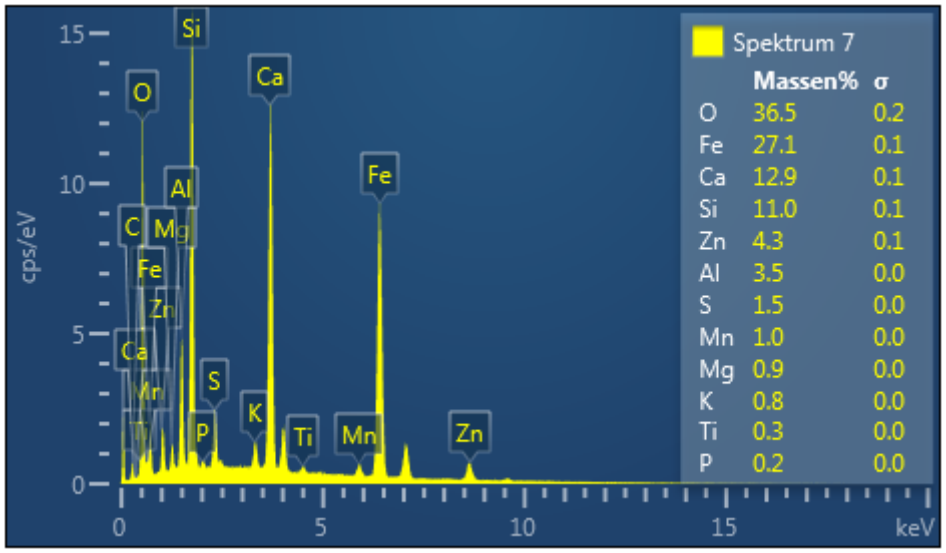


Figure 9.11: Mapping of the utilized slag before the trial

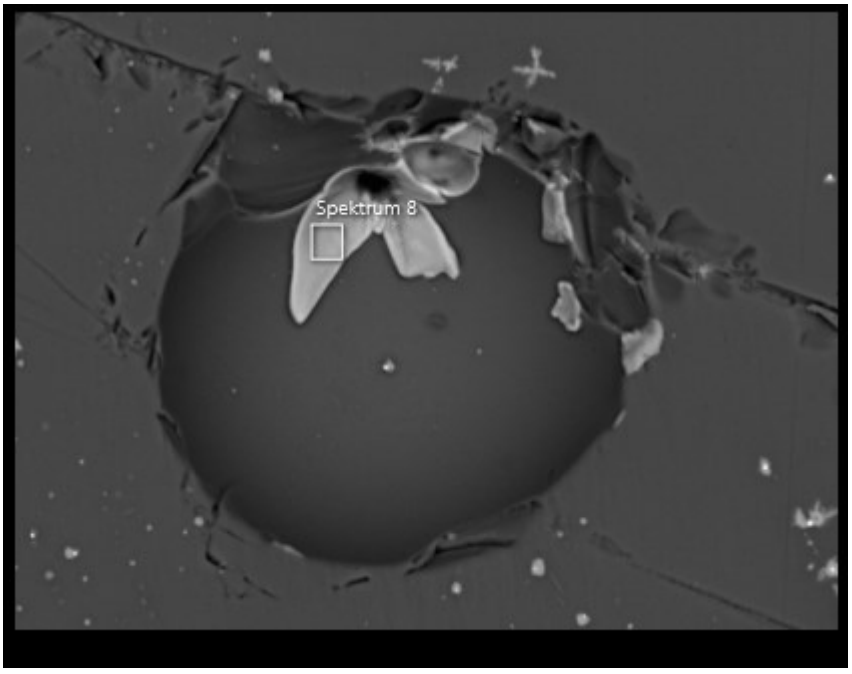


Figure 9.12: Picture of the treated slag of mixture P3

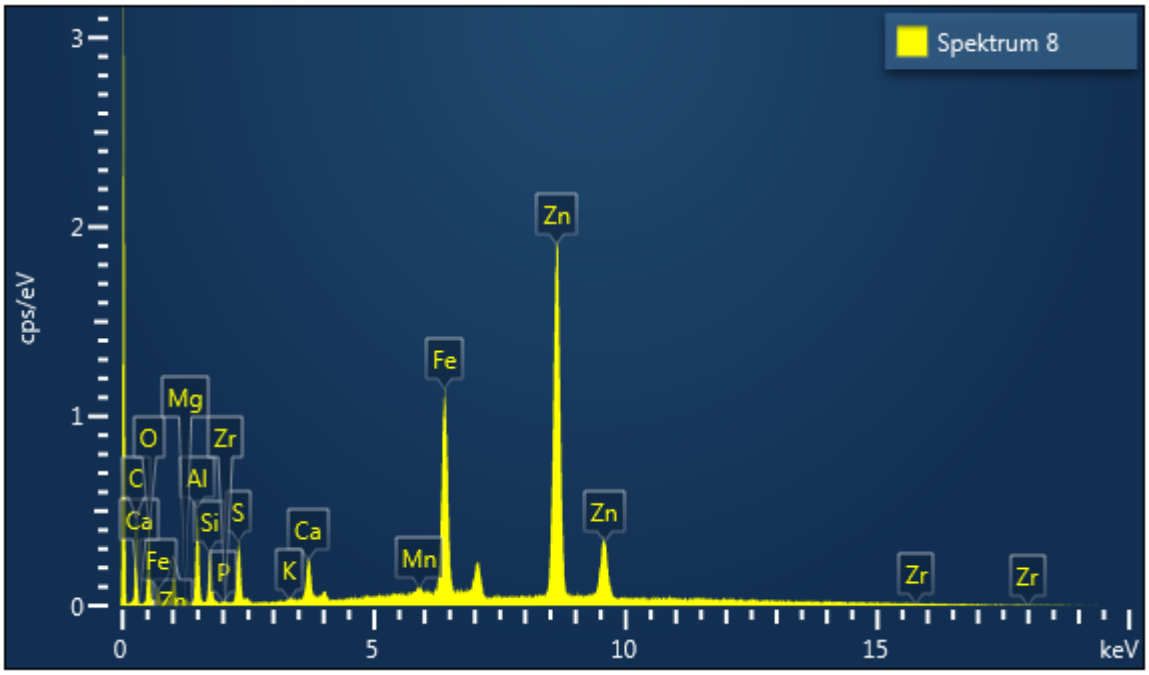


Figure 9.13: Element concentration of spectrum 8 of the treated slag P3

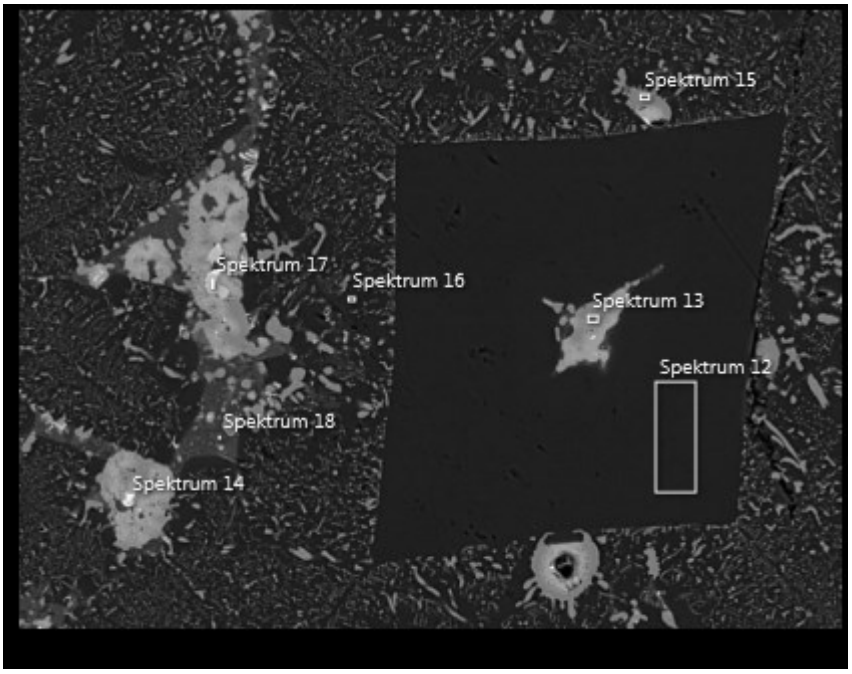


Figure 9.14: Picture of the treated slag of mixture P2

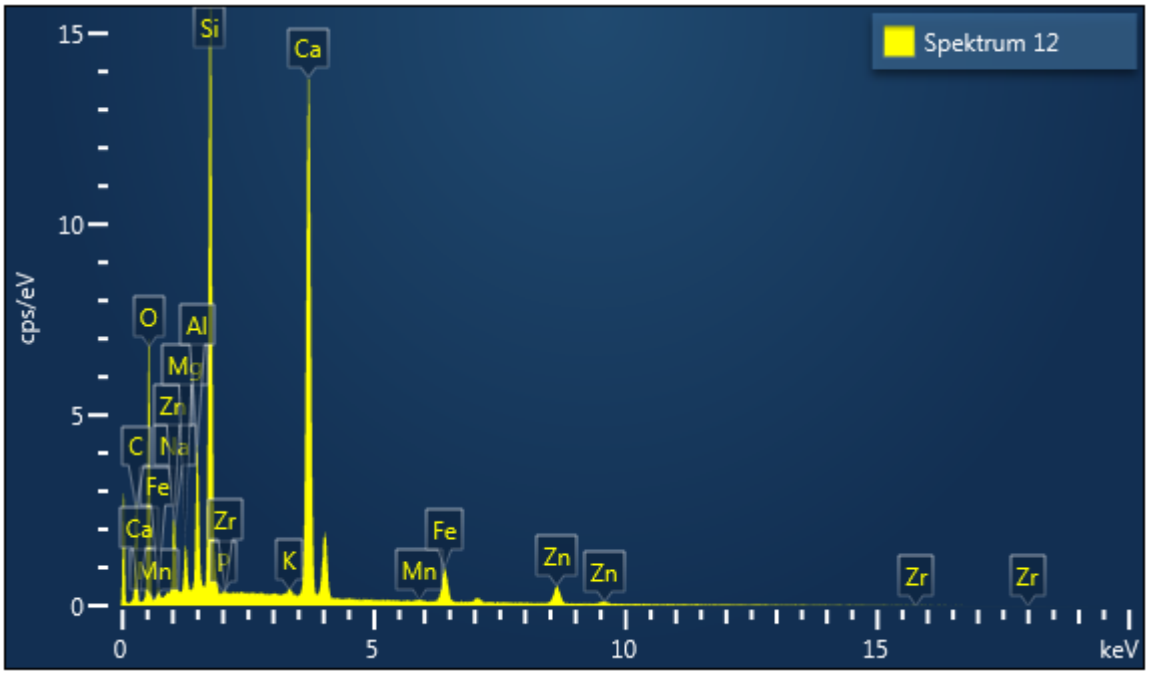


Figure 9.15: Element concentration of spectrum 12 of the treated slag P2

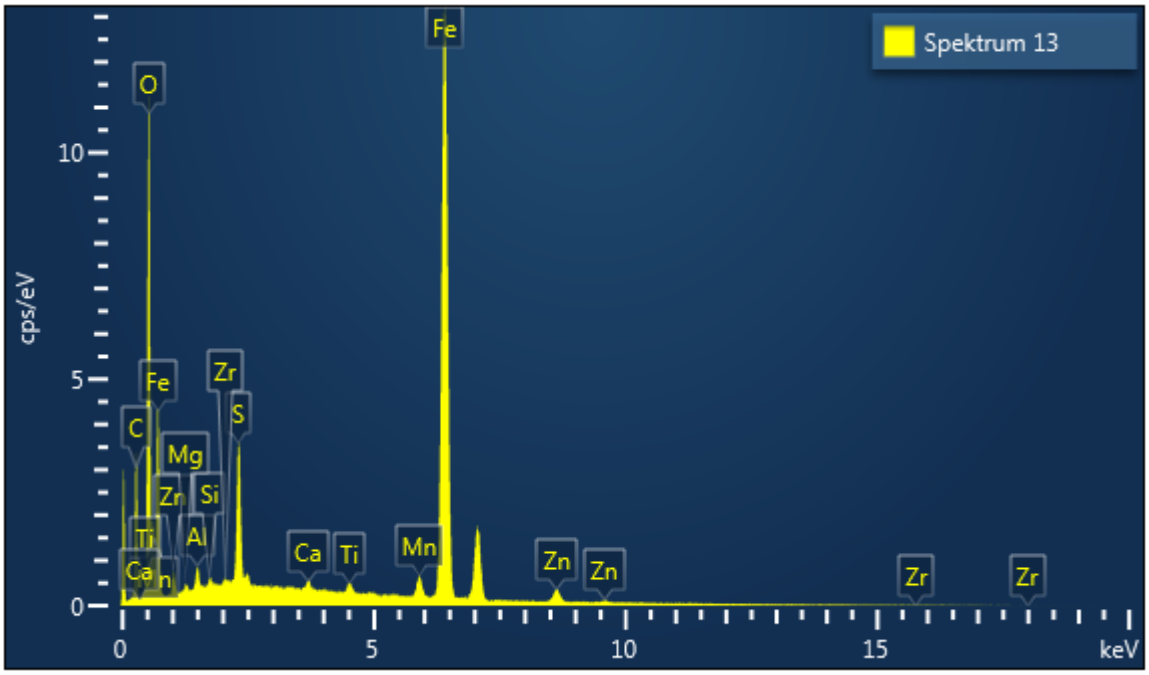


Figure 9.16: Element concentration of spectrum 13 of the treated slag P2

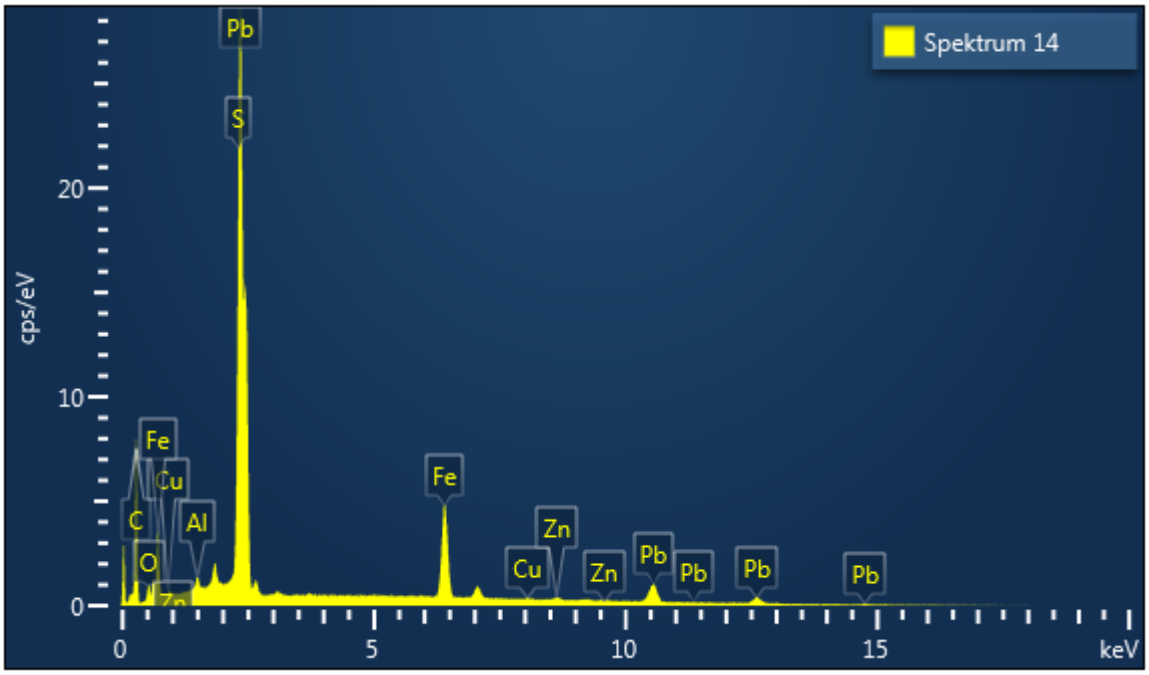


Figure 9.17: Element concentration of spectrum 14 of the treated slag P2

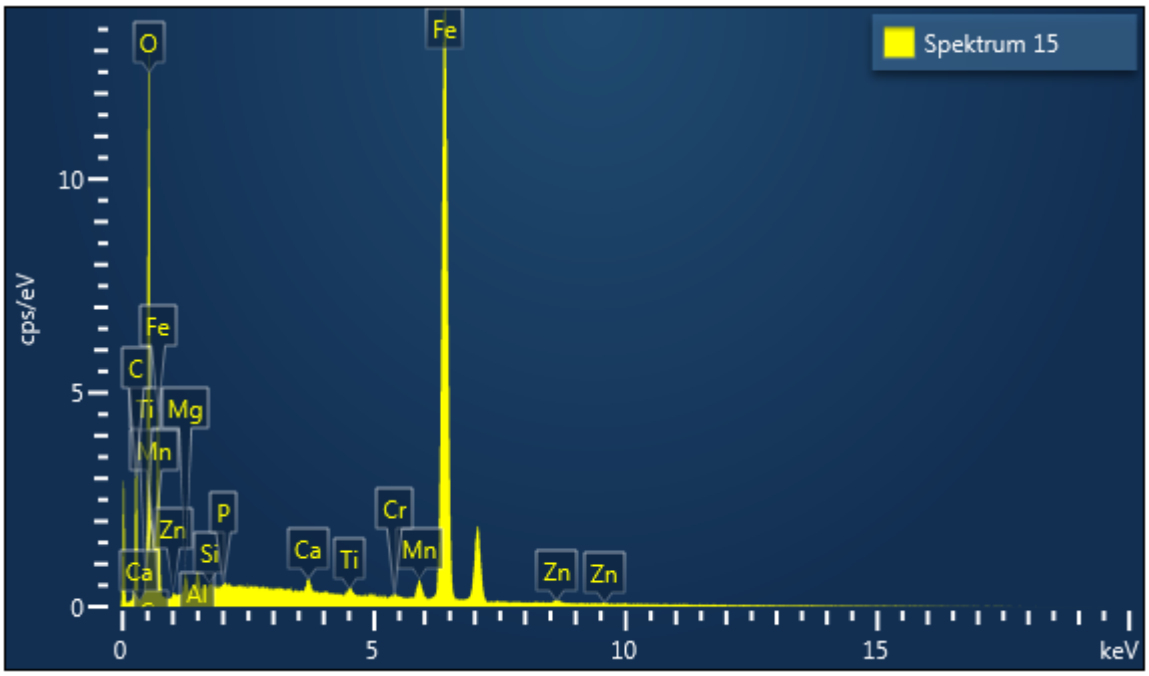


Figure 9.18: Element concentration of spectrum 15 of the treated slag P2

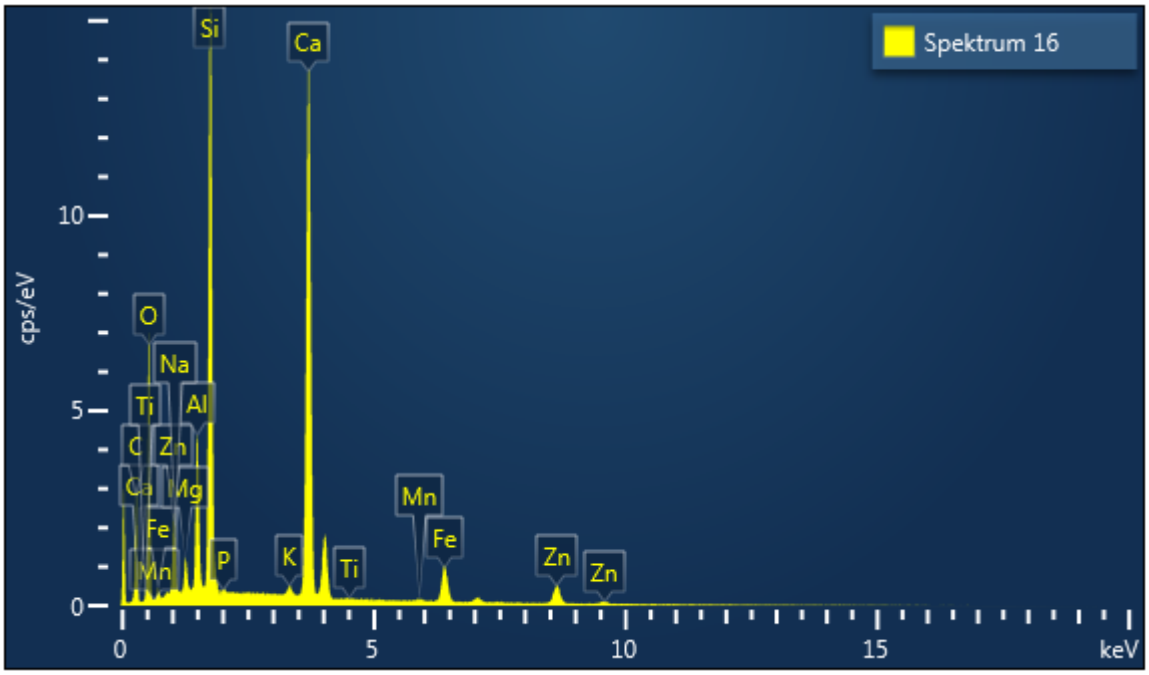


Figure 9.19: Element concentration of spectrum 16 of the treated slag P2

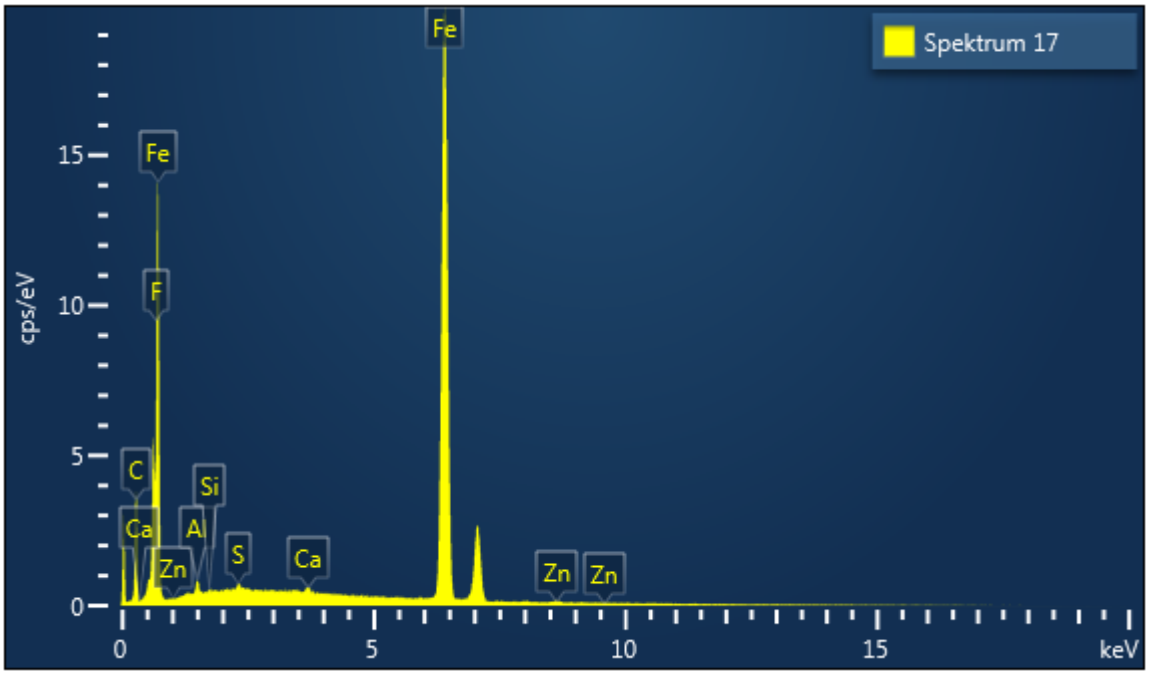


Figure 9.20: Element concentration of spectrum 17 of the treated slag P2

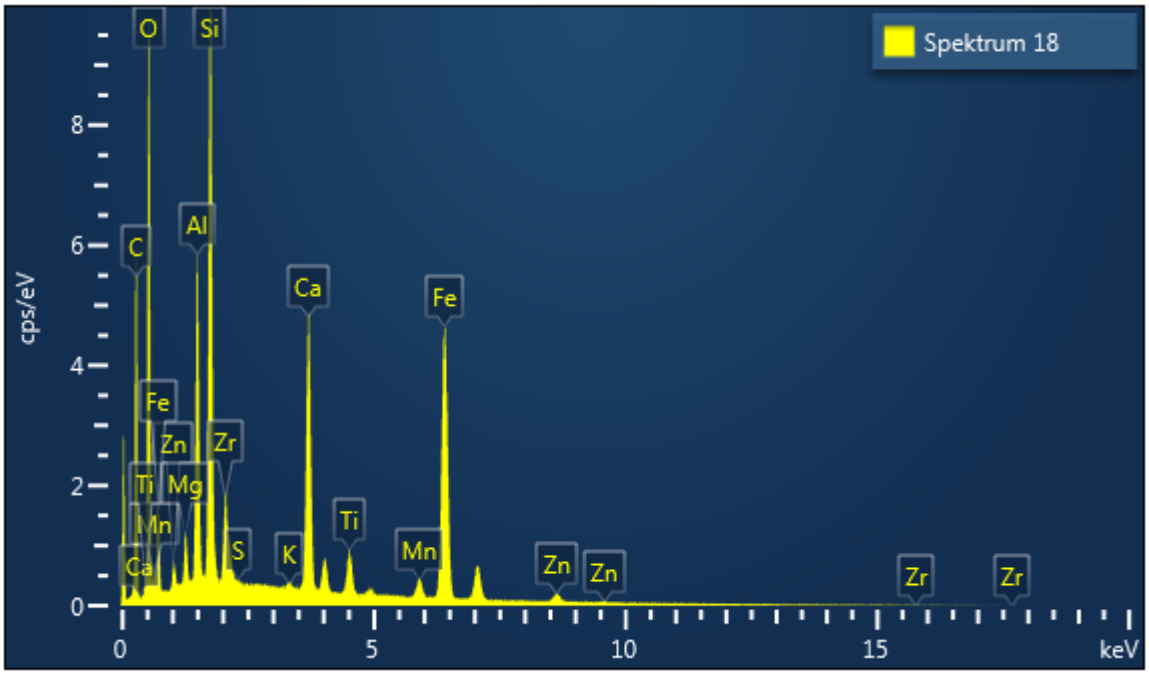


Figure 9.21: Element concentration of spectrum 18 of the treated slag P2

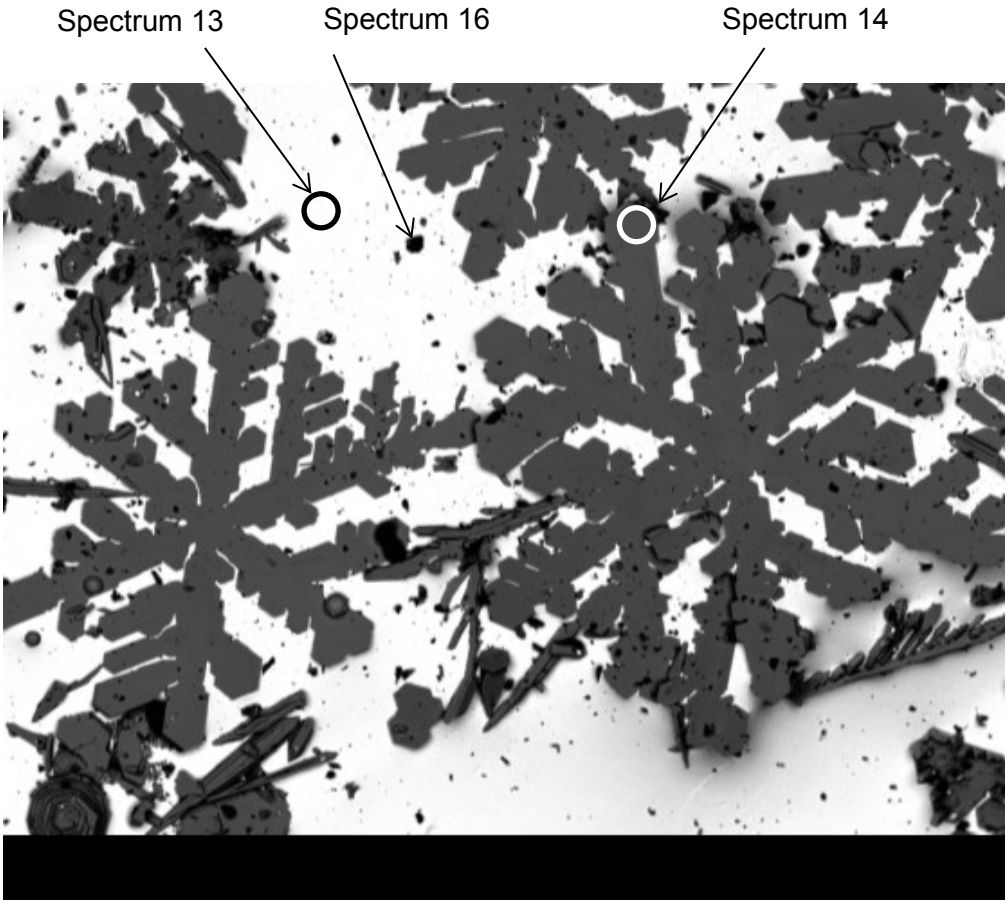


Figure 9.22: Crystalline zinc sulphide structures embedded in a lead matrix

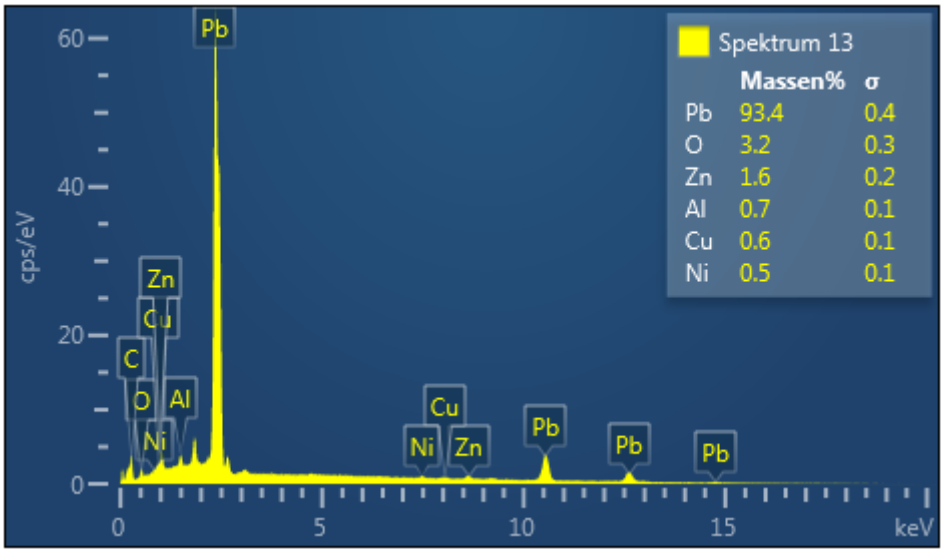


Figure 9.23: Element concentration of spectrum 13 (the lead matrix) of the analysed regulus

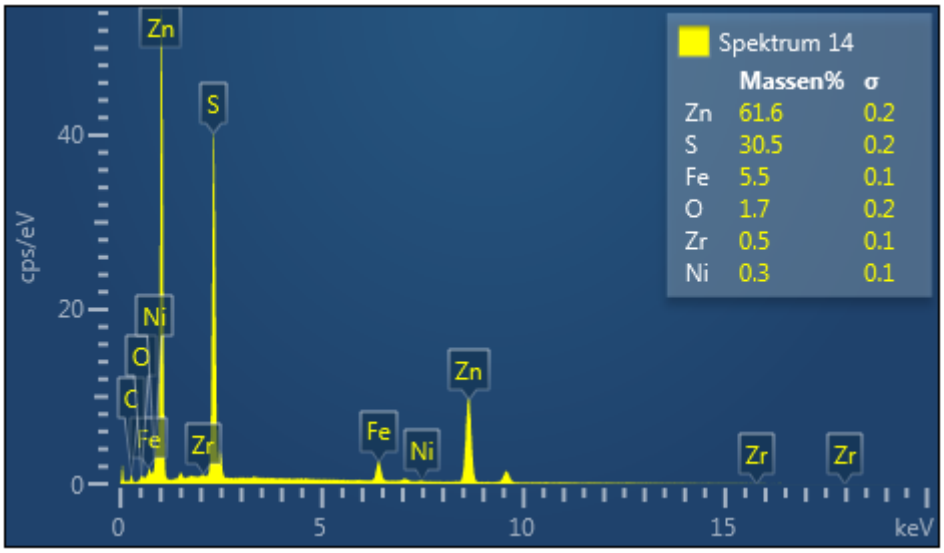


Figure 9.24: Element concentration of spectrum 14 (zinc sulphide structure) of the analysed regulus

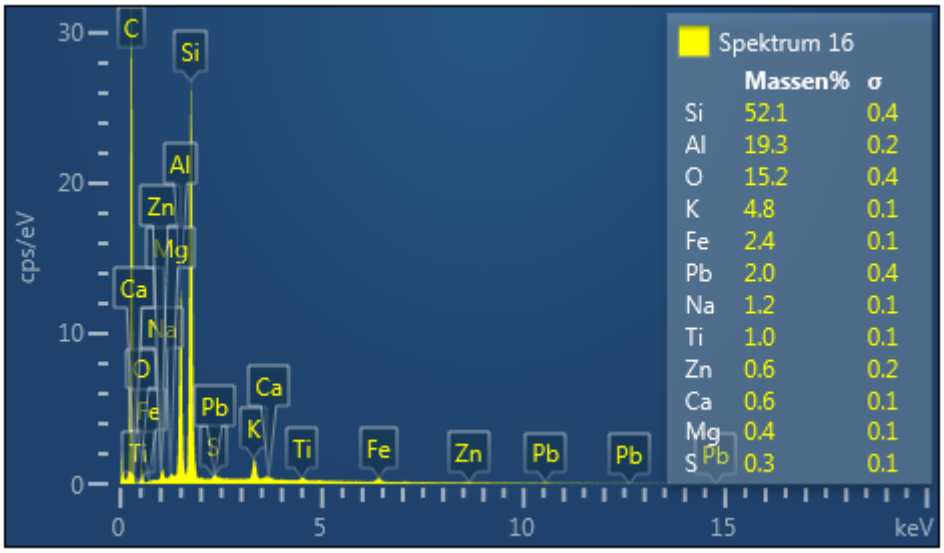


Figure 9.25: Element concentration of spectrum 16 of the analysed regulus

# 10 List of figures

# 11 List of tables

# 12 Literature


[1] International Lead and Zinc Study Group: End Uses of Zinc. Online im Internet: http://www.ilzsg.org/static/enduses.aspx?from=1, last downloaded 19.05.2015

[2] United States Geological Survey: Mineral Commodity Summaries, Reston, Virginia, United States of America, http://minerals.usgs.gov/minerals/pubs/commodity/lead /mcs-2015-lead.pdf , last downloaded 25.05.2015

[3] European Commision: Being wise with waste: the EU's approach to waste management, Brussels, http://ec.europa.eu/environment/waste/pdf /WASTE%20BROCHURE.pdf, last downloaded 19.05.2015

[4] European Commision: Circular Economy Strategy, Brussels, http://ec.europa.eu/smart- regulation/impact/planned_ia/docs/2015_env_065_env +_032_circular_economy_en.pdf, last downloaded 19.05.2015

[5] Univ.-Prof. Dipl.-Ing. Dr. techn. Helmut Antrekowitsch: Metallhüttenkunde II, Leoben, 2014.

[6] International Lead and Zinc Study Group: World Directory 2006: Primary and Secondary Lead Plants , (1–48.)

[7] Wiley-VCH: Ullmanns encyclopedia, Wiley-VCH Verlag GmbH & Co. KGaA.

[8] Pawlek F.: Metallhüttenkunde, Walter de Gruyter & Co, 1983.

[9] Baojun Zhao: Lead and Zinc Sintering, 2012.

[10] Wiley-VCH: Ullmanns encyclopedia, Wiley-VCH Verlag GmbH & Co. KGaA.

[11] A.M.C.O. united samplers and assayers GmbH: Prüfbericht.

[12] Unger A.; Steinlechner S.; Antrekowitsch J.: Simultaneous recovery of valuables from a dumped slag, Leoben, 10/2014.

[13] Weast R. C.: CRC Handbook of Chemistry and Physics 68, CRC Press, 1987-1988.

[14] Unger A.: Developing a recycling process for simultaneous recovery of valuables from a dumped slag, 2014.

[15] A. Longval T.; Jiao Q.; Davis B.: Operational improvements at Brunswick's blast furnace, 2008.

[16] Kenezevic M., Korac M., Kamberovic Z., et al.: Possibility of secondary lead slag stabilization in concrete with presence of selected additives MJoM Vol 16(3) , (2010) 195–204.

[17] Janke D.: Schlacken in der Metallurgie (K. Koch and D. Janke), Verlag Stahleisen mbH, Düsseldorf, 1984.

[18] Krajewski W.; Krüger J.: Schlacken in der Metallurgie (K. Koch and D. Janke),, Verlag Stahleisen mbH,, Düsseldorf, 1984.

[19] Engel H.; Krajewski W.; Krüger J.: Schlacken in der Metallurgie, 1984.

[20] Nabertherm GmbH: Labor-Schmelzöfen. Online im Internet: http://www.nabertherm.com/produkte/details/de/labordental_schmelzoefen, last downloaded 25.05.2015.

[21] Morgan MMS GmbH: Molten Metal Systems Global Technical Data Sheet, Berkatal, Germany.

[22] Rüdel H.; Kösters J.; Schörmann J.: Bestimmung von Elementgehalten in Umweltproben durch ICP-OES. Online im Internet: http://www.ime.fraunhofer.de/content/dam/ime/de/documents/AOe/UPB_SOP_ICP-OES_de.pdf, last downloaded 25.05.2015

[23] A.M.C.O. united samplers and assayers GmbH: Prüfbericht.

[24] JEOL (Germany) GmbH: JEOL JSM-IT300 – die neue Generation der JEOL Rasterelektronenmikroskope. Online im Internet: http://www.jeol.de/electronoptics/produktuebersicht/elektronen-ionenoptische-systeme/rasterelektronenmikroskope/rem-thermische-kathode/jsm-it300.php, last downloaded: 19.05.2015

[25] W. L. Gore & Associates, Inc.: Filter Bags & Cartridges for Bag Houses, Newark, Delaware, United States of America, http://www.gore.com/en_xx/products /filtration/baghouse/filterbags/industrial-baghouse-filters-products.html, last downloaded 16.05.2015

[26] Univ.-Prof. Dipl.-Ing. Dr. techn. Harald Raupenstrauch: Skriptum: Energieformen,-nutzung und -umwandlung, Leoben.

[27] finanzen.net GmbH: Dollarkurs (EUR-USD) – aktueller Kurs. Online im Internet: http://www.finanzen.at/devisen/dollarkurs, last downloaded 25.05.2015

[28] Caterpillar Inc: CatUsed.com Used Equipment, Generators, Engines & Parts from CAT dealers. Online im Internet: http://catused.cat.com/en/search_results_wide.html?mn=174&et=_1016_152504_&et=_1016_79_&mfc=100&pn=0&px=99000&pnr=1&epp=30&sf=relevance&so=false, last downloaded 25.05.2015

[29] Alibaba (China) Co., Ltd: Storage Silo price. Online im Internet: http://www.alibaba.com/showroom/storage-silo-price.html, last downloaded 25.05.2015

[30] finanzen.net GmbH: Aktueller Blei in USD je Tonne. Online im Internet: http://www.finanzen.at/rohstoffe/bleipreis, last downloaded 19.05.2015

[31] Energie-Control Austria für die Regulierung der Elektrizitäts- und Erdgaswirtschaft: Ergebnisse Industriegaspreise. Online im Internet: http://www.e-control.at/de/industrie/gas/gaspreis/industriegaspreise/energiepreis, last downloaded 25.05.2015

[32] finanzen.net GmbH: Aktueller Silber in USD je Feinunze. Online im Internet: http://www.finanzen.at/rohstoffe/silberpreis, last downloaded 19.05.2015

[33] finanzen.net GmbH: Aktueller Zink in USD je Tonne. Online im Internet: http://www.finanzen.at/rohstoffe/zinkpreis, last downloaded 19.05.2015

[34] Verein deutscher Eisenhüttenleute: Werkstoffkunde Stahl Band I: Grundlagen, Springer Verlag, Verlag Stahleisen mbH Düsseldorf, Düsseldorf, Germany, 1984.